

A STUDY OF H-GUIDES WITH  
 ARTIFICIAL DIELECTRICS

Under NASA Research Grant  
 NGR-34-002-047/S1

January 15, 1968

FACILITY FORM 602

N68 27053  
 (ACCESSION NUMBER)

110  
 (PAGES)

CR-92802  
 (NASA CR OR TMX OR AD NUMBER)

1  
 (THRU)

10  
 (CODE)

10  
 (CATEGORY)

GPO PRICE \$ \_\_\_\_\_

CFSTI PRICE(S) \$ \_\_\_\_\_

Hard copy (HC) 3.00

Microfiche (MF) .65

PROGRESS REPORT  
GRANT NGR-34-002-047/S1  
January 15, 1968

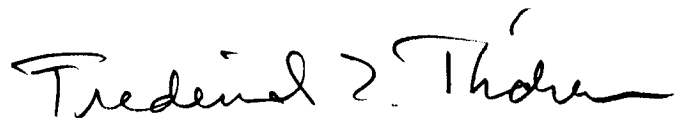
"A STUDY OF H-GUIDES WITH  
ARTIFICIAL DIELECTRICS"

to

The National Aeronautics and Space  
Administration, Washington, D. C.

North Carolina State University  
Raleigh, North Carolina

Submitted:



Dr. Frederick J. Tischer, Professor  
Principal Investigator

## SUMMARY

This report contains in part material presented in previous interim reports and in part new material to present a comprehensive study of the H-guide with artificial dielectrics. The study was carried out by Roy H. Propst under the direction of Dr. Frederick J. Tischer during 1967. The resulting report was submitted by Mr. Propst as a thesis for the Degree of Master of Science at the North Carolina State University at Raleigh, N. C.

The study deals with H-guide structures with artificial dielectrics. The application of artificial dielectrics represents one approach for the reduction of the attenuation caused by the dielectric slab in H-guides. Emphasis is placed on a new type of H-guide, the corrugated H-guide. The attenuation of this guide is computed, evaluated numerically and compared with that of other waveguides. Results of measurements verify the analytical results.

After a review of the literature, the attenuation for three wave-guiding structures is calculated. The structures are: an infinite dielectric sheet, an infinite corrugated plane, and a dielectric H-guide. These preliminary calculations are necessary for developing the method of computation, the normalizations to be used, and for purposes of subsequent comparison.

The distribution of the field components for the corrugated H-guide is determined by employing the method of

field matching. From this, the attenuation is computed and evaluated numerically at various frequencies by computer.

The attenuation of the corrugated H-guide is compared with three other wave guides: a dielectric H-guide, a laminated dielectric H-guide, and a standard rectangular wave guide, all operating at 10 GHz.

Measurements were made at 10 GHz for the verification of the analytical results for the corrugated H-guide structure. They were carried out in a transmission-type cavity which formed a shorted section of H-guide. Experimental techniques are described for determination of the guide wavelength and attenuation.

## TABLE OF CONTENTS

	Page
LIST OF TABLES . . . . .	vi
LIST OF FIGURES. . . . .	vii
1. INTRODUCTION . . . . .	1
2. REVIEW OF THE LITERATURE . . . . .	3
2.1 Surface Waves. . . . .	3
2.2 H-Guide. . . . .	5
2.3 Artificial Dielectrics . . . . .	5
3. ATTENUATION OF A DIELECTRIC SLAB . . . . .	7
3.1 Introduction . . . . .	7
3.2 Development of the Field in Terms of Longitudinal Components . . . . .	7
3.3 Solution for the Field in the Dielectric Region. . . . .	10
3.4 Solution for the Field in the Free-Space Region. . . . .	11
3.5 Power Transport. . . . .	12
3.6 Power Loss . . . . .	13
3.7 Trigonometric Identities . . . . .	13
3.8 Attenuation. . . . .	14
3.9 Physical Parameter Values. . . . .	16
3.10 Computer Program . . . . .	17
3.10.1 Introduction . . . . .	17
3.10.2 Main Program . . . . .	24
3.10.3 Subroutine . . . . .	25
4. ATTENUATION OF AN INFINITE CORRUGATED WAVE GUIDE . . . . .	27
4.1 Introduction . . . . .	27
4.2 Development of the Field in Terms of Longitudinal Components . . . . .	27
4.3 Solution for the Field Within the Corrugations . . . . .	30
4.4 Solution for the Field in the Region Above the Corrugations . . . . .	33
4.5 Continuity of the Field at the Boundary. . . . .	35
4.6 Total Field, after TEM Mode Approximation. . . . .	39
4.7 Power Transport. . . . .	39
4.8 Power Loss . . . . .	40
4.9 Trigonometric Identities . . . . .	41
4.10 Attenuation. . . . .	42
4.11 Computer Program . . . . .	43
4.11.1 Introduction . . . . .	43
4.11.2 Computer Program . . . . .	47
4.11.3 Identification of Program Variables. . . . .	47

## TABLE OF CONTENTS (continued)

	Page
5. DIELECTRIC H-GUIDE . . . . .	48
5.1 Description of Structure . . . . .	48
5.2 Introduction . . . . .	48
5.3 Method of Solution . . . . .	48
5.4 Development of a Wave Equation . . . . .	50
5.5 The Field Within the Dielectric. . . . .	51
5.6 The Field Above the Dielectric . . . . .	54
5.7 Field Matching . . . . .	56
5.8 Trigonometric Identities . . . . .	58
5.9 Simplification of the Field Components . . . . .	59
5.10 Power Transmitted. . . . .	61
5.11 Power Dissipated . . . . .	63
5.12 Attenuation. . . . .	65
5.13 Numerical Results. . . . .	68
6. ARTIFICIAL DIELECTRIC H-GUIDE. . . . .	70
6.1 Description of Structure . . . . .	70
6.2 Introduction . . . . .	70
6.3 Method of Solution . . . . .	70
6.4 Development of a Wave Equation . . . . .	72
6.5 Solution of the Wave Equation Under Special Periodic Conditions . . . . .	73
6.6 The Field Above the Corrugations . . . . .	77
6.7 The Field Within the Corrugations. . . . .	80
6.8 Field Matching . . . . .	86
6.9 Power Transport. . . . .	93
6.10 Power Loss . . . . .	94
6.11 Identities . . . . .	96
6.12 Attenuation. . . . .	98
6.13 Group Velocity . . . . .	102
6.14 Numerical Results. . . . .	104
6.14.1 Introduction . . . . .	104
6.14.2 Computer Program . . . . .	104
7. COMPARISON OF ATTENUATIONS . . . . .	119
7.1 Laminated Dielectric H-Guide . . . . .	119
7.2 A Comparison of Three H-Guides with the Rectangular Wave Guide . . . . .	122
8. EXPERIMENTAL PROCEDURES AND RESULTS. . . . .	123
8.1 Introduction . . . . .	123
8.2 Description of the Test Cavity . . . . .	123

## TABLE OF CONTENTS (continued)

	Page
8.3 Determination of the Resonant Frequencies for the Empty Cavity . . . . .	125
8.4 Determination of the Resonant Frequencies of the Dielectric-Loaded Cavity . . . . .	128
8.5 Excitation of Cavity Modes . . . . .	130
8.6 Wideband Measurement Technique . . . . .	132
8.7 Q-Value Measurement Technique. . . . .	134
8.8 Wideband Measurement Results . . . . .	135
8.9 Q-Value Measurement Results. . . . .	143
8.10 Theoretical Technique for Unloaded Q-Value Measurement . . .	148
8.11 Experimental Technique for Q-Value Measurements. . . . .	153
8.12 A Relationship Between Attenuation and Q-Value . . . . .	157
9. CONCLUSION . . . . .	161
9.1 Summary. . . . .	161
9.2 Findings . . . . .	161
10. LIST OF REFERENCES . . . . .	162

## LIST OF TABLES

	Page
7.1 Relative permittivity and loss tangent of several materials at 10 GHz . . . . .	121
7.2 Attenuation for various wave guides at 10 GHz . . . . .	122
8.1 Frequencies of cavity modes . . . . .	127
8.2 Frequencies of cavity modes with central slab loading . . . . .	128
8.3 Loaded Q-values of the test cavity . . . . .	147
8.4 Results of insertion loss and loaded Q-value measurements . . . . .	156



## LIST OF FIGURES

	Page
3.1 Infinite dielectric slab over perfectly conducting plane . . .	8
3.2 Flow chart for main program . . . . .	18
3.3 Flow chart for subroutine . . . . .	19
3.4 Attenuation of infinite dielectric slab at 10 GHz . . . . .	20
3.5 Attenuation of infinite dielectric slab at 35 GHz . . . . .	21
3.6 Thickness of infinite dielectric slab at 10 GHz . . . . .	22
3.7 Thickness of infinite dielectric slab at 35 GHz . . . . .	23
4.1 Infinite corrugated wave guide over perfectly conducting plane . . . . .	28
4.2 Flow chart for program . . . . .	44
4.3 Attenuation of infinite corrugated wave guide at 35 GHz . . . .	45
4.4 Attenuation of infinite corrugated wave guide at 10 GHz . . . .	46
5.1 Dielectric H-guide on perfectly conducting plane. . . . .	49
5.2 Attenuation of dielectric H-guide for 10 GHz with a sidewall spacing of 2.286 cm . . . . .	69
6.1 Corrugated H-guide over perfectly conducting plane. . . . .	71
6.2 Flow chart. . . . .	108
6.3 Attenuation of corrugated H-guide at 10 GHz with 2.286 cm sidewall spacing. . . . .	109
6.4 Attenuation of corrugated H-guide at 10 GHz with 4.572 cm sidewall spacing. . . . .	110
6.5 Attenuation of corrugated H-guide at 35 GHz with 2.286 cm sidewall spacing. . . . .	111
6.6 Attenuation of corrugated H-guide at 35 GHz with 4.572 cm sidewall spacing. . . . .	112
6.7 Attenuation of corrugated H-guide at 70 GHz with 2.286 cm sidewall spacing. . . . .	113

## LIST OF FIGURES (continued)

	Page
6.8 Attenuation of corrugated H-guide at 70 GHz with 4.572 cm sidewall spacing. . . . .	114
6.9 Attenuation of corrugated H-guide at 150 GHz with 2.286 cm or 2.572 cm sidewall spacing. . . . .	115
6.10 Normalized phase velocity or guide wavelength for the corrugated H-guide . . . . .	116
6.11 Omega-beta diagram for corrugated H-guide with $p$ , a normalized x-decay constant of two tenths and a sidewall spacing of 2.286 cm . . . . .	117
6.12 Normalized group velocity for corrugated H-guide at 10 GHz for two sidewall spacing (SS) values . . . . .	118
8.1 Test cavity. . . . .	124
8.2 Assembly view of test cavity end section . . . . .	126
8.3 Cutaway view of test cavity with central dielectric loading. . .	129
8.4 Cross-sectional view at test cavity end. . . . .	131
8.5 Circuit used for wideband and Q-value measurements . . . . .	133
8.6 Mode spectrum of empty test cavity . . . . .	136
8.7 Mode spectrum of test cavity fully loaded with inexpensive dielectric described in text . . . . .	137
8.8 Mode spectrum of test cavity centrally loaded with a one- inch strip of inexpensive dielectric described in text . . . . .	139
8.9 Mode spectrum of test cavity centrally loaded with a one- eighth-inch strip of Rexolite. . . . .	140
8.10 Mode spectrum of test cavity centrally loaded with a one- quarter-inch strip of Rexolite . . . . .	141
8.11 Mode spectrum of test cavity centrally loaded with a one- quarter-inch strip of Rexolite and one-quarter-inch plywood on top and bottom surfaces . . . . .	142

## LIST OF FIGURES (continued)

	Page
8.12 Mode spectrum of test cavity loaded with one-half-inch strips of Eccofoam absorbing material on top and bottom surfaces . . . . .	144
8.13 Mode spectrum of test cavity centrally loaded with one-quarter-inch strip of Rexolite and one-half-inch strips of Eccofoam absorbing material on top and bottom surfaces. . .	145
8.14 Q-value measurement spectrum of test cavity for the $TE_{107}$ mode in empty cavity . . . . .	146
8.15 Equivalent circuit of transmission cavity with coupling irises shown as ideal transformers . . . . .	149
8.16 Alternative form for the circuit shown in Figure 8.15. . . . .	150
8.17 Generator, $V$ , feeding a matched load $z_0$ . . . . .	152
8.18 Circuit used for INSERTION LOSS and Q-value measurement. . . . .	154

## 1. INTRODUCTION

As frequency increases beyond X-band (10 GHz), the low-loss qualities of rectangular wave guides become degraded considerably; for example, the attenuation of standard rectangular wave guides operating at 70 GHz is approximately twenty times that of X-band wave guide at 10 GHz. This occurs because of the reduction in the ratio of cross-sectional area to wall area, and increase in surface resistance. There is further a degradation in the power handling capability as the size becomes small.

One alternative solution is the use of "oversize" wave guides; that is wave guides with a width of several half-wavelengths. However, this introduces modes of higher order than the fundamental, which means there will be losses incurred when the power is extracted.

Semi-open wave guides, such as the H-guide which may also be "oversize", offer another possibility in that the top and bottom walls of a rectangular guide are removed and replaced by a central dielectric slab whose loss can be less than that of the walls removed. The H-guide behaves somewhat as a surface wave guide since the field decays exponentially with distance from the central dielectric slab, thus confining the field to a region near the slab. An interesting feature of the dielectric H-guide is the disappearance of the component of the magnetic portion of the field normal to the slab, thereby eliminating longitudinal wall currents. This means that the contact resistance between H-guide sections is of no consequence and does not introduce significant losses as in the case of rectangular wave guides.

It is intended for this investigation to determine quantitatively the advantage in using artificial dielectrics, as opposed to a single dielectric slab, within the H-guide. Two cases will be considered: a corrugated

structure, and a laminated dielectric structure. The corrugated structure consists of an array of rectangular metallic plates placed in parallel within a low-loss foam dielectric; and the laminated, an array of dielectric slabs each of which occupies a position similar to the slab in the usual H-guide.

Initially, the attenuation for three other structures--infinite dielectric plane, infinite corrugated plane, and dielectric H-guide--is found. This is necessary since the attenuation for the infinite corrugated plane was not available elsewhere, and that for the infinite dielectric plane and the dielectric H-guide was not available in a form suitable for comparisons. The attenuations for the infinite cases also provide a validity check for the attenuation of the H-guides, since in the limit as the width of the H-guides becomes infinite, the attenuations approach that of the infinite planes.

## 2. REVIEW OF THE LITERATURE

### 2.1 Surface Waves

A surface wave is defined as a wave which propagates along an interface between two different media without radiation; radiation meaning energy converted from the surface-wave field to some other form.

Hertz was probably the first to examine surface waves analytically (Jones, 1893). In 1889, he determined the electric field produced by a wave propagating along a wire of infinitesimal thickness. However, he did not solve the problem completely; this was left to Sommerfeld (1899). In 1888, Hertz constructed a single wire transmission line excited by resonant spark discharges (Jones, 1893). He found that the wavelength, as measured between adjacent modes on the wire, was independent of the size of the wire and the material from which it was made, and, thus, concluded the velocity of propagation to be independent of these parameters. This line is a surface wave transmission line in that the waves are traveling along the air-conductor interface.

The Harms-Goubau line, a single wire covered with a layer of dielectric material, is perhaps one of the most widely known surface wave guides. This was first analyzed by Harms (1907) by direct solution of the Maxwell equations. Goubau (1950) extended the work, and later performed measurements on such a line. The attenuation of a two-mile line of this type was measured at 200 MHz, and found to be only six decibels per mile (Goubau, 1954). It was found that the sum of the conductor and dielectric losses for this line was less than the conductor losses for a conventional two-wire transmission line; however, launching loss and loss due to supports was fairly large; therefore short lines would not be practical.

Zucker (1954) classifies traveling waves into two categories; if the phase velocity,  $v_p$ , of a wave is slower than the velocity of light,  $c$ , in the medium, then most of the energy of the wave is contained within a small region near the interface and the wave is termed a guided or "trapped" wave (surface wave); if  $v_p$  is greater than  $c$ , then the wave radiates and is termed a "leaky" wave. This can be observed from the equation relating the propagation constants of a wave traveling in the  $z$ -direction along an infinite interface. If  $x$  is the direction normal to the interface, the propagation constants are related by

$$\alpha_x^2 = k_z^2 - k^2 \quad (2.1)$$

or, in terms of velocities, as

$$\alpha_x^2 = \frac{\omega}{v_p} - \frac{\omega}{c} . \quad (2.2)$$

It follows from (2.2) that if  $v_p$  is greater than  $c$ , then  $\alpha_x$  must be complex and, therefore, eliminating the guiding property of the interface.

If the guiding structure is closed in the  $y$ -direction, then (2.1) becomes

$$\alpha_x^2 = k_y^2 + k_z^2 - k^2 , \quad (2.3)$$

or (2.2) may be written as

$$\alpha_x^2 = \frac{\omega}{v_p} - \frac{\omega}{c} + k_y^2 . \quad (2.4)$$

Now, if  $v_p$  is greater than  $c$ ,  $\alpha_x$  need not necessarily be imaginary due to the presence of  $k_y$ . This illustrates the difference between a semi-open and a completely open (infinite) guiding structure.

## 2.2 H-Guide

The H-guide was proposed by Tischer (1953). The cross-sectional area view, from which the name is derived, is in the form of an "H"; essentially a parallel-plate wave guide with a dielectric bar separating the plates. An investigation of the properties of the structure carrying the low-loss wave mode was made by Tischer (1956) and extended to other wave modes by Cohn (1959). Attenuation was calculated but not placed in a form suitable for comparison with later structures. Tischer (1959) investigated the properties of an H-guide with a central bar composed of two dielectric slabs separated by air; it was found that losses could be reduced in this manner. In the same paper, an H-guide with multiple laminations of dielectric slabs for the central bar was proposed; however, no calculations were performed.

An experimental investigation of the dielectric H-guide was performed by Tischer (1959) whereby a distribution of the electric portion of the field was plotted. Griemsman and Birenbaum (1959) also investigated the same structure and demonstrated that losses are definitely reduced by the insertion of the dielectric slab; thus, H-guide as opposed to parallel plates alone.

This work indicates that the H-guide is a feasible wave guiding structure, and that the possibility exists for reducing attenuation by the use of artificial dielectrics.

## 2.3 Artificial Dielectrics

An artificial dielectric is a large-scale model of an actual dielectric, which can be obtained by arranging conducting obstacles in some three-dimensional pattern (Collin, 1960). In actuality, the obstacles are supported by some material such as styrofoam which has a dielectric constant nearly equal to unity. When an external field is applied, charge on the surfaces



of the obstacles is displaced, thus establishing an electric dipole. Each obstacle thereby behaves as molecule in an ordinary dielectric. The combined effect of all of the obstacles produces a net average dipole polarization,  $\underline{P}$ . The permittivity,  $\epsilon$ , is greater than  $\epsilon_0$ , since

$$\underline{\epsilon E} = \epsilon_0 \underline{E} + \underline{P} .$$

The analysis of the artificial dielectric problem is approached in three manners. The simplest solution is obtained by considering only dipole interaction between obstacles. This is valid if the obstacle size is small, as compared to spacing, and spacings are less than one-tenth wavelength. For larger obstacles, all of the multipoles can be accounted for by a complete static field solution (the second method). A third method is to solve the Maxwell equations directly in some approximate manner; this approach will be used for the solution of the corrugated wave guide problems, which follow.

Brillouin (1948) discussed several types of structures capable of supporting waves whose phase velocity is less than the velocity of light in the medium. These structures were corrugated plates of rectangular or cylindrical geometry.

Elliott (1954) examined a rectangular wave guide with a corrugated bottom surface. He was interested primarily in the structure as a means of exciting a corrugated radiator, and therefore did not compute the attenuation for the structure.

### 3. ATTENUATION OF A DIELECTRIC SLAB

#### 3.1 Introduction

The purpose of this section is to determine the attenuation of waves of the fundamental TM (Transverse Magnetic) mode propagating along an infinite dielectric slab in terms of the medium properties, and a normalized decay constant ( $p = \alpha_x/k_0$ ) of the field above the dielectric.

To facilitate the solution of the problem, an equivalent problem may be considered (Figure 3.1); namely, the dielectric slab placed on a perfectly conducting sheet, which later will be removed using the method of images. Another slab, whose thickness is the same as that of the original, will be substituted in its place. Implicit is, of course, the necessity for excitation which is symmetrical about  $x = 0$ . The solution will be obtained by the use of field matching at the boundary between the dielectric and air regions. Two solutions to the wave equation, one for each region, will be found; one valid for  $x \geq a$  (air).

There is, of course, another set of solutions which would arise if the plane were a perfect magnetic conductor. In this case, the electric field would be a maximum at the conductor rather than zero.

#### 3.2 Development of the Field in Terms of Longitudinal Components

The source-free, time harmonic Maxwell equations are

$$\nabla \times \underline{E} = -j \omega \mu_0 \underline{H} \quad (3.1)$$

and

$$\nabla \times \underline{H} = j \omega \epsilon_0 \epsilon_r \underline{E} . \quad (3.2)$$

Expansion in rectangular coordinates yields

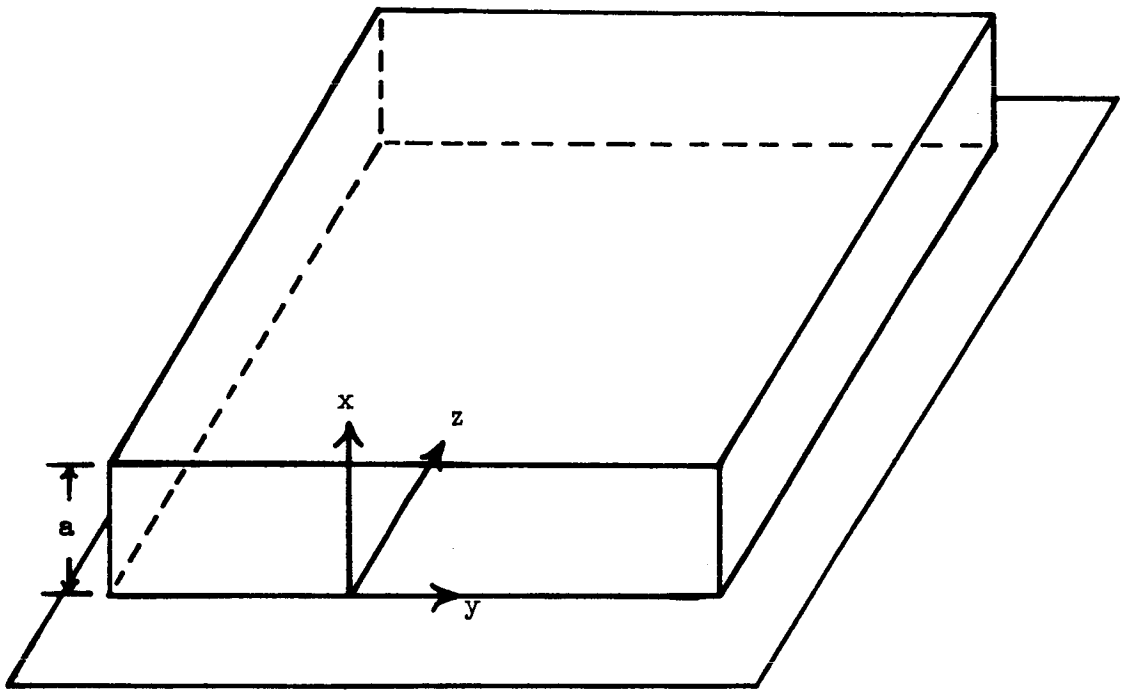


Figure 3.1 Infinite dielectric slab over perfectly conducting plane

$$\frac{\partial E_z}{\partial y} - \frac{\partial E_y}{\partial z} = -j \omega \mu_0 H_x, \quad (3.3)$$

$$\frac{\partial E_x}{\partial z} - \frac{\partial E_z}{\partial x} = -j \omega \mu_0 H_y, \quad (3.4)$$

$$\frac{\partial E_y}{\partial x} - \frac{\partial E_x}{\partial y} = -j \omega \mu_0 H_z, \quad (3.5)$$

$$\frac{\partial H_z}{\partial y} - \frac{\partial H_y}{\partial z} = j \omega \epsilon_0 \epsilon_r E_x, \quad (3.6)$$

$$\frac{\partial H_x}{\partial z} - \frac{\partial H_z}{\partial x} = j \omega \epsilon_0 \epsilon_r E_y, \quad (3.7)$$

and

$$\frac{\partial H_y}{\partial x} - \frac{\partial H_x}{\partial y} = j \omega \epsilon_0 \epsilon_r E_z, \quad (3.8)$$

The solution is now restricted to the fundamental TM mode ( $H_z = 0$ ), and by symmetry considerations the y-variation is zero ( $\frac{\partial}{\partial y} = 0$ ); therefore, only three field components will remain. In this type structure, the z-variation, upon separating variables, must be of the form  $e^{-jk_z z}$  for waves traveling in the positive z-direction; (3.3) through (3.8) reduce to

$$H_y = \frac{-j \omega \epsilon_0 \epsilon_r}{k_0^2 \epsilon_r - k_z^2} \frac{\partial E_z}{\partial x} \quad (3.9)$$

and

$$E_x = \frac{-j k_z}{k_0^2 \epsilon_r - k_z^2} \frac{\partial E_z}{\partial x}, \quad (3.10)$$

where

$$k_0^2 = \omega^2 \mu_0 \epsilon_0 \quad (3.11)$$

and

$$\frac{\partial^2 E_z}{\partial x^2} + (k_0^2 \epsilon_r - k_z^2) E_z = 0 . \quad (3.12)$$

### 3.3 Solution for the Field in the Dielectric Region

Boundary conditions specify

$$E_z = 0$$

for

$$x = 0 .$$

Therefore, (3.12) yields a solution of the form

$$E_{ze} = A \sin(k_x x) , \quad (3.13)$$

where

$$k_x^2 = k_0^2 \epsilon_r - k_z^2 . \quad (3.14)$$

The other two field components may be obtained from (3.9) and (3.10); the total field variation is then

$$E_{ze} = \frac{jk_x}{\omega \epsilon_0 \epsilon_r} H_0 \sin(k_x x) , \quad (3.15)$$

$$H_{ye} = H_0 \cos(k_x x) , \quad (3.16)$$

and

$$E_{xe} = \frac{k_z}{\omega \epsilon_0 \epsilon_r} H_0 \cos(k_x x) , \quad (3.17)$$

defining

$$H_0 = \frac{-j \omega \epsilon_0 \epsilon_r A}{k_x} . \quad (3.18)$$

### 3.4 Solution for the Field in the Free-Space Region

It is desired to have a solution which describes waves traveling along the interface between the dielectric and free-space regions, which means the field must decay as  $x$  increases from the value  $a$ . The only type of solution of (3.12) meeting this requirement is of the form

$$E_z = B e^{-\alpha_x x}, \quad (3.19)$$

where

$$\alpha_x^2 = k_z^2 - k_0^2. \quad (3.20)$$

Requiring continuity of  $E_z$  at  $x = a$ , i.e.,

$$E_z = E_{ze} \quad (3.21)$$

for  $x = a$ , this yields

$$B = \frac{jk_x}{\omega \epsilon_0 \epsilon_r} H_0 \sin(k_x a) e^{\alpha_x a}. \quad (3.22)$$

The remaining two field components may be obtained from (3.9) and (3.10); the total field is then

$$E_z = \frac{j\alpha_x}{\omega \epsilon_0} H'_0 e^{-\alpha_x x}, \quad (3.23)$$

$$H_y = H'_0 e^{-\alpha_x x}, \quad (3.24)$$

and

$$E_x = \frac{k_z}{\omega \epsilon_0} H'_0 e^{-\alpha_x x}, \quad (3.25)$$

where

$$H'_0 = \frac{H_0 k_x}{\alpha_x \epsilon_r} \sin(k_x a) e^{\alpha_x a} . \quad (3.26)$$

Requiring further, that the other tangential field component,  $H_y$ , must also be continuous at  $x = a$ , i.e.,

$$H_y = H_{y\epsilon} \quad (3.27)$$

for  $x = a$ , which yields

$$k_x \tan(k_x a) = \epsilon_r \alpha_x . \quad (3.28)$$

### 3.5 Power Transport

The total power,  $P$ , carried by the guide will be due partly to the dielectric,  $P_\epsilon$ , and partly to the free-space region,  $P_0$ ; hence,

$$P = P_\epsilon + P_0 . \quad (3.29)$$

The Poynting identity yields

$$P_\epsilon = \frac{1}{2} \operatorname{Re} \int_0^a \int_0^1 E_{x\epsilon} H_{y\epsilon}^* dy dx \quad (3.30)$$

and

$$P_0 = \frac{1}{2} \operatorname{Re} \int_0^\infty \int_0^1 E_x H_y^* dy dx . \quad (3.31)$$

Equations (3.15) and (3.16) yield

$$P_\epsilon = \frac{k_z H_0^2}{8\omega \epsilon_0 \epsilon_r k_x} \{ 2k_x a + \sin(2k_x a) \} ; \quad (3.32)$$

also, (3.23), (3.24), and (3.31) yield

$$P_0 = \frac{k_z H_0^2 k_x^2}{4\omega \epsilon_0 \epsilon_r^2 \alpha_x^3} \sin^2(k_x a) . \quad (3.33)$$

Combining (3.29), (3.32), and (3.33), the total power transported is

$$P = \frac{k_z H_0^2}{4\omega \epsilon_0 \epsilon_r} \left\{ \frac{1}{2k_x} [(2k_x a + \sin(2k_x a))] + \frac{k_x^2 \sin^2(k_x a)}{\epsilon_0 \epsilon_r \alpha_x^3} \right\}. \quad (3.34)$$

### 3.6 Power Loss

Power losses due to the conducting plane are not considered since, in the last analysis, it will be removed. The total losses are, therefore, due to the dielectric alone; they are predicted by the Poynting identity as

$$P_L = \frac{1}{2} R_e \int_0^a \int_0^1 \underline{J}_{-\epsilon} \cdot \underline{E}_{\epsilon}^* dy dx, \quad (3.35)$$

which becomes

$$P_L = \frac{\omega \epsilon_0 \epsilon_r}{2} \tan(\delta) R_e \int_0^a \int_0^1 (E_{x\epsilon} E_{x\epsilon}^* + E_{z\epsilon} E_{z\epsilon}^*) dy dx, \quad (3.36)$$

when Ohm's law,  $\underline{J} = \sigma \underline{E}$ , is substituted into (3.35). Introducing (3.15) and (3.17) into (3.36) and performing the integration,

$$P_L = \frac{H_0^2 \tan(\delta)}{8 \omega \epsilon_0 \epsilon_r k_x} \left\{ 2k_x a k_0^2 \epsilon_r + [k_0^2 (2 - \epsilon_r) + 2\alpha_x^2] \sin(2k_x a) \right\}. \quad (3.37)$$

### 3.7 Trigonometric Identities

It will be useful to consider the following identities before calculation of the attenuation

$$\sin(2k_x a) = 2 \sin(k_x a) \cos(k_x a), \quad (3.38)$$

$$\sin(k_x a) = \frac{1}{\sqrt{1 + \cot^2(k_x a)}}, \quad (3.39)$$

and

$$\cos(k_x a) = \frac{1}{\sqrt{1 + \tan^2(k_x a)}}. \quad (3.40)$$



Combining (3.14) and (3.20), yields

$$k_x^2 = k_0^2(\epsilon_r - 1) - \alpha_x^2 . \quad (3.41)$$

Equations (3.39) and (3.40) can now be evaluated in terms of nontrigonometric functions by using (3.38),

$$\sin(k_x a) = \frac{\epsilon_r \alpha_x}{h} , \quad (3.42)$$

where

$$h^2 = k_0^2(\epsilon_r - 1) + \alpha_x^2(\epsilon_r^2 - 1) \quad (3.43)$$

and

$$\cos(k_x a) = \frac{k_x}{h} . \quad (3.44)$$

Combining (3.38), (3.42) and (3.44) yield

$$\sin(2k_x a) = \frac{2k_x \epsilon_r \alpha_x}{h^2} . \quad (3.45)$$

### 3.8 Attenuation

Having completed the preliminaries, the attenuation can be evaluated.

The attenuation, power loss per unit length, in the z-direction is given by

$$\alpha = \frac{P_L}{2P} . \quad (3.46)$$

From (3.34) and (3.37), it follows that

$$\alpha = \frac{\tan(\delta) \{ 2k_x a k_0^2 \epsilon_r + [k_0^2(2 - \epsilon_r) + 2\alpha_x^2] \sin(2k_x a) \}}{4k_x k_z \left\{ \frac{1}{2k_x} [2k_x a + \sin(2k_x a)] + \frac{k_x^2 \sin^2(k_x a)}{\epsilon_0 \epsilon_r \alpha_x^3} \right\}} . \quad (3.47)$$

Using now the identities, (3.42) and (3.45), and multiplying numerator and denominator by  $h^2 \alpha_x$  yields

$$\alpha = \frac{\tan(\delta)\alpha_x \{ 2ak_0^2\epsilon_r h^2 + [k_0^2(2-\epsilon_r) + 2\alpha_x^2]2\epsilon_r\alpha_x \}}{4k_z \{ a\alpha_x h^2 + \alpha_x^2\epsilon_r + k_x^2\epsilon_r \}} . \quad (3.48)$$

Introducing (3.41) and simplifying,

$$\alpha = \frac{\tan(\delta) \{ k_0^2\epsilon_r\alpha_x[ah^2 + (2-\epsilon_r)\alpha_x] + 2\epsilon_r\alpha_x^4 \}}{2k_z \{ ah^2\alpha_x + k_0^2\epsilon_r(\epsilon_r-1) \}} . \quad (3.49)$$

The thickness,  $a$ , of the slab is given by (3.28). When this is combined with (3.41), it becomes

$$a = \frac{1}{\sqrt{k_0^2(\epsilon_r-1) - \alpha_x^2}} \tan^{-1} \left\{ \frac{\epsilon_r\alpha_x}{\sqrt{k_0^2(\epsilon_r-1) - \alpha_x^2}} \right\} , \quad (3.50)$$

defining  $p$ , the normalized decay in the  $x$ -direction as

$$p = \frac{\alpha_x}{k_0} .$$

Substitution of  $p$  into (3.50) and multiplying by  $h^2$  then specifies

$$ah^2 = \frac{k_0(\epsilon_r-1)[1 + p^2(\epsilon_r+1)]}{\sqrt{\epsilon_r - 1 - p^2}} \tan^{-1} \left\{ \frac{\epsilon_r p}{\sqrt{\epsilon_r - 1 - p^2}} \right\} , \quad (3.51)$$

after defining

$$H = \frac{(\epsilon_r-1)[1 + p^2(\epsilon_r+1)]}{\sqrt{\epsilon_r - 1 - p^2}} \tan^{-1} \left\{ \frac{\epsilon_r p}{\sqrt{\epsilon_r - 1 - p^2}} \right\} . \quad (3.52)$$

Equation (3.51) may be written

$$ah^2 = k_0 H , \quad (3.53)$$

noting that  $H$  depends on frequency only through  $p$ . The attenuation can now be written in terms of  $p$  and  $H$  by using (3.51) and (3.53);

$$\alpha = \frac{\tan(\delta)k_0}{2} \cdot \frac{\epsilon_r p [H + p(2 - \epsilon_r) + 2p^3]}{\sqrt{1 + p^2 [H_p + \epsilon_r(\epsilon_r + 1)]}} \quad (3.54)$$

$\alpha$  is now explicitly a function of  $H$ ,  $p$ ,  $\epsilon_r$ , and  $\tan(\delta)$  except for the linear  $k_0$  dependence.

### 3.9 Physical Parameter Values

It would now be useful to determine the numerical range of physically meaningful values for  $\alpha_x$  and  $p$ . Suppose it is desired that the fields decay to 100/M percent of the value at  $x = a$ , at a distance  $s\lambda_0$ , viz.,

$$e^{-\alpha_x s \lambda_0} = \frac{1}{M} ;$$

that is,

$$\alpha_x = \frac{\ln(M)}{s \lambda_0} \quad (3.55)$$

If the following conditions are desired:

$$M = 10 ,$$

$$s = 1.5 ,$$

and

$$\lambda_0 = 3 \times 10^{-2} \text{ meters (} f = 10 \text{ GHz) ,}$$

then

$$\alpha_x = 51 \frac{\text{neper}}{\text{meter}} \quad (3.56a)$$

or

$$p_{10} = 0.242 \frac{\text{neper}}{\text{radian}} , \quad (3.56b)$$

since

$$k_0 \approx 210 \frac{\text{radian}}{\text{meter}} \quad (3.56c)$$

Similarly for the same value of  $M$  and  $s$ , but for

$$\lambda_0 = .857 \times 10^{-2} \text{ meters } (f = 35 \text{ GHz}) ,$$

$$\alpha_x = 192 \frac{\text{neper}}{\text{meter}}$$

and

$$p_{as} = 0.0261 \frac{\text{neper}}{\text{meter}} . \quad (3.57)$$

Examination of (3.51) yields the possible range of  $\epsilon_r$  for a given  $\alpha_x$  as

$$\epsilon_r > p^2 + 1 .$$

### 3.10 Computer Program

#### 3.10.1 Introduction

Listed below is the computer program which was used to determine the attenuation of the infinite-dielectric surface wave guide; a flow chart, Figure 3.2, is also included. The normalized decay constant ( $p$ ), initial relative permittivity, frequency, and loss tangent are initially-fixed parameters. Relative permittivity is varied from the initial value to one hundred; attenuation and thickness are computed for each value of permittivity, all of which are printed.

A subroutine, GRAPH, is used to plot the results by utilization of a Calcomp Model 563 plotter in conjunction with an I.B.M. 360 series, Model 30 computer;<sup>1</sup> a flow chart can be seen in Figure 3.3. The language used for all of the programming was Basic FORTRAN IV.

The numerical results appear in Figures (3.4) through (3.7).

---

<sup>1</sup>Triangle Universities Computation Center, Research Triangle Park, Research Triangle, North Carolina.

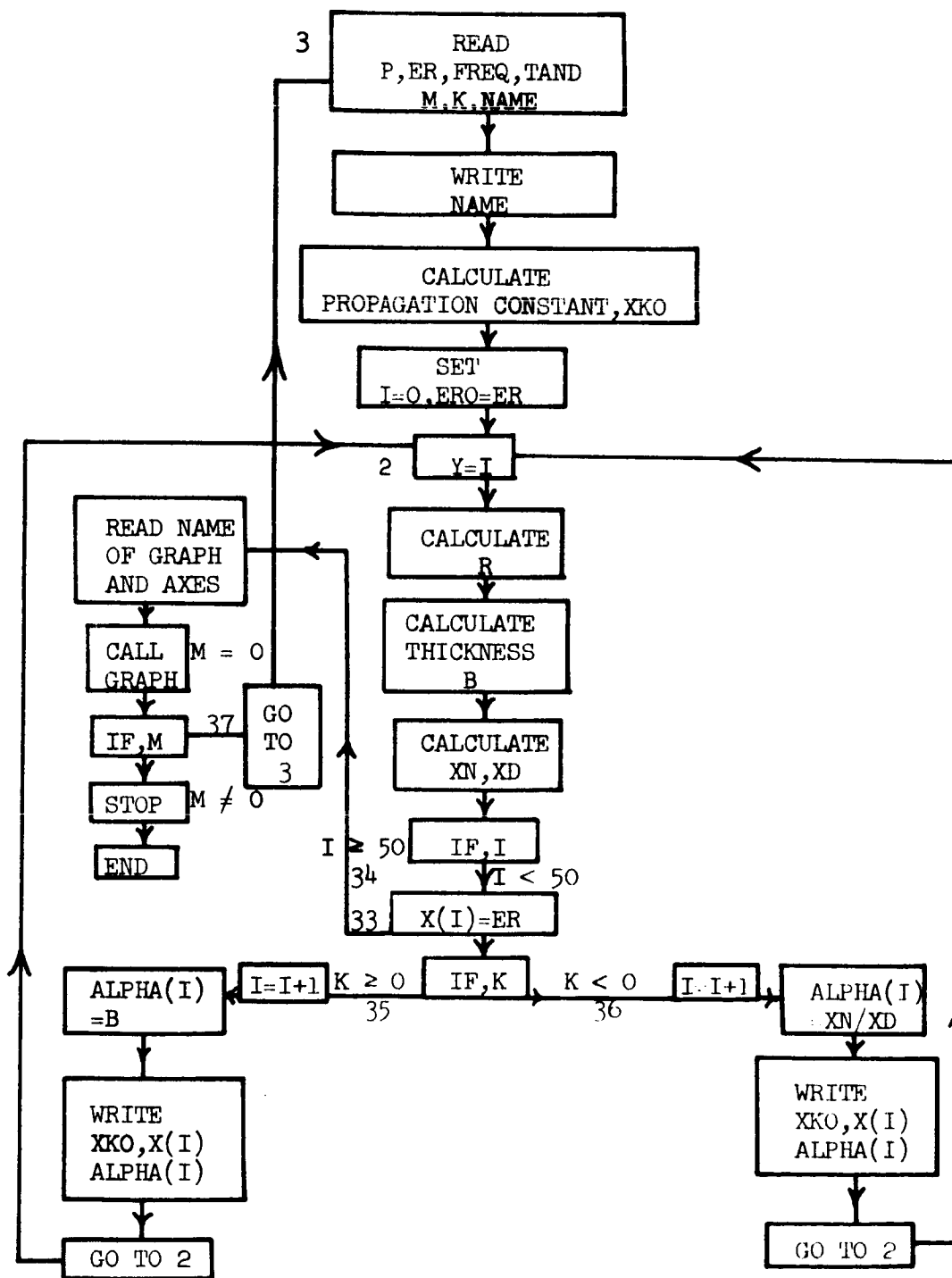


Figure 3.2 Flow chart for main program

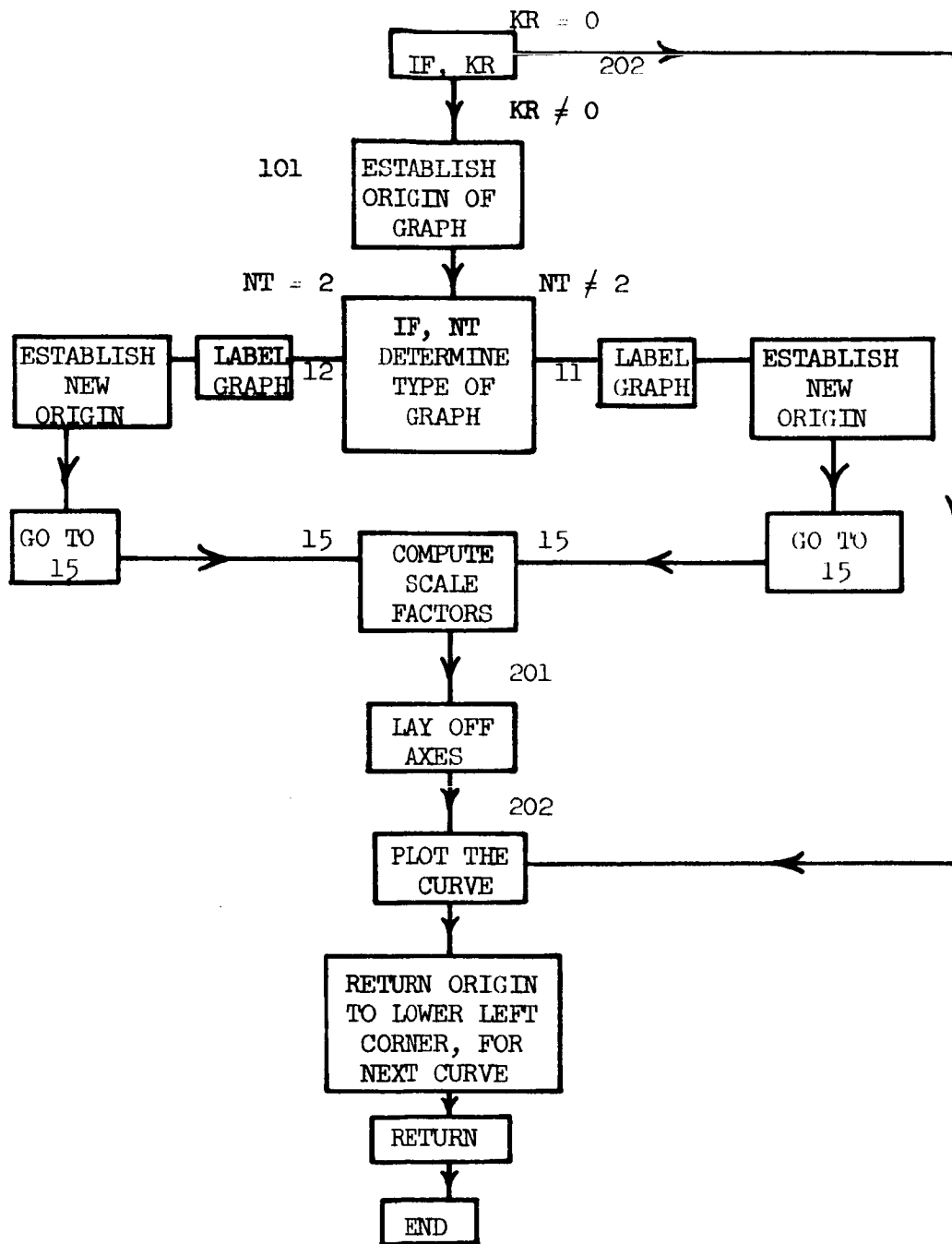


Figure 3.3 Flow chart for subroutine

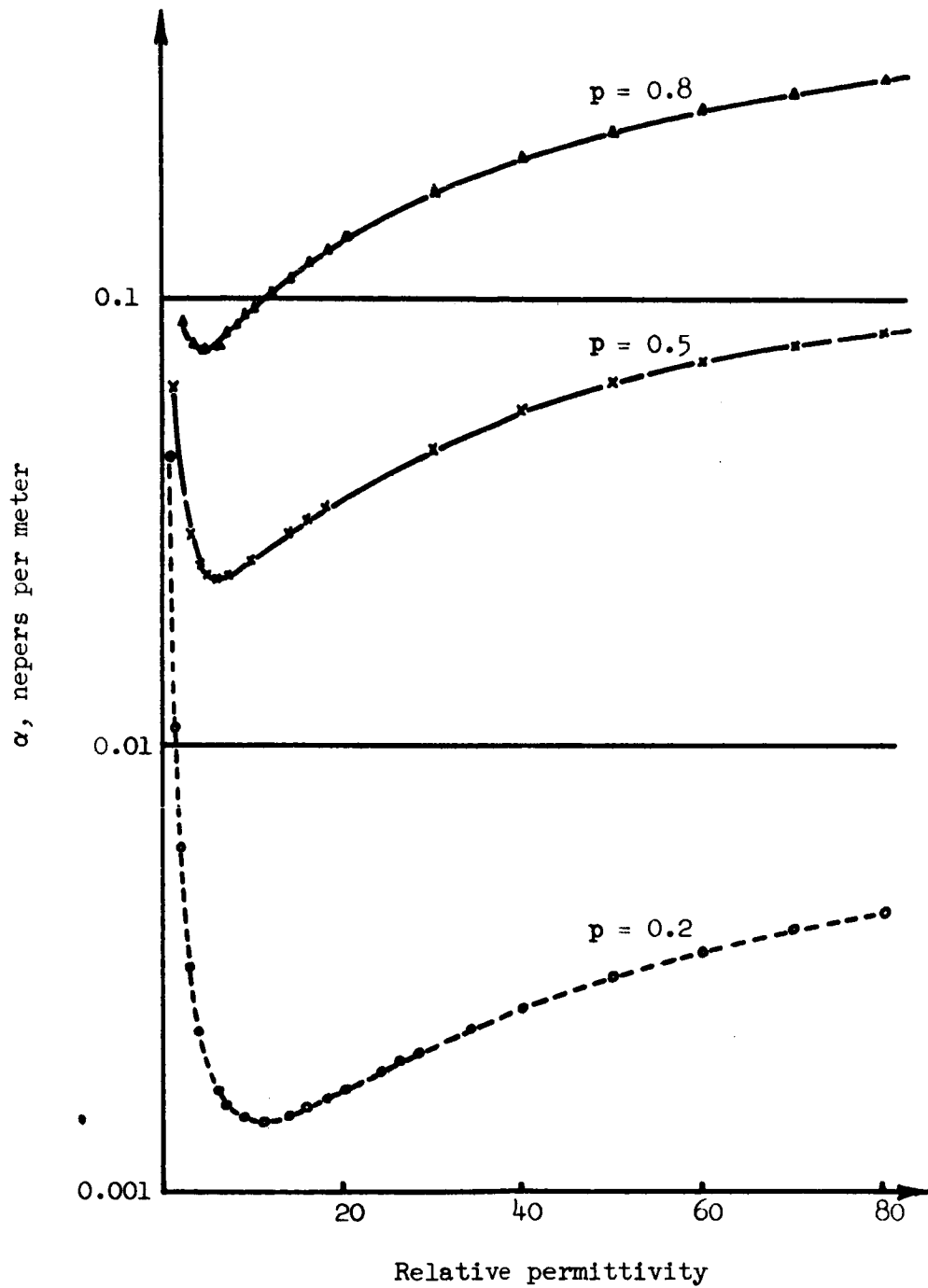


Figure 3.4 Attenuation of infinite dielectric slab at 10 GHz

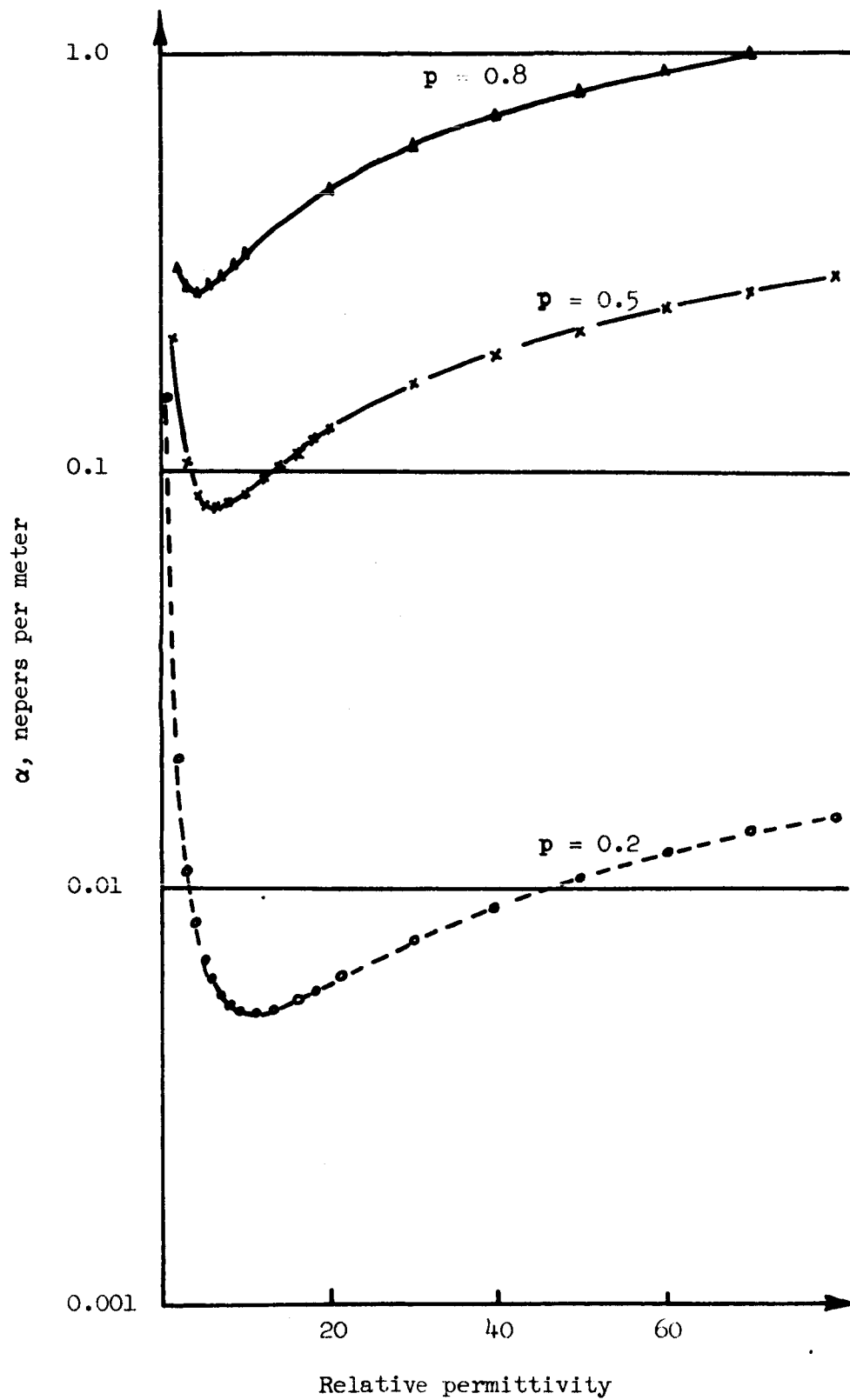


Figure 3.5 Attenuation of infinite dielectric slab at 35 GHz



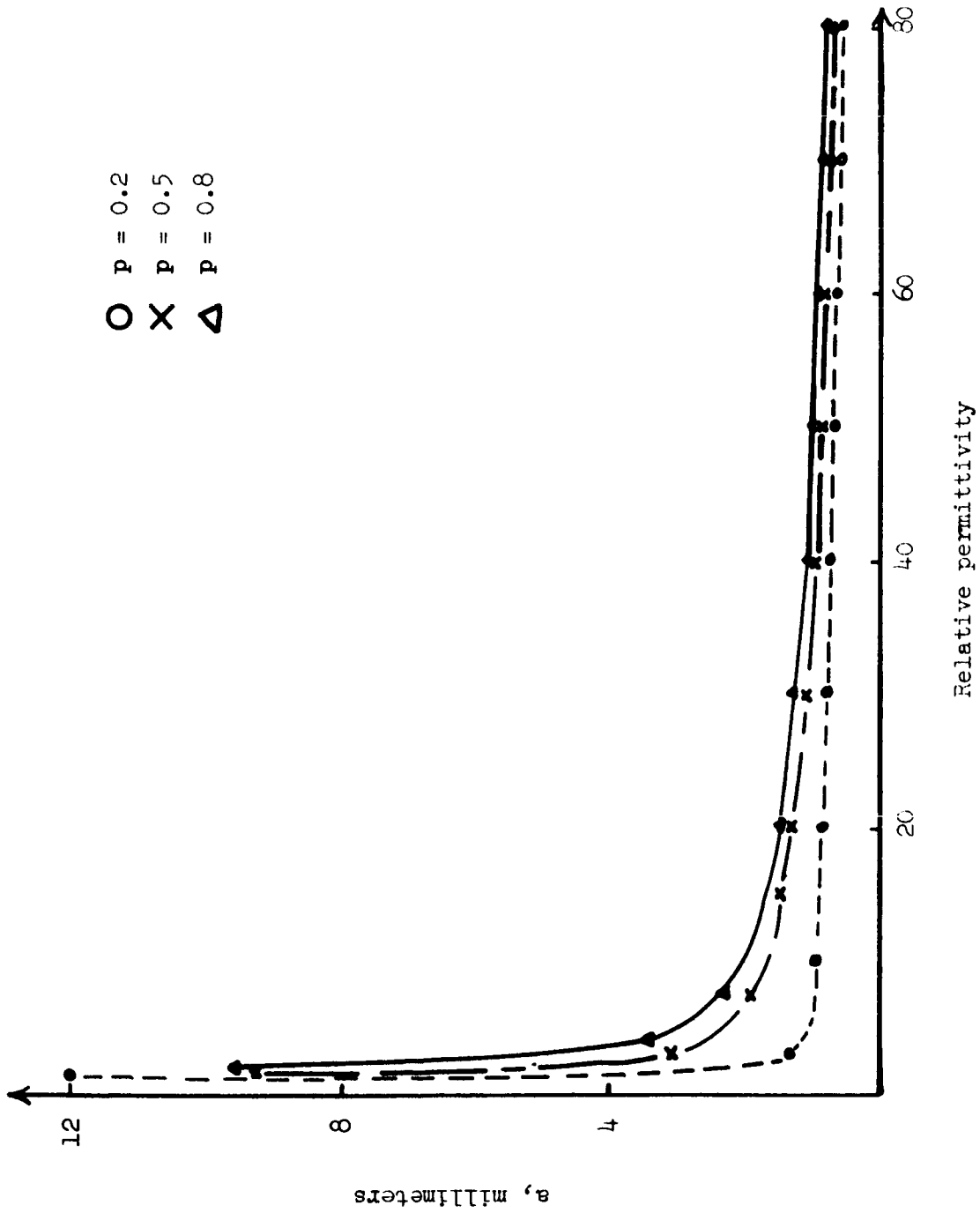


Figure 3.6 Thickness of infinite dielectric slab at 10 GHz

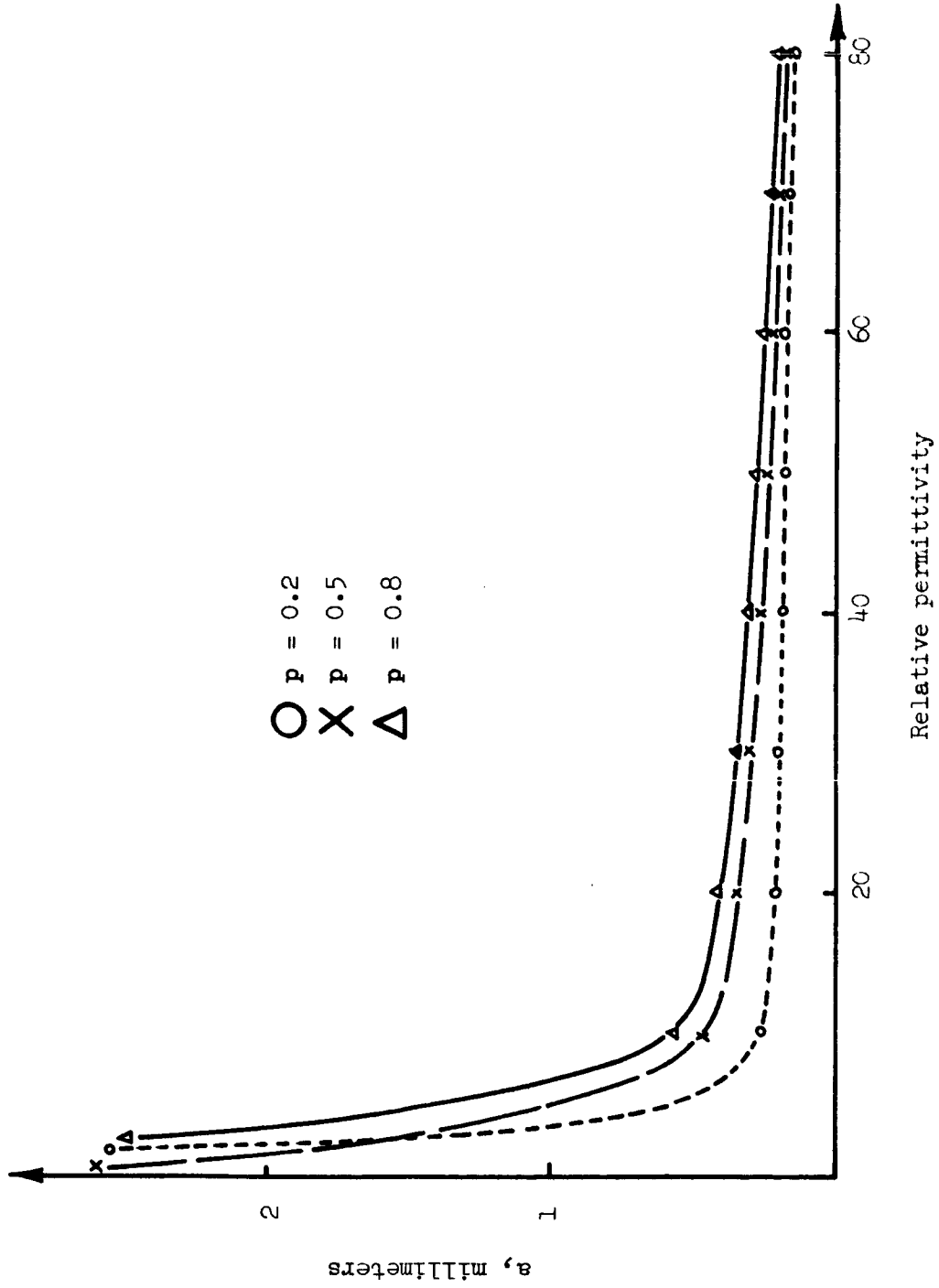


Figure 3.7 Thickness of infinite dielectric slab at 35 GHz

3.10.2 Main Program

```

C   X IS RELATIVE PERMITTIVITY
C   IF K=0  ALPHA IS THICKNESS
C   IF K=1  ALPHA IS ATTENUATION
C   TAND IS LOSS TANGENT
C   P IS NORMALIZED DECAY CONSTANT
C   NAME IS APPROPRIATE COLUMN NAME
C   DEPENDING ON VALUE OF K
C   EO IS FREE-SPACE PERMITTIVITY
C   XMO IS FREE-SPACE PERMEABILITY
C   XKOS IS PROP. CONSTANT SQUARED
C   XKO IS PROP. CONSTANT
C   B IS THICKNESS OF SLAB
C   ERO IS INITIAL PERMITTIVITY
DIMENSION X(55),ALPHA(55), WORK(210),ANAME(3)
3   READ(1,199)P,ER,FREQ,TAND,M,K,NAME
199  FORMAT(2F10.5,E15.8,E15.8,15,15,A12)
WRITE(3,306)NAME
306  FORMAT(1H1,'PROP. CONSTANT',1X,'RELATIVE EPSILON',3X,A12)
PI=3.14159
EO=(1.E-09)/(36.*PI)
XMO=(1.E-07)*4.*PI
XKOS=4.*PI*PI*FREQ*FREQ*XMO*EO
XKO=SQRT(XKOS)
I=0
ERO=ER
2   Y=I
ER=ERO+Y*Y*.04
Z=1./(XKO*SQRT(ER-1.-P*P))
B=7*ATAN(ER*P/SQRT(ER-1.-P*P))
H=B*XKO*(ER-1.)*(1.+P*P*P(ER+1.))
XN=TAND*ER*XKO*P*(H+P*(2.-ER)+2.*P*P*P)
XD=2.*SQRT(P*P+1.)*(H*P+ER*(ER-1.))
IF(I-50)33,34,34
33  X(I)=ER
IF(K-1)35,36,36
35  I=I+1
ALPHA(I)=B
WRITE(3,405)XKO,X(I),ALPHA(I)
405  FORMAT(1X,3E15.8)
GO TO 2
36  I=I+1
ALPHA(I)=XN/XD
WRITE(3,405)XKO,X(I),ALPHA(I)
GO TO 2
34  READ(1,20) ANAME(1),ANAME(2),ANAME(3)
20  FORMAT(3(A4,6X))
J=0
CALL GRAPH (X,ALPHA,WORK,50,ANAME,36,2,1,J)

```

```

CALL PLOT (0.,0.,999)
IF(M)38,37,38
37 GO TO 3
38 STOP
END

```

### 3.10.3 Subroutine

```

SUBROUTINE GRAPH(X,Y,WORK,N,ANAME,L,NT,KR,J)
C WORK IS A DUMMY MATRIX USED IN PLOTTER INSTRUCTIONS
C DIMENSION OF WORK IS DIMENSION OF X PLUS DIMENSION OF Y PLUS 100
C N IS NUMBER OF DATA POINTS
C ANAME(1) NAME OF GRAPH
C ANAME(2) NAME OF X-AXIS
C ANAME(3) NAME OF Y-AXIS
C X IS HORIZONTAL AXIS
C Y IS VERTICAL AXIS
C DIMENSION OF X IS N+2 DIMENSION OF Y IS N+2
C L IS THE DECIMAL INTEGER CODE INDICATING POINT SYMBOL USED
C NT=1 LONG AXIS VERTICAL IE Y-AXIS VERTICAL
C NT=2 LONG AXIS HORIZONTAL IE X-AXIS HORIZONTAL
C KR=0 PLOT CURVE ON SAME AXIS
C KR=1 DRAW NEW AXIS EACH TIME
C J=0 NO DATA POINTS OUTLINED
C J=1 DATA POINTS OUTLINED WITH CHARACTER TYPE L
C DUMMY DIMENSION STATEMENT SW, SH GET DUMMY INITIAL VALUES
C DIMENSION X(1),Y(1),WORK(1),ANAME(1)
C NBYTE=2*N+2
C SH=5.
C SW=5.
C ESTABLISH WORK AREA
C CALL PLOTS(WORK(1),NBYTE)
C IS THIS A REPEAT
C IF(KR)101,202,101
C IS THIS THE FIRST GRAPH. IF SO,ESTABLISH PEN LOCATION AND ORIGIN.
C FIND BOTTOM OF PAPER
101 CALL PLOT(0.,-11.,-3)
C ESTABLISH ORIGIN OF WORK AREA
C CALL PLOT(12.,.5,-3)
C AREA ORIGIN IS NOW ESTABLISHED
C DETERMINE TYPE GRAPH TO BE PLOTTED TYPE 1 HAS LONG AXIS VERTICAL,
C TYPE 2 HAS LONG AXIS HORIZONTAL.
C IF(NT-2) 11,12,11
C TYPE 1
C LABEL GRAPH NAME WITH .25 INCH LETTER LOWER LEFT CORNER 3.5,10.0
11 CALL SYMBOL(7.5,10.0,25,ANAME(1),0.,4)
C ESTABLISH NEW ORIGIN
C CALL PLOT(2.,.5,-3)
C SW=8.
C SH=10.
C GO TO 15

```

```
C   TYPE 2
    12 CALL SYMBOL(6.5,8.50,.25,ANAME(1),0.,4)
C   ESTABLISH NEW ORIGIN
    CALL PLOT(2.,1.,-3)
    SW=10.
    SH=8.
C   COMPUTE SCALE FACTORS
    15 CALL SCALE(X,SW,N,1,10.)
    CALL SCALE(Y,SH,N,1,10.)
C   LAY OFF AXES
    201 CALL AXIS(0.,0.,ANAME(2),-4,SW,0.,X(N=1),X(N+2),10.)
    CALL PLOT(0.,0.,3)
    CALL AXIS(0.,0.,ANAME(3),4,SH,90.,Y(N+1),Y(N+2),10.)
    CALL PLOT(0.,0.,3)
C   PLOT THE CURVE
    202 CALL LINE(X,Y,N,1,J,L)
    CALL PLOT(0.,0.,3)
C   CHECK FOR COMPLETION OF CURVE
C   RETURN ORIGIN TO LOWER LEFT ORIGIN OF WORK REGION
    IF(NT-2) 21,22,21
C   TYPE 1
    21 CALL PLOT(-2.,-.5,-3)
    RETURN
C   TYPE 2
    22 CALL PLOT(-2.,-1.,-3)
    RETURN
    END
```

## 4. ATTENUATION OF AN INFINITE CORRUGATED WAVE GUIDE

### 4.1 Introduction

The infinite corrugated wave guide, Figure 4.1, behaves much the same as the dielectric surface wave guide in that the field is confined to a region just above the corrugations; that is, the corrugations perform as an artificial dielectric.

The attenuation for the corrugated guide is to be calculated and compared with that of the dielectric guide; as a comparison criterion, the normalized decay constant,  $p$ , will be the same for both cases.

Here again, the same technique as in the dielectric case will be employed; namely, the problem will be solved under the assumption of symmetrical excitation, with a perfectly conducting plane passing through the center of the corrugated guide, which requires finding the field for  $x$ -positive, the other half being symmetrical. The field matching technique will be utilized, matching the field solution above the corrugations with that below at  $x = a$ .

### 4.2 Development of the Field in Terms of Longitudinal Components

The source-free, time-harmonic Maxwell equations are

$$\nabla \times \underline{E} = -j \omega \mu_0 \underline{H} \quad (4.1)$$

and

$$\nabla \times \underline{H} = j \omega \epsilon_0 \underline{E} , \quad (4.2)$$

which become, upon expansion in rectangular coordinates

$$\frac{\partial E_z}{\partial y} - \frac{\partial E_y}{\partial z} = -j \omega \mu_0 H_x , \quad (4.3)$$

$$\frac{\partial E_x}{\partial z} - \frac{\partial E_z}{\partial x} = -j \omega \mu_0 H_y , \quad (4.4)$$

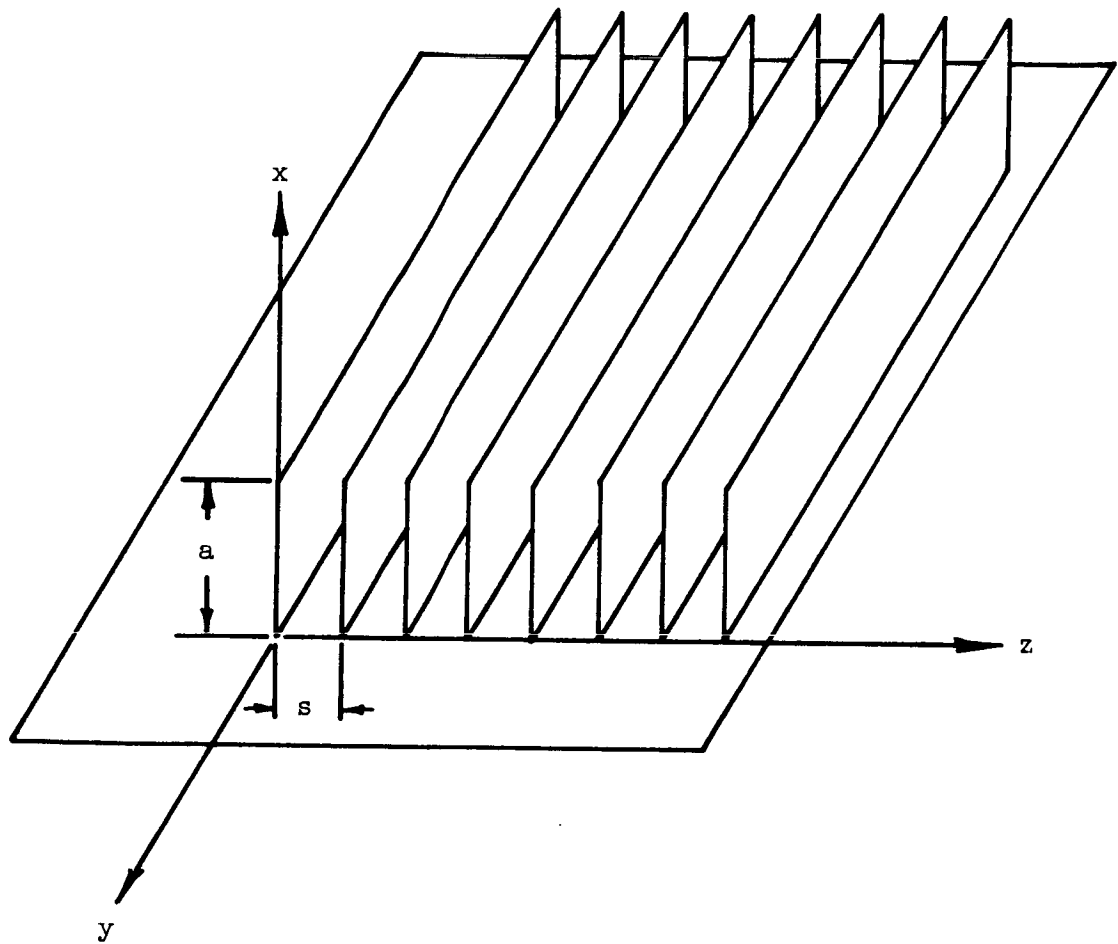


Figure 4.1 Infinite corrugated wave guide over perfectly conducting plane

$$\frac{\partial E_y}{\partial x} - \frac{\partial E_x}{\partial y} = -j \omega \mu_0 H_z, \quad (4.5)$$

$$\frac{\partial H_z}{\partial y} - \frac{\partial H_y}{\partial z} = +j \omega \epsilon_0 E_x, \quad (4.6)$$

$$\frac{\partial H_x}{\partial z} - \frac{\partial H_z}{\partial x} = +j \omega \epsilon_0 E_y, \quad (4.7)$$

and

$$\frac{\partial H_y}{\partial x} - \frac{\partial H_x}{\partial y} = +j \omega \epsilon_0 E_z. \quad (4.8)$$

For the case under consideration, the field may be separated into TE (Transverse Electric) and TM (Transverse Magnetic) modes. If now it is assumed that only TM modes are present and symmetry is considered, (4.3) through (4.8) become

$$H_z = 0, \quad (4.9)$$

$$\frac{\partial}{\partial y} = 0, \quad (4.10)$$

$$-\frac{\partial E_y}{\partial z} = -j \omega \mu_0 H_x, \quad (4.11)$$

$$\frac{\partial E_x}{\partial z} - \frac{\partial E_z}{\partial x} = -j \omega \mu_0 H_y, \quad (4.12)$$

$$\frac{\partial E_y}{\partial x} = 0, \quad (4.13)$$

$$-\frac{\partial H_y}{\partial z} = j \omega \epsilon_0 E_x, \quad (4.14)$$

$$\frac{\partial H_x}{\partial z} = j \omega \epsilon_0 E_y, \quad (4.15)$$



and

$$\frac{\partial H_y}{\partial x} = j \omega \epsilon_0 E_z . \quad (4.16)$$

#### 4.3 Solution for the Field Within the Corrugations

Boundary conditions require  $E_y = 0$  at  $x = a$ , but (4.13) specifies  $E_y$  to be independent of  $x$ ; it must therefore be concluded that

$$E_y = 0 \quad (4.17)$$

for all  $x$ . Equation (4.17) together with (4.11) now yield the further restriction

$$H_x = 0 . \quad (4.18)$$

The remaining field components, (4.12), (4.14), and (4.16), can now be written

$$\frac{\partial E_x}{\partial z} - \frac{\partial E_z}{\partial x} = - j \omega \mu_0 H_y , \quad (4.19)$$

$$E_x = \frac{j}{\omega \epsilon_0} \frac{\partial H_y}{\partial z} , \quad (4.20)$$

and

$$E_z = \frac{-j}{\omega \epsilon_0} \frac{\partial H_y}{\partial x} . \quad (4.21)$$

If now (4.19) through (4.21) are combined, a wave equation results; namely

$$\frac{\partial^2 H_y}{\partial x^2} + \frac{\partial^2 H_y}{\partial z^2} + k_0^2 H_y = 0 , \quad (4.22)$$

where

$$k_0^2 = \omega^2 \mu_0 \epsilon_0 . \quad (4.23)$$

In rectangular coordinates, variables may be separated, and (4.22) becomes

$$\frac{1}{X} \frac{\partial^2 X}{\partial x^2} + \frac{1}{Z} \frac{\partial^2 Z}{\partial z^2} + k_0^2 = 0 , \quad (4.24)$$

where

$$H_y = X(x) Z(z) .$$

Therefore, upon separation,

$$\frac{\partial^2 X}{\partial x^2} + k_x^2 X = 0 \quad (4.25)$$

and

$$\frac{\partial^2 Z}{\partial z^2} + k_z^2 Z = 0 , \quad (4.26)$$

where

$$k_x^2 + k_z^2 = k_0^2 . \quad (4.27)$$

Equations (4.25) and (4.26) yield solutions of the form

$$X = A_{xm} \cos(k_{xm} x) + B_{xm} \sin(k_{xm} x) \quad (4.28)$$

and

$$Z = A_{zn} \cos\left(\frac{n\pi}{s} z\right) + B_{zn} \sin\left(\frac{n\pi}{s} z\right) . \quad (4.29)$$

The total  $H_{ye}$  variation, the product of X and Z, must be

$$H_{ye} = \sum_{m=-\infty}^{\infty} [A_{xm} \cos(k_{xm} x) + B_{xm} \sin(k_{xm} x)] \\ \cdot \sum_{n=-\infty}^{\infty} [A_{zn} \cos\left(\frac{n\pi}{s} z\right) + B_{zn} \sin\left(\frac{n\pi}{s} z\right)] , \quad (4.30)$$

which reduces to

$$H_{ye} = \sum_{n=-\infty}^{\infty} [A_{xn} \cos(k_{xn}x) + B_{xn} \sin(k_{xn}x)] \cdot [A_{zn} \cos(\frac{n\pi}{s}z) + B_{zn} \sin(\frac{n\pi}{s}z)] , \quad (4.31)$$

since upon substitution of  $k_z = n\pi/s$  into (4.27) yields

$$k_{xm}^2 + (\frac{n\pi}{s})^2 = k_0^2 , \quad (4.32)$$

implying  $m = n$ ; therefore becoming

$$k_{xn}^2 + (\frac{n\pi}{s})^2 = k_0^2 . \quad (4.33)$$

In actuality, this requires each individual term of the series expansion for  $H_{ye}$  to satisfy the wave equation; however, this does not necessarily mean that each term (mode) must satisfy the boundary conditions stipulated by the Maxwell equations, since these boundary conditions need apply only to the total field. The boundary conditions are

$$E_{xe} = 0$$

for

$$z = i/s,$$

where

$$i = 0 , \pm 1 , \pm 2 , \dots$$

and

$$E_{ze} = 0$$

for

$$x = 0 .$$

If it is now assumed that the series describing  $H_{ye}$  is uniformly convergent, (4.20) and (4.21) together with (4.31) specify

$$\begin{aligned}
E_{x\epsilon} = & \frac{j}{\omega\epsilon_0} \sum_{n=-\infty}^{\infty} \left(\frac{n\pi}{s}\right) [A_{xn} \cos(k_{xn} x) + B_{xn} \sin(k_{xn} x)] \\
& \cdot [-A_{zn} \sin\left(\frac{n\pi}{s} z\right) + B_{zn} \cos\left(\frac{n\pi}{s} z\right)]
\end{aligned} \tag{4.34}$$

and

$$\begin{aligned}
E_{z\epsilon} = & \frac{-j}{\omega\epsilon_0} \sum_{n=-\infty}^{\infty} k_{xn} [-A_{xn} \sin(k_{xn} x) + B_{xn} \cos(k_{xn} x)] \\
& \cdot [A_{zn} \cos\left(\frac{n\pi}{s} z\right) + B_{zn} \sin\left(\frac{n\pi}{s} z\right)] .
\end{aligned} \tag{4.35}$$

Noting the boundary conditions have not, as yet, been enforced.

The uniform convergence is in fact true, since the series is actually a Fourier expansion of the field, and the field will be required to be continuous (Lanczos, 1966).

#### 4.4 Solution for the Field in the Region Above the Corrugations

In this region, as before, the same restrictions apply to the field, i.e.,

$$H_z = 0 , \tag{4.36}$$

$$\frac{\partial}{\partial y} = 0 , \tag{4.37}$$

$$E_y = 0 , \tag{4.38}$$

and

$$H_x = 0 , \tag{4.39}$$

yielding again, (4.19) through (4.23).

Surface wave propagation is desired, and by definition, this requires the field to decay with increasing distance normal to the wave guide (increasing  $x$ ). The following form for the  $x$ -variation is therefore imposed upon the field

$$X = \sum_{m=-\infty}^{\infty} a_m e^{-\alpha_{xm}x}, \quad (4.40)$$

which, of course, satisfies the wave equation

$$\frac{\partial^2 X_m}{\partial x^2} - \alpha_{xm}^2 X_m = 0, \quad (4.41)$$

$X_m$  being the  $m^{\text{th}}$  term of the series. Since the total field variation for  $H_y$  must satisfy (4.22), then the  $z$ -variation must satisfy

$$\frac{\partial^2 Z_m}{\partial z^2} + k_{zm}^2 Z_m = 0, \quad (4.42)$$

where

$$k_{zm}^2 = k_0^2 + \alpha_{xm}^2. \quad (4.43)$$

The periodicity of the structure in the  $z$ -direction requires the Floquet theorem (Collin, 1960) to be satisfied by the  $z$ -variation. That is, between any two points separated by a distance,  $s$ , the field differs only by a phase change; namely

$$Z(z+s) = Z(z) e^{-jk_{z0}s},$$

requiring

$$Z(z) = \varphi(z) e^{-jk_{z0}z},$$

where

$$\varphi(z+s) = \varphi(z).$$

Since this is true for  $\varphi(z)$ , then  $\varphi(z)$  may be expanded in Fourier series of period  $s$ ,

$$\varphi(z) = \sum_{m=-\infty}^{\infty} b_m e^{-j\left(\frac{2m\pi}{s}\right)z}.$$

It follows that the total z-variation must then be of the form

$$Z(z) = \sum_{m=-\infty}^{\infty} b_m e^{-jk_{zm}z}, \quad (4.44)$$

where

$$k_{zm} = k_{z0} + \frac{2m\pi}{s}. \quad (4.45)$$

This, with (4.40), specifies the total  $H_y$  variation as

$$H_y = \sum_{m=-\infty}^{\infty} H'_m e^{-\alpha_{xm}x} e^{-jk_{zm}z}. \quad (4.46)$$

Since, as before, there exist no "cross terms" where the series, (4.40) and (4.44), are multiplied because of (4.43). Equations (4.20) and (4.21) then yield with (4.46):

$$E_x = \frac{1}{\omega\epsilon_0} \sum_{m=-\infty}^{\infty} H'_m k_{zm} e^{-\alpha_{xm}x} e^{-jk_{zm}z} \quad (4.47)$$

and

$$E_z = \frac{j}{\omega\epsilon_0} \sum_{m=-\infty}^{\infty} H'_m \alpha_{xm} e^{-\alpha_{xm}x} e^{-jk_{zm}z}. \quad (4.48)$$

#### 4.5 Continuity of the Field at the Boundary

Requiring the tangential field components to be continuous at the boundary specifies

$$E_{z\epsilon} = E_z \quad (4.49)$$

and

$$H_{y\epsilon} = H_y \quad (4.50)$$

for  $x = a$ . This will yield two equations from which others may be generated by using the orthogonality property of the field components, from which all of

the unknown constants may be found. The results specifying exactly (as the chosen model permits) the field everywhere; however, the solution will be lengthy.

Alternatively, the corrugated regions may be considered as infinite parallel-plate wave guides which, for  $s < \lambda/2$ , would be cut-off for TE and TM modes, i.e., only allowing the TEM mode to propagate. For the TEM mode, it must be that  $E_x = 0$ , which occurs if

$$n = 0 , \quad (4.51)$$

reducing (4.31) and (4.35) to

$$H_{y\epsilon} = A_{x0} \cos(k_{x0}x) + B_{x0} \sin(k_{x0}x) \quad (4.52)$$

and

$$E_{z\epsilon} = \frac{-j}{\omega\epsilon_0} k_{x0} A_{z0} [-A_{x0} \sin(k_{x0}x) + B_{x0} \cos(k_{x0}x)] . \quad (4.53)$$

Boundary conditions require

$$B_{x0} = 0 . \quad (4.54)$$

Therefore, with (4.33), (4.52) and (4.53)

$$H_{y\epsilon} = H_0 \cos(k_{x0}x) \quad (4.55)$$

and

$$E_{z\epsilon} = j Z_0 H_0 \sin(k_{x0}x) , \quad (4.56)$$

where

$$H_0 = A_{x0} , \quad (4.57)$$

$$A_{z0} = 1 , \quad (4.58)$$

and

$$Z_0 = \sqrt{\mu_0/\epsilon_0} . \quad (4.59)$$

Tangential field components can now be matched using (4.49) and (4.50), yielding

$$H_0 \cos(k_0 a) = \sum_{m=-\infty}^{\infty} H'_m e^{-\alpha_{xm} a} e^{-jk_{zm} z} \quad (4.60)$$

and

$$k_0 H_0 \sin(k_0 a) = \sum_{m=-\infty}^{\infty} H'_m \alpha_{xm} e^{-\alpha_{xm} a} e^{-jk_{zm} z} . \quad (4.61)$$

By use of the orthogonality property of the harmonics forming the total field, (4.60) and (4.61) can be simplified. The procedure is as follows: multiply (4.60) and (4.61) by  $e^{jk_{zr} z}$ , integrate the resulting equations over the fundamental period,  $s$ , of the field, and note the right sides of the equations are zero if  $r$  is not equal to  $m$ . Upon setting  $r = m$ , the results are

$$H_0 \cos(k_0 a) \int_0^s e^{jk_{zm} z} dz = H'_m e^{-\alpha_{xm} a} s \quad (4.62)$$

and

$$k_0 H_0 \sin(k_0 a) \int_0^s e^{jk_{zm} z} dz = H'_m \alpha_{xm} e^{-\alpha_{xm} a} s , \quad (4.63)$$

the  $s$ , appearing in the right sides, resulting from the integration. If (4.62) is now divided by (4.63),

$$\alpha_{xm} = k_0 \tan(k_0 a) \quad (4.64)$$

results. This specifies that there is only a single value for  $m$ , i.e., only a single term in the series expansion for the field, since the right side of (4.64) is a constant. Equation (4.43) essentially declares this value of  $m$  to be zero since  $k_{zm}$  is a constant. After evaluation of the integrals, (4.62) through (4.64) become



$$H_0 \cos(k_0 a) \left[ \frac{e^{jk_{z0}s} - 1}{jk_{z0}} \right] = H'_0 e^{-\alpha_{x0} a} s, \quad (4.65)$$

$$k_0 H_0 \sin(k_0 a) \left[ \frac{e^{jk_{z0}s} - 1}{jk_{z0}} \right] = H'_0 \alpha_{x0} e^{-\alpha_{x0} a} s, \quad (4.66)$$

and

$$\alpha_{x0} = k_0 \tan(k_0 a). \quad (4.67)$$

The solution of (4.66), in terms of  $H_0$  explicitly, yields

$$H'_0 = \frac{k_0 H_0 \sin(k_0 a) e^{\alpha_{x0} a}}{\alpha_{x0} s} \left[ \frac{e^{jk_{z0}s} - 1}{jk_{z0}} \right]. \quad (4.68)$$

Equation (4.43) then stipulates

$$k_{z0} = k_0 \left[ \frac{1}{\cos(k_0 a)} \right]. \quad (4.69)$$

Now, substitution of (4.67) and (4.69) into (4.70) gives

$$H'_0 = \Phi H_0 [j - j e^{jk_{z0}s}], \quad (4.70)$$

where

$$\Phi = \frac{\cos^2(k_0 a) e^{\alpha_{x0} a}}{k_0 s}. \quad (4.71)$$

Expanding (4.70) yields

$$H'_0 = \Phi H_0 \{ \sin(k_{z0}s) + j[1 - \cos(k_{z0}s)] \} \quad (4.72)$$

and, therefore,

$$H_0^{*'} = \Phi H_0^* \{ \sin(k_{z0}s) - j[1 - \cos(k_{z0}s)] \}, \quad (4.73)$$

combining

$$H_0' H_0'^* = \frac{1}{4} H_0 H_0^* 2[1 - \cos(k_{z0}s)] , \quad (4.74)$$

which will later be useful in the calculation of the attenuation.

#### 4.6 Total Field, after TEM Mode Approximation

For  $0 \leq x \leq a$  ,

$$H_{ye} = H_0 \cos(k_0 x) \quad (4.56)$$

and

$$E_{ze} = j Z_0 H_0 \sin(k_0 x) . \quad (4.57)$$

For  $a \leq x < \infty$  ,

$$H_y = H_0' e^{-\alpha_{x0}x} e^{-jk_{z0}z} , \quad (4.75)$$

$$E_x = \frac{k_{z0} H_0'}{\omega \epsilon_0} e^{-\alpha_{x0}x} e^{-jk_{z0}z} , \quad (4.76)$$

and

$$E_z = \frac{j \alpha_{x0} H_0'}{\omega \epsilon_0} e^{-\alpha_{x0}x} e^{-jk_{z0}z} . \quad (4.77)$$

#### 4.7 Power Transport

The power is transported totally in the region above the corrugations, and is, from the Poynting identity, given by

$$P = \frac{1}{2} R_e \int_a^\infty \int_0^1 \underline{E} \times \underline{H}^* \cdot d\underline{s} \quad (4.78)$$

or

$$P' = \frac{1}{2} R_e \int_a^\infty \underline{E} \times \underline{H}^* \cdot d\underline{s} , \quad (4.79)$$

$P'$  being the power transported per unit width of guide. Substitution of (4.75) and (4.76) into (4.79) yields

$$P' = \frac{k_{z0}}{2\omega\epsilon_0} H_0' H_0^{*'} \int_a^\infty e^{-2\alpha_{x0}x} dx ; \quad (4.80)$$

now, performing the integration

$$P' = \frac{k_{z0} H_0' H_0^{*'}}{4\omega\epsilon_0\alpha_{x0}} e^{-2\alpha_{x0}a} . \quad (4.81)$$

#### 4.8 Power Loss

Power will be dissipated by the walls of the corrugations, since in actuality these will be nonperfect conductors. The power loss is given by

$$P_L = \frac{R_s}{2} \int_0^a |H_{ye}|^2 dx . \quad (4.82)$$

$P_L$  is only the power dissipated by one vertical wall in a single corrugation. There are, however, two walls per corrugation and  $\frac{1}{s}$  corrugations per meter. The total power dissipated per meter, is then

$$P_L' = \frac{R_s}{s} \int_0^a |H_{ye}|^2 dx . \quad (4.83)$$

With (4.56), it becomes

$$P_L' = \frac{R_s}{s} H_0 H_0^* \int_0^a \cos^2(k_0 x) dx . \quad (4.84)$$

Integrating yields

$$P_L' = \frac{R_s H_0 H_0^*}{4 s k_0} [2k_0 a + \sin(2k_0 a)] . \quad (4.85)$$

#### 4.9 Trigonometric Identities

Before the task of computing the attenuation is undertaken, the details can be greatly simplified by considering the following identities.

It will be advantageous to define a normalized decay constant,  $p$ , as

$$p = \frac{\alpha_{x0}}{k_0} . \quad (4.86)$$

Equation (4.43) then becomes

$$\frac{k_{z0}}{\alpha_{x0}} = \frac{\sqrt{1 + p^2}}{p} . \quad (4.87)$$

Consider

$$\sin(2k_0 a) = 2\sin(k_0 a)\cos(k_0 a) , \quad (4.88)$$

$$\sin(k_0 a) = \frac{1}{\sqrt{1 + \cot^2(k_0 a)}} , \quad (4.89)$$

and

$$\cos(k_0 a) = \frac{1}{\sqrt{1 + \tan^2(k_0 a)}} . \quad (4.90)$$

Equation (4.64) then yields

$$\tan(k_0 a) = p . \quad (4.91)$$

Equations (4.88) through (4.91) become

$$\sin(k_0 a) = \frac{p}{\sqrt{p^2 + 1}} , \quad (4.92)$$

$$\cos(k_0 a) = \frac{1}{\sqrt{p^2 + 1}} , \quad (4.93)$$

and

$$\sin(2k_0 a) = \frac{2p}{1 + p^2} . \quad (4.94)$$

The attenuation may now be computed.

#### 4.10 Attenuation

The attenuation,  $\alpha$ , is defined as the average power loss per unit length of wave guide, which means

$$\alpha = \frac{P'_L}{2P'} . \quad (4.95)$$

Using (4.81) and (4.85), this becomes

$$\alpha = \frac{R_s H_0 H_0^* [2k_0 a + \sin(2k_0 a)] 4\omega \epsilon_0 \alpha_{x0}}{2.4 s k_0 k_{z0} H_0 H_0^* e^{-2\alpha_{x0} a}} . \quad (4.96)$$

Substitution of (4.71), (4.74), and (4.87) into (4.96) will remove the  $H_0$  and  $H_0^*$  dependency and simplify the attenuation as

$$\alpha = \frac{R_s k_0 \omega \epsilon_0 p s (2k_0 a + \sin 2k_0 a)}{4 \cos^4 k_0 a \sqrt{1 + p^2} [1 - \cos(k_{z0} s)]} . \quad (4.97)$$

The previously developed trigonometric identities, (4.93) and (4.94), may now be used

$$\alpha = \frac{R_s k_0 \omega \epsilon_0 p s (1 + p^2)^{3/2} (2k_0 a + \frac{2p}{1 + p^2})}{4 [1 - \cos(k_{z0} s)]} . \quad (4.98)$$

Introducing for  $a$ , (4.91) and simplifying,

$$\alpha = \frac{R_s k_0 \omega \epsilon_0 p s [2(1 + p^2)^{3/2} \tan^{-1}(p) + 2p \sqrt{1 + p^2}]}{4 [1 - \cos(k_{z0} s)]} . \quad (4.99)$$

Using  $k_{z0}$  from (4.43), then expressing this in terms of  $p$ , yields

$$k_{z0} = k_0 \sqrt{1 + p^2} . \quad (4.100)$$

Using this,  $\alpha$  at last becomes

$$\alpha = \frac{R_s k_0 \omega \epsilon_0 p s [2(1+p^2)^{3/2} \tan^{-1}(p) + 2p \sqrt{1+p^2}]}{4 [1 - \cos(k_0 \sqrt{1+p^2} s)]} . \quad (4.101)$$

It would be expected that the attenuation would become quite large as  $s$  becomes small, since the number of corrugations per meter increases, hence, increasing the losses. This can be observed if the Maclaurin expansion for the cosine is considered. For small  $s$ ,

$$\cos(k_0 \sqrt{1+p^2} s) \approx 1 - \frac{k_0^2 (1+p^2) s^2}{2} . \quad (4.102)$$

The attenuation is now given by

$$\alpha = \frac{R_s \omega \epsilon_0 p \left[ 2(1+p^2)^{\frac{1}{2}} \tan^{-1}(p) + 2 \left( \frac{1}{p \sqrt{1+p^2}} \right) \right]}{k_0 s} , \quad (4.103)$$

which, as expected, does increase as  $s$  decreases.

#### 4.11 Computer Program

##### 4.11.1 Introduction

A computer program, written in Basic FORTRAN IV, appears below, along with a flow chart in Figure 4.2. The normalized decay constant ( $p$ ), frequency and loss tangent are input parameters. The spacing of the corrugations ( $s$ ) is varied; height of corrugations ( $a$ ) and attenuation ( $\alpha$ ) are output variables.

The results of the numerical calculation are given in Figures 4.3 and 4.4.

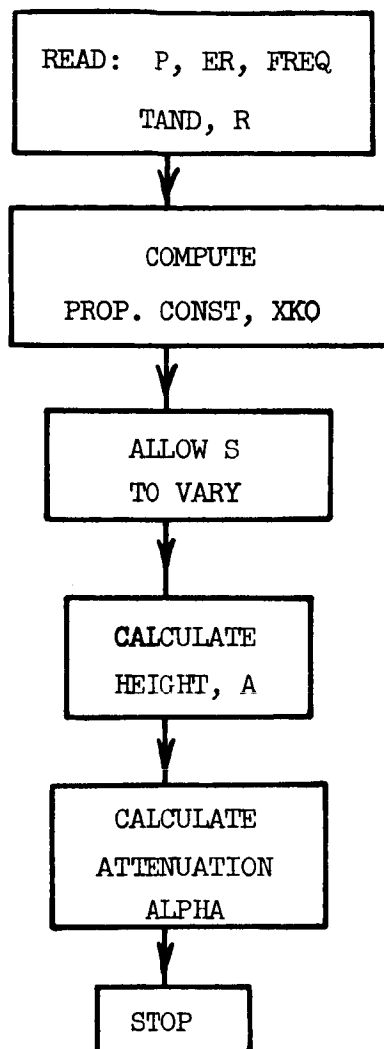


Figure 4.2 Flow chart for program

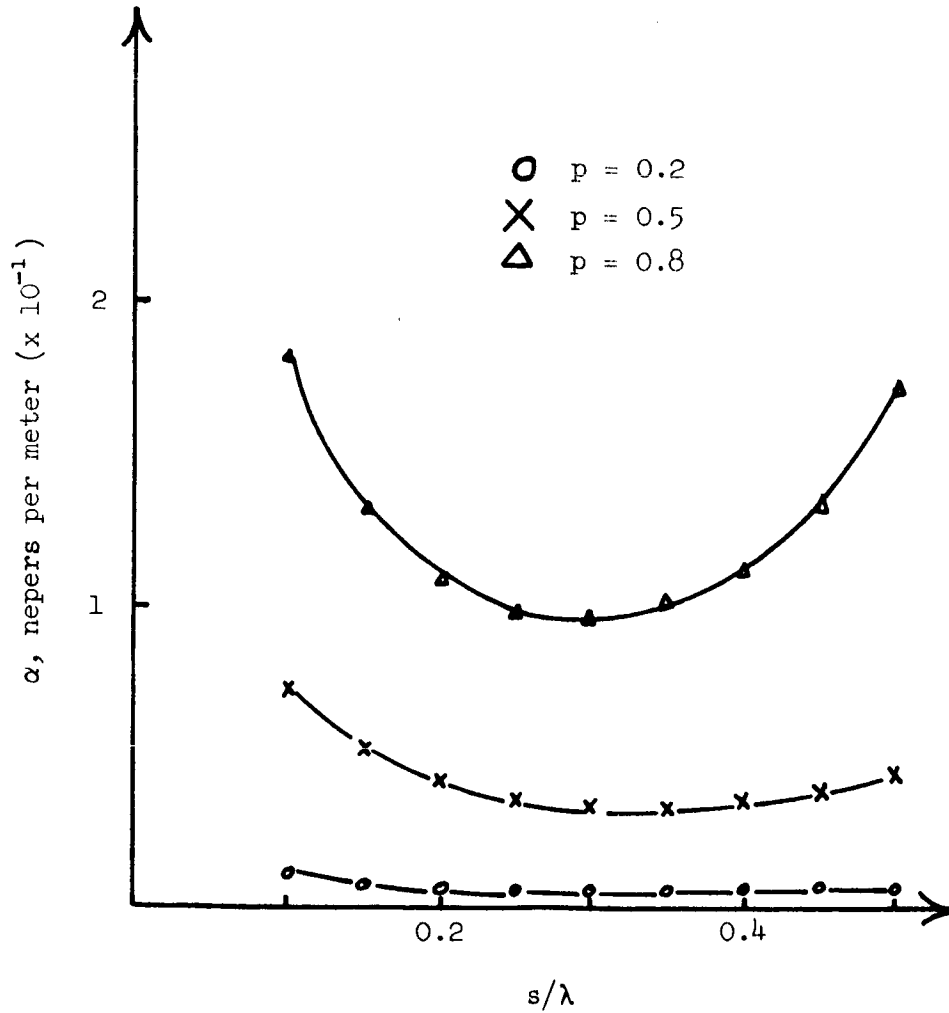


Figure 4.3 Attenuation of infinite corrugated wave guide at 35 GHz



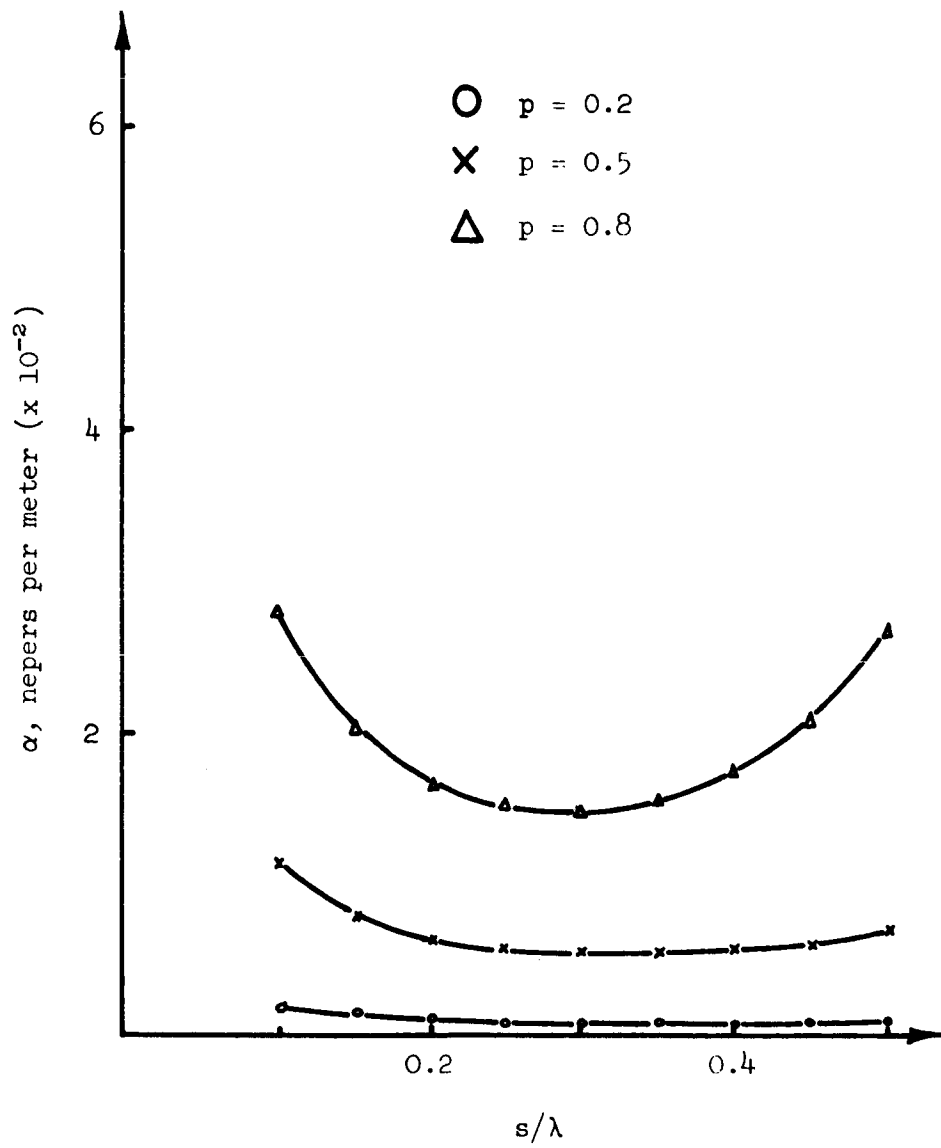


Figure 4.4 Attenuation of infinite corrugated wave guide at 10GHz

4.11.2 Computer Program

```

      DIMENSION X(55),A(55),ALPHA(55)
3    READ(1,199)P,ER,FREQ,TAND,M,K,R
199  FORMAT(2F10.5,E15.8,E15.8,15,15,F10.5)
      WRITE(3,404)P,ER,FREQ,TAND,M,K,R
404  FORMAT(1X,4E15.8,15,15,F10.5)
      WRITE(3,105)
105  FORMAT('1',4X,'SEPARATION',8X,'HEIGHT',8X,'ATTENUATION',4X,'PROP.'
      $,'CONSTANT')
      PI=3.14159
      EO=(1.E-09)/(36.*PI)
      XMO=(1.E-07)*4.*PI
      XKOS=4.*PI*PI*FREQ*FREQ*XMO*EO
      XKO=SQRT(XKOS)
      DO 88 I=1,50
      Q=I
      Y=Q*.01
      XL=(.3E+09)/FREQ
      S=(.09+Y)*XL
      B=(1./XKO)*ATAN(P)
      Z=2.*XKO*B*(1.+P*P)*SQRT(1.+P*P) +2.*P*SQRT(1.+P*P)
      XN=R*XKO*2.*PI*FREQ*EO*P*S*Z
      XD=4.*(1.-COS(XKO*SQRT(1.+P*P)*S))
      X(I)=S
      A(I)=B
      ALPHA(I)=XN/XD
88   WRITE(3,100)X(I),A(I),ALPHA(I),XKOS
100  FORMAT(1X,4E16.8)
      STOP
      END

```

4.11.3 Identification of Program Variables

A IS HEIGHT OF CORRUGATIONS  
 ALPHA IS ATTENUATION  
 P IS NORMALIZED DECAY CONSTANT

DEFINED P=ALPHA/XKO

FREQ IS FREQUENCY  
 TAND IS LOSS TANGENT  
 ER, M AND K ARE NOT USED  
 R IS SURFACE RESISTANCE  
 XMO IS FREE SPACE PERMEABILITY  
 XKO IS PROPAGATION CONSTANT OF FREE SPACE

## 5. DIELECTRIC H-GUIDE

### 5.1 Description of Structure

The structure considered is that of a H-guide utilizing a dielectric slab for the center section (Figure 5.1). The dielectric slab has dimensions  $2a$  by  $b$ . The sidewalls are assumed to be large enough in the  $x$ -direction such that the field components are essentially zero at  $x = h$ , and therefore may be considered unbounded in the field analysis.

### 5.2 Introduction

The dielectric H-guide is examined analytically by employing the field matching technique. Upon matching the field components, it was found that the  $H_x$  component vanishes, implying the longitudinal wall currents are zero. Attenuation is found for the guide and plotted as a function of relative permittivity for various values of  $p$ ; the normalized  $x$ -decay constant, defined  $p = \alpha_x/k$ ,  $\alpha_x$ , being the  $x$ -decay constant.

### 5.3 Method of Solution

To facilitate the solution, that portion of the guide for  $x \geq 0$  may be considered alone, if a perfect electrically conducting plane is placed at  $x = 0$ , and removed later. Generally applicable expressions for the field are found; one set useful above the dielectric and another within. The field matching technique is employed to assure continuity of tangential (it may also happen normal) field components at the boundary  $x = a$ . The field now having been completely specified, the conducting plane may be removed and a symmetrical portion of guide revealed in the region, where  $x < 0$ , as predicted by the method of images. Excitation must be forced to meet the symmetry requirements imposed by this technique.

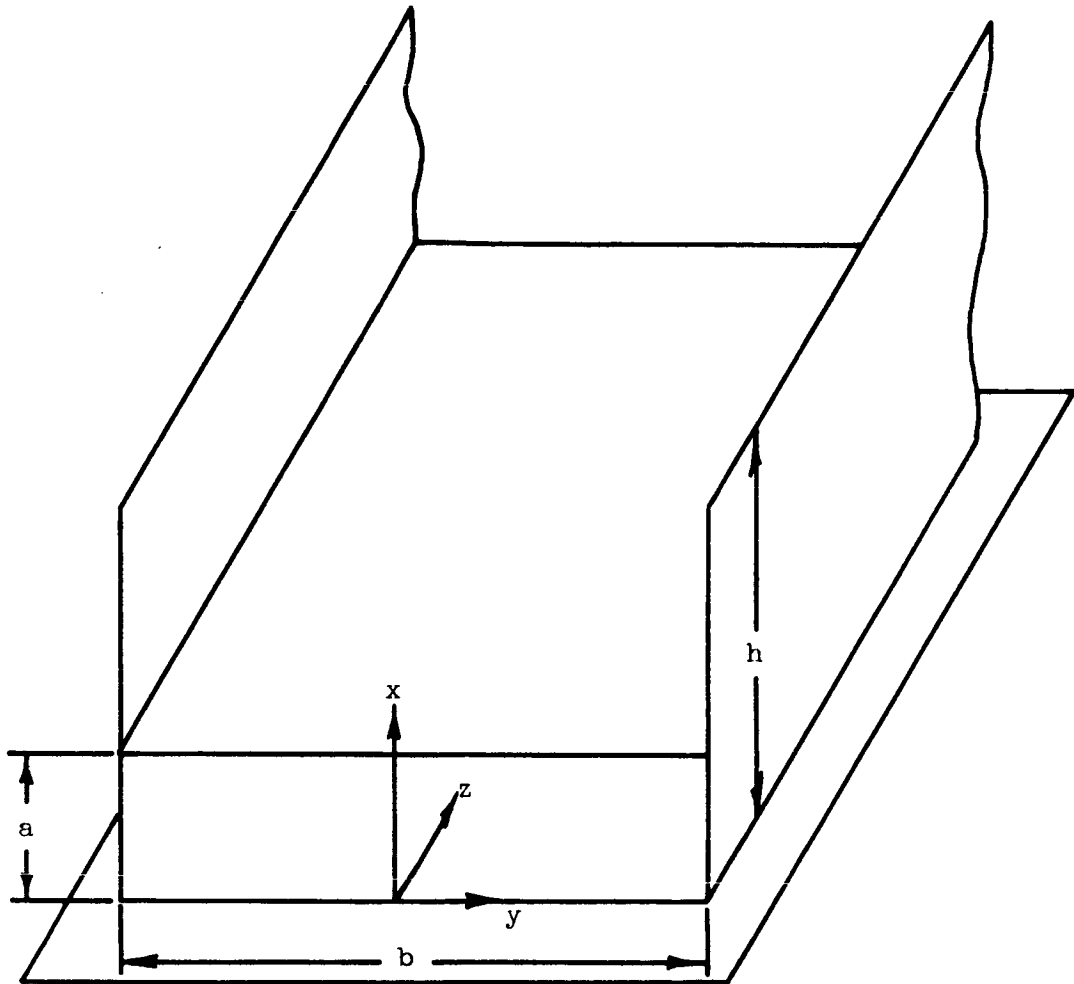


Figure 5.1 Dielectric H-guide on perfectly conducting plane

It should be noted that the above considers only one-half of the total solution to the problem; that is, there also exists a set of field components which would arise from placing a perfect magnetically conducting plane at the center of the wave guide. In this case, the tangential magnetic field would be zero at the center rather than the electric; the electric being a maximum in this case. These two types of solutions are sometimes denoted the even and odd modes, depending on whether the transverse magnetic field is odd or even with respect to the center of the wave guide.

#### 5.4 Development of a Wave Equation

The total field in a linear, isotropic, homogeneous region free of sources, must satisfy the Maxwell equations, which are, under the assumption of sinusoidal time variation

$$\nabla \times \underline{E} = -j \omega \mu \underline{H} , \quad (5.1)$$

$$\nabla \times \underline{H} = j \omega \epsilon \underline{E} , \quad (5.2)$$

$$\nabla \cdot \underline{E} = 0 , \quad (5.3)$$

and

$$\nabla \cdot \underline{H} = 0 . \quad (5.4)$$

Applying the curl operator to (5.1) and using (5.2) and (5.3), a wave equation for  $\underline{E}$  is obtained that is

$$\nabla^2 \underline{E} + k^2 \underline{E} = 0 , \quad (5.5)$$

where

$$k^2 = \omega^2 \mu \epsilon . \quad (5.6)$$

Similarly, a wave equation for  $\underline{H}$  may be obtained, which is

$$\nabla^2 \underline{H} + k^2 \underline{H} = 0 . \quad (5.7)$$

In the case of rectangular coordinates, any one of the six field components, denoted  $f(x,y,z)$ , can be seen to satisfy

$$\frac{\partial^2 f(x,y,z)}{\partial x^2} + \frac{\partial^2 f(x,y,z)}{\partial y^2} + \frac{\partial^2 f(x,y,z)}{\partial z^2} + k^2 f(x,y,z) = 0 . \quad (5.8)$$

It follows that by knowing any two field components, two E-components, or two H-components, a third component can be found from either (5.3) or (5.4), specifying completely either E or H. The remaining three unknown components can be found from either (5.1) or (5.2).

Solutions of (5.8) must now be found for two field components.

### 5.5 The Field Within the Dielectric

The choice of components which satisfy (5.8) is arbitrary;  $E_x$  and  $E_y$  will therefore be chosen. Before the choice is made, it will be assumed that since the H-guide will be excited by a  $TE_{10}$  field within a rectangular wave guide, then only a single half-sinusoidal variation will be present in the y-direction. The tangential E components will be required to be zero, as specified by the Maxwell equations at the boundary of a perfect conductor. Under these requirements,  $E_x$  and  $E_y$  have the form

$$E_{x\epsilon} = A_\epsilon [\cos(k_x x) + C_\epsilon \sin(k_x x)] \cos(k_y y) e^{-jk_z z} \quad (5.9)$$

and

$$E_{y\epsilon} = B_\epsilon \sin(k_x x) [\sin(k_y y) + D_\epsilon \cos(k_y y)] e^{-jk_z z} . \quad (5.10)$$

Now, by using (5.3), the third component must be

$$E_{z\epsilon} = - \int \left( \frac{\partial E_x}{\partial x} + \frac{\partial E_y}{\partial y} \right) dz + C_1 ,$$

which becomes upon substitution from (5.9) and (5.10):

$$E_{z\epsilon} = - \int \{ A_{\epsilon} k_x [-\sin(k_x x) + C_{\epsilon} \cos(k_x x)] \cos(k_y y) \\ + B_{\epsilon} k_y \sin(k_x x) [\cos(k_y y) - D_{\epsilon} \sin(k_y y)] \} e^{-jk_z z} dz ,$$

becoming, after simplification and integration,

$$E_{z\epsilon} = - (-A_{\epsilon} k_x + B_{\epsilon} k_y) \sin(k_x x) \cos(k_y y) \frac{e^{-jk_z z}}{-jk_z} ,$$

if the possibility of a static solution is eliminated. It will be convenient to redefine the constants  $A_{\epsilon}$  and  $B_{\epsilon}$  as

$$A_{\epsilon} \rightarrow A_{\epsilon} k_z$$

and

$$B_{\epsilon} \rightarrow B_{\epsilon} k_z .$$

The total  $\underline{E}$  component of the field now becomes

$$E_{x\epsilon} = A_{\epsilon} k_z \cos(k_x x) \cos(k_y y) e^{-jk_z z} , \quad (5.11)$$

$$E_{y\epsilon} = B_{\epsilon} k_z \sin(k_x x) \sin(k_y y) e^{-jk_z z} , \quad (5.12)$$

$$E_{z\epsilon} = j(A_{\epsilon} k_x - B_{\epsilon} k_y) \sin(k_x x) \cos(k_y y) e^{-jk_z z} , \quad (5.13)$$

$$k_x^2 + k_y^2 + k_z^2 = \epsilon_r k_0^2 , \quad (5.14)$$

$$k_y = \frac{\pi}{b} , \quad (5.15)$$

and

$$k_0^2 = \omega^2 \mu_0 \epsilon_0 . \quad (5.16)$$

The magnetic portion of the field may be found from (5.1) with the aid of (5.11) through (5.13); it is therefore given by

$$H_{xe} = \frac{j}{\omega\mu} \left[ -j(A_{\epsilon} k_x - B_{\epsilon} k_y) k_y \sin(k_x x) \sin(k_y y) e^{-jk_z z} \right. \\ \left. + jk_z B_{\epsilon} k_z \sin(k_x x) \sin(k_y y) e^{-jk_z z} \right],$$

$$H_{ye} = \frac{j}{\omega\mu} \left[ -jA_{\epsilon} k_z^2 \cos(k_x x) \cos(k_y y) e^{-jk_z z} \right. \\ \left. - jk_x (A_{\epsilon} k_x - B_{\epsilon} k_y) \cos(k_x x) \cos(k_y y) e^{-jk_z z} \right],$$

and

$$H_{ze} = \frac{j}{\omega\mu} \left[ k_x k_z B_{\epsilon} \cos(k_x x) \sin(k_y y) e^{-jk_z z} \right. \\ \left. + A_{\epsilon} k_z k_y \cos(k_x x) \sin(k_y y) e^{-jk_z z} \right],$$

which become after simplification

$$H_{xe} = \frac{1}{\omega\mu} \left[ (A_{\epsilon} k_x - B_{\epsilon} k_y) k_y - k_z^2 B_{\epsilon} \right] \sin(k_x x) \sin(k_y y) e^{-jk_z z}, \quad (5.17)$$

$$H_{ye} = \frac{1}{\omega\mu} \left[ (A_{\epsilon} k_x - B_{\epsilon} k_y) k_x + k_z^2 A_{\epsilon} \right] \cos(k_x x) \cos(k_y y) e^{-jk_z z}, \quad (5.18)$$

and

$$H_{ze} = \frac{j}{\omega\mu} \left[ (A_{\epsilon} k_y + B_{\epsilon} k_x) k_z \right] \cos(k_x x) \sin(k_y y) e^{-jk_z z}. \quad (5.19)$$



### 5.6 The Field Above the Dielectric

In the same manner, as for the field within the dielectric,  $E_x$  and  $E_y$  will be chosen for the field above; they become, after enforcing the boundary conditions,

$$E_x = A e^{-\alpha_x x} \cos(k_y y) e^{-jk_z z} \quad (5.20)$$

and

$$E_y = B e^{-\alpha_x x} [\sin(k_y y) + C \cos(k_y y)] e^{-jk_z z}; \quad (5.21)$$

and again, (5.3) yields  $E_z$  to be

$$E_z = - \int \left\{ -A \alpha_x e^{-\alpha_x x} \cos(k_y y) e^{-jk_z z} + B k_y e^{-\alpha_x x} [\cos(k_y y) - C \sin(k_y y)] e^{-jk_z z} \right\},$$

which becomes upon simplification,

$$E_z = - [-A \alpha_x + B k_y] \cos(k_y y) e^{-\alpha_x x} \frac{e^{-jk_z z}}{-jk_z}. \quad (5.22)$$

Again, redefining the constants, A and B, as

$$A \rightarrow A k_z$$

and

$$B \rightarrow B k_z,$$

(5.20) through (5.22) become respectively

$$E_x = A k_z e^{-\alpha_x x} \cos(k_y y) e^{-jk_z z}, \quad (5.23)$$

$$E_y = B k_z e^{-\alpha_x x} \sin(k_y y) e^{-jk_z z}, \quad (5.24)$$

and

$$E_z = j[A \alpha_x - B k_y] e^{-\alpha_x x} \cos(k_y y) e^{-jk_z z}. \quad (5.25)$$

Equation (5.1) along with (5.23) through (5.25) now specify the magnetic portion of the field as

$$H_x = \frac{j}{\omega \mu} \left[ -k_y j(A \alpha_x - B k_y) e^{-\alpha_x x} \sin(k_y y) e^{-jk_z z} + jk_z^2 B e^{-\alpha_x x} \sin(k_y y) e^{-jk_z z} \right],$$

$$H_y = \frac{j}{\omega \mu} \left[ -jk_z^2 A e^{-\alpha_x x} \cos(k_y y) e^{-jk_z z} + \alpha_x j(A \alpha_x - B k_y) e^{-\alpha_x x} \cos(k_y y) e^{-jk_z z} \right],$$

and

$$H_z = \frac{j}{\omega \mu} \left[ -\alpha_x B k_z e^{-\alpha_x x} \sin(k_y y) e^{-jk_z z} + k_y A k_z e^{-\alpha_x x} \sin(k_y y) e^{-jk_z z} \right],$$

which become after simplification

$$H_x = \frac{1}{\omega \mu} \left[ (A \alpha_x - B k_y) k_y - k_z^2 B \right] e^{-\alpha_x x} \sin(k_y y) e^{-jk_z z}, \quad (5.26)$$

$$H_y = \frac{1}{\omega \mu} \left[ k_z^2 A - \alpha_x (A \alpha_x - B k_y) \right] e^{-\alpha_x x} \cos(k_y y) e^{-jk_z z}, \quad (5.27)$$

$$H_z = \frac{j}{\omega\mu} [(A k_y - B \alpha_x) k_z] e^{-\alpha_x x} \sin(k_y y) e^{-jk_z z}, \quad (5.28)$$

and

$$k_0^2 = -\alpha_x^2 + k_y^2 + k_z^2. \quad (5.29)$$

### 5.7 Field Matching

All of the field components will be matched at the boundary,  $x = a$ .

Equations (5.11) and (5.23) yield for  $E_x$

$$\epsilon_0 \epsilon_r A \cos(k_x a) = \epsilon_0 A e^{-\alpha_x a}; \quad (5.30)$$

(5.12) and (5.24) yield for  $E_y$

$$B \sin(k_x a) = B e^{-\alpha_x a}; \quad (5.31)$$

(5.13) and (5.25) yield for  $E_z$

$$(A \epsilon k_x - B \epsilon k_y) \sin(k_x a) = (A \alpha_x - B k_y) e^{-\alpha_x a}; \quad (5.32)$$

(5.16) and (5.26) yield for  $\mu_0 H_x$

$$[A \epsilon k_x k_y - B \epsilon (k_y^2 + k_z^2)] \sin(k_x a) = [A \alpha_x k_y - B (k_y^2 + k_z^2)] e^{-\alpha_x a}; \quad (5.33)$$

(5.17) and (5.27) yield for  $H_y$

$$[A \epsilon (k_x^2 + k_z^2) - B \epsilon k_x k_y] \cos(k_x a) = [A (-\alpha_x^2 + k_z^2) + B \alpha_x k_y] e^{-\alpha_x a}; \quad (5.34)$$

(5.18) and (5.28) yield for  $H_z$

$$(A \epsilon k_y + B \epsilon k_x) \cos(k_x a) = (A k_y - B \alpha_x) e^{-\alpha_x a}; \quad (5.35)$$

(5.30) and (5.31) yield

$$A_{\epsilon} = \frac{A}{\epsilon_r} \frac{e^{-\alpha_x a}}{\cos(k_x a)}, \quad (5.36)$$

and

$$B_{\epsilon} = B \frac{e^{-\alpha_x a}}{\sin(k_x a)}. \quad (5.37)$$

Equations (5.32) with (5.36) and (5.37) specify

$$\left[ \frac{A}{\epsilon_r} \frac{e^{-\alpha_x a} k_x}{\cos(k_x a)} - \frac{B e^{-\alpha_x a} k_y}{\sin(k_x a)} \right] \sin(k_x a) = (A \alpha_x - B k_y) e^{-\alpha_x a},$$

and after simplification this becomes

$$A \left[ \frac{k_x \sin(k_x a)}{\epsilon_r \cos(k_x a)} - \alpha_x \right] = B(k_y - k_x).$$

It follows that

$$\epsilon_r \alpha_x = k_x \tan(k_x a), \quad (5.38)$$

since it is not desirable to have  $A = 0$ . Now  $B$  can be obtained in terms of  $A$  from (5.35) by utilizing (5.36) and (5.37); that is,

$$\left[ \frac{A}{\epsilon_r} \frac{e^{-\alpha_x a} k_y}{\cos(k_x a)} + \frac{B e^{-\alpha_x a} k_x}{\sin(k_x a)} \right] \cos(k_x a) = (A k_y - B \alpha_x) e^{-\alpha_x a},$$

which becomes

$$-A \left( \frac{k_y}{\epsilon_r} + k_y \right) + B \left( \frac{k_x}{\tan(k_x a)} + \alpha_x \right) = 0,$$

and therefore

$$B = A \frac{k_y \left( 1 - \frac{1}{\epsilon_r} \right) \tan(k_x a)}{k_x + \alpha_x \tan(k_x a)}$$

or, after simplification

$$B = A \frac{k_x k_y \tan(k_x a)}{\epsilon_r (k_y^2 + k_z^2)}, \quad (5.39)$$

after using (5.14), (5.29), and (5.38). This can be written as

$$B(k_y^2 + k_z^2) = A k_y \cdot \frac{k_x \tan(k_x a)}{\epsilon_r},$$

but (5.38) specifies this as

$$B(k_y^2 + k_z^2) = A k_y \alpha_x. \quad (5.40)$$

Comparing this with (5.33), it must be concluded that  $H_x$  and  $H_{x\epsilon}$  are zero everywhere.

### 5.8 Trigonometric Identities

It is advantageous to consider the following identities, which will simplify the field equations considerably:

$$\sin(k_x a) = \frac{1}{\sqrt{1 + \cot^2(k_x a)}}, \quad (5.41)$$

$$\cos(k_x a) = \frac{1}{\sqrt{1 + \tan^2(k_x a)}}, \quad (5.42)$$

and

$$\sin(2k_x a) = 2 \sin(k_x a) \cos(k_x a). \quad (5.43)$$

Utilizing (5.38), (5.41) through (5.43) become respectively

$$\sin(k_x a) = \frac{\epsilon_r \alpha_x}{h}, \quad (5.44)$$

$$\cos(k_x a) = \frac{k_x}{h}, \quad (5.45)$$

and

$$\sin(2k_x a) = \frac{2\epsilon_r \alpha_x k_x}{h^2}, \quad (5.46)$$

where

$$h^2 = k_x^2 + \epsilon_r^2 \alpha_x^2. \quad (5.47)$$

### 5.9 Simplification of the Field Components

The field components can now be obtained in terms of a single variable,  $A$ , by utilizing (5.36), (5.37) and (5.40). The field within the dielectric becomes

$$E_{xe} = \frac{k_z e^{-\alpha_x a}}{\epsilon_r \cos(k_x a)} \cos(k_x x) \cos(k_y y) e^{-jk_z z}, \quad (5.48)$$

$$E_{ye} = \frac{A \alpha_x k_y k_z e^{-\alpha_x a}}{\sin(k_x a)(k_y^2 + k_z^2)} \sin(k_x x) \sin(k_y y) e^{-jk_z z}, \quad (5.49)$$

$$E_{ze} = jA \left[ \frac{k_x}{\epsilon_r \cos(k_x a)} - \frac{\alpha_x k_y^2}{(k_y^2 + k_z^2) \sin(k_x a)} \right] e^{-\alpha_x a} \cdot \sin(k_x x) \cos(k_y y) e^{-jk_z z}, \quad (5.50)$$

$$H_{ye} = \frac{A}{\omega \mu} \left[ \frac{k_x^2 + k_z^2}{\epsilon_r \cos(k_x a)} - \frac{\alpha_x k_x k_y^2}{\sin(k_x a)(k_y^2 + k_z^2)} \right] e^{-\alpha_x a} \cdot \cos(k_x x) \cos(k_y y) e^{-jk_z z}, \quad (5.51)$$

and

$$H_{ze} = \frac{j\omega}{\omega_p} \left[ \frac{k_y k_z}{\epsilon_r \cos(k_x a)} + \frac{k_x k_z k_y \alpha_x}{\sin(k_x a)(k_y^2 + k_z^2)} \right] e^{-\alpha_x a} \cdot \cos(k_x x) \sin(k_y y) e^{-jk_z z} \quad (5.52)$$

The identities, (5.44) and (5.45), can now be employed simplifying the field to be

$$E_{xe} = \frac{A' k_z h}{\epsilon_r k_x} \cos(k_x x) \cos(k_y y) e^{-jk_z z}, \quad (5.53)$$

$$E_{ye} = \frac{A' k_y k_z h}{\epsilon_r (k_y^2 + k_z^2)} \sin(k_x x) \sin(k_y y) e^{-jk_z z}, \quad (5.54)$$

$$E_{ze} = \frac{jA' k_z^2 h}{\epsilon_r (k_y^2 + k_z^2)} \sin(k_x x) \cos(k_y y) e^{-jk_z z}, \quad (5.55)$$

$$H_{ye} = \frac{A' \omega \epsilon_0 k_z^2 h}{k_x (k_y^2 + k_z^2)} \cos(k_x x) \cos(k_y y) e^{-jk_z z}, \quad (5.56)$$

and

$$H_{ze} = \frac{jA' \omega \epsilon_0 k_y k_z h}{k_x (k_y^2 + k_z^2)} \cos(k_x x) \sin(k_y y) e^{-jk_z z}, \quad (5.57)$$

where, for convenience,

$$A' = A e^{-\alpha_x a}.$$

The field components above the dielectric region will now be simplified in the same manner that is

$$E_x = A k_z e^{-\alpha_x x} \cos(k_y y) e^{-jk_z z}, \quad (5.58)$$

$$E_y = \frac{A \alpha_x k_y k_z}{(k_y^2 + k_z^2)} e^{-\alpha_x x} \sin(k_y y) e^{-jk_z z}, \quad (5.59)$$

$$E_z = \frac{jA \alpha_x k_z^2}{(k_y^2 + k_z^2)} e^{-\alpha_x x} \cos(k_y y) e^{-jk_z z}, \quad (5.60)$$

$$H_y = \frac{A \omega \epsilon_0 k_z^2}{(k_y^2 + k_z^2)} e^{-\alpha_x x} \cos(k_y y) e^{-jk_z z}, \quad (5.61)$$

and

$$H_z = \frac{jA \omega \epsilon_0 k_z k_y}{(k_y^2 + k_z^2)} e^{-\alpha_x x} \sin(k_y y) e^{-jk_z z}. \quad (5.62)$$

The entire field is thus expressible in terms of a single variable which depends upon the excitation.

#### 5.10 Power Transmitted

The power transmitted by the wave guide will have two contributing factors; that delivered by the field within the dielectric,  $P_\epsilon$ , and that delivered by the field above the dielectric,  $P_0$ . Consequently, the total power,  $P$ , is given by

$$P = P_\epsilon + P_0. \quad (5.63)$$

The power transmitted within the dielectric region is

$$P_\epsilon = \frac{R_e}{2} \int_{-b/2}^{b/2} \int_0^a E_{x\epsilon} H_{y\epsilon}^* dx dy. \quad (5.64)$$

Upon substitution from (5.53) and (5.56), it becomes

$$P_\epsilon = \frac{A^2 \omega \epsilon_0 k_z^2 h^2}{2 \epsilon_r k_x^2 (k_y^2 + k_z^2)} \int_{-b/2}^{b/2} \int_0^a \left\{ \frac{[1 + \cos(2k_x x)]}{2} \frac{[1 + \cos(2k_y y)]}{2} \right\} dx dy$$



or, after integrating,

$$P_{\epsilon} = \frac{A'^2 \omega \epsilon_0 k_z^3 h^2 b}{16 \epsilon_r k_x^3 (k_y^2 + k_z^2)} [2k_x a + \sin(2k_x a)] . \quad (5.65)$$

The power transmitted above the dielectric region is similarly given by

$$P_0 = \frac{R_e}{2} \int_{-b/2}^{b/2} \int_a^{\infty} E_x H_y^* dx dy . \quad (5.66)$$

Using now (5.58) and (5.61), the power becomes

$$P_0 = \frac{A'^2 \omega \epsilon_0 k_z^3}{2(k_y^2 + k_z^2)} \int_{-b/2}^{b/2} \int_a^{\infty} e^{-2\alpha_x x} \frac{[1 + \cos(2k_y y)]}{2} dx dy \quad (5.67)$$

and, upon integration,

$$P_0 = \frac{A'^2 \omega \epsilon_0 k_z^3 b}{8(k_y^2 + k_z^2) \alpha_x} .$$

The total power is now given by (5.63); that is

$$P = \frac{A'^2 \omega \epsilon_0 k_z^3 b}{8(k_y^2 + k_z^2)} \left\{ \frac{h^2}{2 \epsilon_r k_x^3} [2k_x a + \sin(2k_x a)] + \frac{1}{\alpha_x} \right\} .$$

Equation (5.46) will simplify this to be

$$P = \frac{A'^2 \omega \epsilon_0 k_z^3 b}{8(k_y^2 + k_z^2)} \left[ \frac{ah^2 \alpha_x + \epsilon_r (\alpha_x^2 + k_x^2)}{\epsilon_r k_x^2 \alpha_x} \right] .$$

Equations (5.20) and (5.29) simplify this further as

$$P = \frac{A'^2 \omega \epsilon_0 k_z^3 b}{8(k_y^2 + k_z^2) \epsilon_r k_x^2 \alpha_x} [ah^2 \alpha_x + \epsilon_r k_0^2 (\epsilon_r - 1)] . \quad (5.68)$$

The total power transmitted is available in terms of a single unknown; the power dissipated must be now developed in a similar manner.

### 5.11 Power Dissipated

The power dissipated will have two sources, the dielectric loss and the imperfect conductor loss. The total power dissipated will, thus, be composed of three terms: the dielectric loss,  $P_{L\epsilon}$ ; the wall loss within the dielectric region,  $P_{Lb}$ ; and the wall loss above the dielectric region,  $P_{La}$ . The total power dissipated,  $P_L$ , is therefore given by

$$P_L = P_{L\epsilon} + P_{La} + P_{Lb} . \quad (5.69)$$

The power dissipated within the dielectric is given by

$$P_{L\epsilon} = \frac{R_e}{2} \int_{-b/2}^{b/2} \int_0^a \frac{J}{-\epsilon} \cdot \underline{E}^* dx dy , \quad (5.70)$$

which is

$$P_{L\epsilon} = \frac{\omega \epsilon_0 \epsilon_r \tan(\delta)}{2} R_e \int_{-b/2}^{b/2} \int_0^a (|E_{x\epsilon}|^2 + |E_{y\epsilon}|^2 + |E_{z\epsilon}|^2) dx dy .$$

Substitution from (5.53) through (5.55) into this yields

$$\begin{aligned} P_{L\epsilon} = & \frac{\omega \epsilon_0 \epsilon_r \tan(\delta) A'^2}{8 \epsilon_r} \int_{-b/2}^{b/2} \int_0^a \left[ \frac{k_z^2}{k_x^2} \{ [1 + \cos(2k_x x)][1 + \cos(2k_y y)] \right. \\ & + \frac{k_y^2 k_z^2}{(k_y^2 + k_z^2)} \{ [1 - \cos(2k_x x)][1 - \cos(2k_y y)] \\ & \left. + \frac{k_z^4}{(k_y^2 + k_z^2)} \{ [1 - \cos(2k_x x)][1 + \cos(2k_y y)] \} \right] \end{aligned}$$

or, after performing the integration and simplifying with (5.46),

$$P_{Le} = \frac{\omega \epsilon_0 \tan(\delta) A'^2 b}{8 \epsilon_r (k_y^2 + k_z^2) k_x} \left\{ \frac{k_z^2 (k_y^2 + k_z^2)}{k_x^2} [k_x a h^2 + \epsilon_r \alpha_x k_x] \right. \\ \left. + \frac{k_z^2}{(k_y^2 + k_z^2)} [k_y^2 (k_x a h^2 - \epsilon_r \alpha_x k_x) + k_z^2 (k_x a h^2 - \epsilon_r \alpha_x k_x)] \right\} .$$

Combining further, it becomes

$$P_{Le} = \frac{\omega \epsilon_0 \tan(\delta) A'^2 b k_z^2}{8 \epsilon_r (k_y^2 + k_z^2) k_x^2} [(k_y^2 + k_z^2)(a h^2 + \epsilon_r \alpha_x) + k_x^2 (a h^2 - \epsilon_r \alpha_x)] .$$

Simplifying once again and using (5.14), it is given by

$$P_{Le} = \frac{\omega \epsilon_0 \tan(\delta) A'^2 b k_z^2}{8 k_x^2 (k_y^2 + k_z^2)} \{ a h^2 k_0^2 + \alpha_x [k_0^2 (2 - \epsilon_r) + 2 \alpha_x^2] \} . \quad (5.71)$$

The power dissipated within the walls below the dielectric is given by

$$P_{Lb} = \frac{(2)R_s}{2} \int_0^a |H_{ze}|^2 dx \quad (5.72)$$

per meter in the z-direction, where y is evaluated at the wall ( $y = b/2$ ).

Substituting from (5.77) yields

$$P_{Lb} = R_s \left[ \frac{A'^2 (\omega \epsilon_0 k_y k_z)^2 h^2}{k_x^2 (k_y^2 + k_z^2)^2} \right] \int_0^a \frac{[1 + \cos(2k_x x)]}{2} dx$$

and, after evaluation of the integral, this becomes

$$P_{Lb} = \frac{R_s A'^2 (\omega \epsilon_0 k_y k_z)^2 h^2}{2 k_x^3 (k_y^2 + k_z^2)^2} [2k_x a + \sin(2k_x a)] .$$

Simplification, by use of (5.46), yields

$$P_{Lb} = \frac{R_s A'^2 (\omega \epsilon_0 k_y k_z)^2}{k_x^2 (k_y^2 + k_z^2)^2} [a h^2 + \epsilon_r \alpha_x] . \quad (5.73)$$

The power dissipated within the walls above the dielectric is similarly given by

$$P_{La} = \frac{(2)R_s}{2} \int_a^\infty |H_z|^2 dx, \quad (5.74)$$

and again  $y$  is evaluated at the wall. Substitution from (5.62) yields

$$P_{La} = \frac{R_s A^2 (\omega \epsilon_0 k_z k_y)^2}{(k_y^2 + k_z^2)^2} \int_a^\infty e^{-2\alpha_x x} dx,$$

which becomes upon performing the integration

$$P_{La} = \frac{R_s A^2 (\omega \epsilon_0 k_z k_y)^2}{2\alpha_x (k_y^2 + k_z^2)^2}. \quad (5.75)$$

### 5.12 Attenuation

The attenuation for a wave guide is given by

$$\alpha = \frac{P_L}{2P}. \quad (5.76)$$

For the wave guide under consideration, this may be separated into three terms: that due to the dielectric,  $\alpha_d$ ; that due to the walls within the dielectric region,  $\alpha_b$ ; and that due to the walls above the dielectric region,  $\alpha_a$ . That is, the total attenuation,  $\alpha$ , is given by

$$\alpha = \alpha_d + \alpha_b + \alpha_a.$$

The attenuation due to the dielectric is given by

$$\alpha_d = \frac{P_{Ld}}{2P},$$

which may be evaluated using (5.68) and (5.71). Hence,

$$\alpha_d = \frac{\omega \epsilon_0 \tan(\delta) b k_z^2 \{ ah^2 k_0^2 + \alpha_x [k_0^2(2 - \epsilon_r) + 2\alpha_x^2] \}}{16 \epsilon_r (k_y^2 + k_z^2) k_x^2 \frac{\omega \epsilon_0 k_z^3 b}{8(k_y^2 + k_z^2) \epsilon_r k_x^2 \alpha_x} [ah^2 \alpha_x + \epsilon_r k_0^2 (\epsilon_r - 1)]}$$

It will be advantageous to define two new parameters, the normalized x-decay constant, p, and the normalized y-propagation constant, q, as

$$p = \frac{\alpha_x}{k_0} \quad (5.77)$$

and

$$q = \frac{k_y}{k_0} \quad (5.78)$$

Using these, (5.30) can be written in the form

$$k_z = k_0 \sqrt{1 + p^2 - q^2} \quad (5.79)$$

Substitution of (5.77) through (5.79) into  $\alpha_d$ , it becomes

$$\alpha_d = \frac{\tan(\delta) \epsilon_r k_0 p k_0^3 \left\{ \frac{ah^2}{k_0} + p[2 - \epsilon_r + 2p^2] \right\}}{2k_0 \sqrt{1 + p^2 - q^2} k_0^2 \left[ \frac{ah^2}{k_0} p + \epsilon_r (\epsilon_r - 1) \right]} \quad (5.80)$$

This can be simplified in the following manner. Equation (5.38) can be written as

$$a = \frac{1}{k_x} \tan^{-1} \left( \frac{\epsilon_r \alpha_x}{k_x} \right), \quad (5.81)$$

but (5.14) and (5.29) specify  $k_x$  in terms of  $\alpha_x$ ; therefore,

$$k_x = k_0 \sqrt{\epsilon_r - 1 - p^2} \quad (5.82)$$

Equation (5.81) can now be obtained in terms of p and q by using (5.82);

that is,

$$\frac{ah^2}{k_0} = \frac{(\epsilon_r - 1)[1 + p^2(\epsilon_r + 1)]}{\sqrt{\epsilon_r - 1 - p^2}} \tan^{-1} \left[ \frac{\epsilon_r p}{\sqrt{\epsilon_r - 1 - p^2}} \right] \quad (5.83)$$

after multiplying by  $h^2$  and using (5.47). Now defining for convenience,

$$\frac{ah^2}{k_0} = H. \quad (5.84)$$

The attenuation,  $\alpha_d$ , can now be written as

$$\alpha_d = \frac{\tan(\delta)k_0}{2} \cdot \frac{\epsilon_r p [H + p(2 - \epsilon_r + 2p^2)]}{\sqrt{1 + p^2 - q^2} [H + \epsilon_r(\epsilon_r - 1)]}. \quad (5.85)$$

This result can be compared with that of the infinite dielectric slab, allowing the width to become infinite hence  $q$  tends to zero; the results are identical.

The attenuation due to the wall losses within the dielectric region may now be computed; it is given by

$$\alpha_b = \frac{P_{Lb}}{2P}, \quad (5.86)$$

which, becomes upon substitution from (5.68) and (5.73),

$$\alpha_b = \frac{R_s (\omega \epsilon_0 k_y k_z)^2 [ah^2 + \epsilon_r \alpha_x]}{2k_x^2 (k_y^2 + k_z^2)^2 \frac{\omega \epsilon_0 k_z^2 b}{8(k_y^2 + k_z^2) \epsilon_r k_x^2 \alpha_x} [ah^2 \alpha_x + \epsilon_r k_0^2 (\epsilon_r - 1)]},$$

and after simplifying, it becomes

$$\alpha_b = \frac{4R_s \omega \epsilon_0 k_y^2 \epsilon_r \alpha_x [ah^2 + \epsilon_r \alpha_x]}{(k_y^2 + k_z^2) k_z b [ah^2 \alpha_x + \epsilon_r k_0^2 (\epsilon_r - 1)]}. \quad (5.87)$$

Using now (5.79), (5.84), and normalizing in terms of  $p$  and  $q$ , it becomes

$$\alpha_b = \frac{4R_s \epsilon_r}{b \sqrt{\mu/\epsilon_0}} \cdot \frac{q^2 p [H + \epsilon_r p]}{(1+p^2)[Hp + \epsilon_r(\epsilon_r-1)] \sqrt{1+p^2-q^2}} \quad (5.88)$$

The final attenuation term, that due to the walls above the dielectric is given by

$$\alpha_a = \frac{P_{La}}{2P} \quad (5.89)$$

and substitution from (5.68) and (5.75) yields

$$\alpha_a = \frac{R_s (\omega \epsilon_0 k_z k_y)^2}{4\alpha_x (k_y^2 + k_z^2)^2 \frac{\omega \epsilon_0 k_z^3 b}{8(k_y^2 + k_z^2) \epsilon_r k_z^2 \alpha_x} [ah^2 \alpha_x + \epsilon_r k_z^2 (\epsilon_r - 1)]}$$

becoming, after simplification,

$$\alpha_a = \frac{2R_s \omega \epsilon_0 k_y^2 \epsilon_r k_x^2}{bk_z (k_y^2 + k_z^2) [ah^2 \alpha_x + \epsilon_r k_z^2 (\epsilon_r - 1)]}$$

The same normalization will be performed as previously, namely using (5.79), (5.82), and (5.84) with  $p$  and  $q$ ,  $\alpha_a$ , therefore, becomes

$$\alpha_a = \frac{2R_s \epsilon_r}{b \sqrt{\mu/\epsilon_0}} \cdot \frac{q^2 (\epsilon_r - 1 - p^2)}{(1+p^2)[Hp + \epsilon_r(\epsilon_r-1)] \sqrt{1+p^2-q^2}} \quad (5.90)$$

Equations (5.88) and (5.90) tend to zero as  $b$  becomes infinite, as expected.

### 5.13 Numerical Results

A computer program was written<sup>2</sup> to evaluate the attenuation as a function of relative permittivity for fixed values of  $p$ . The results appear in Figure 5.2.

---

<sup>2</sup>Personal communication. C. W. Bostian, Department of Electrical Engineering, North Carolina State University, Raleigh, N. C.

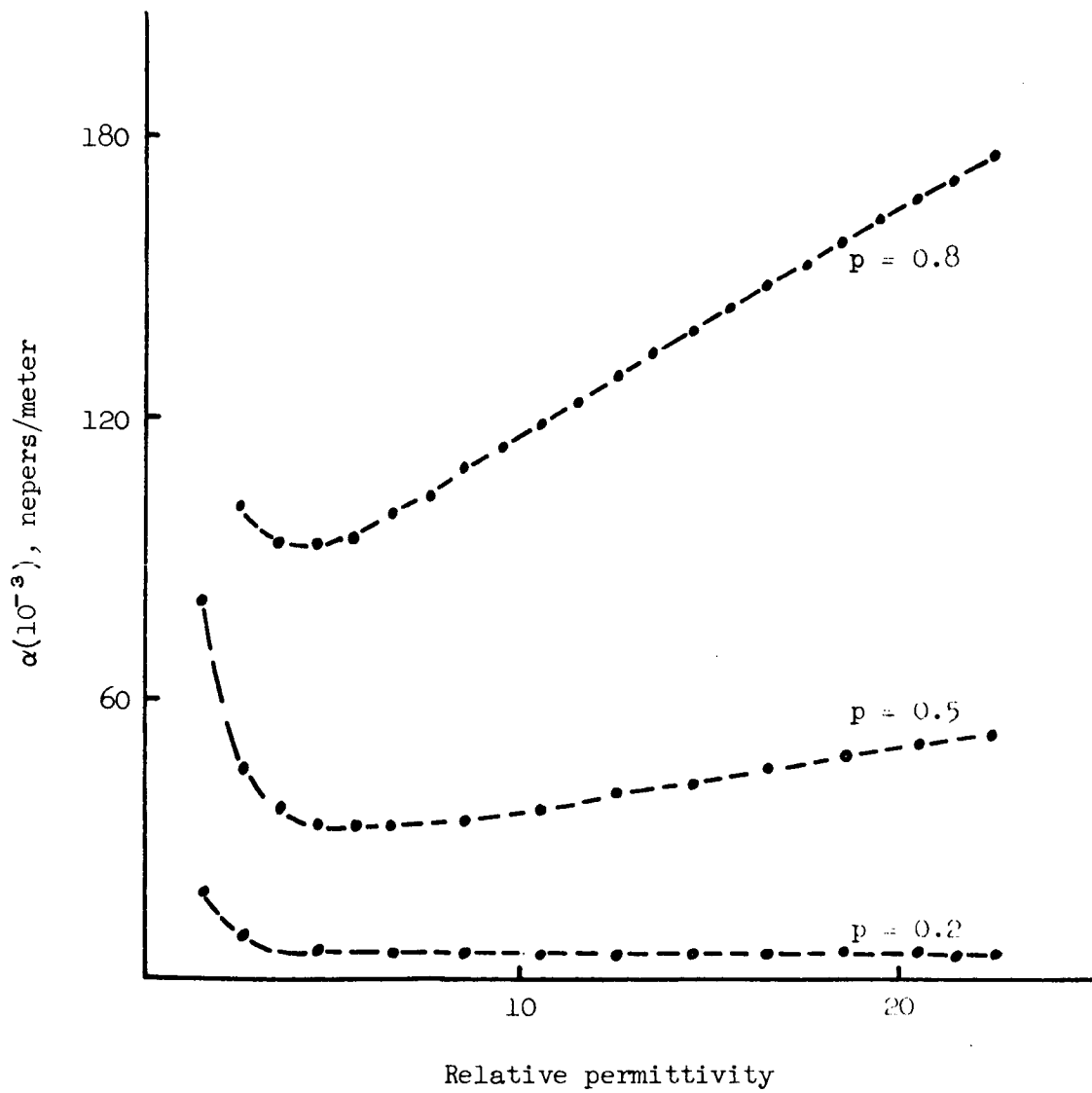


Figure 5.2 Attenuation of dielectric H-guide for 10 GHz with a sidewall spacing of 2.286 cm



## 6. ARTIFICIAL DIELECTRIC H-GUIDE

### 6.1 Description of Structure

The structure under consideration is an H-guide, utilizing a corrugated section in the center, which behaves as an artificial dielectric (Figure 6.1). Each corrugation is a metallic plate whose dimensions are  $2a$  by  $b$ ; the thickness is assumed to be negligible as compared to one wavelength of the operating frequency. The sidewalls are assumed to be large enough in the  $x$ -direction such that the field components are essentially zero at  $x = h$ ; therefore, they may be considered unbounded in the field analysis.

### 6.2 Introduction

The artificial dielectric H-guide structure is examined analytically by employing the field matching technique. The zero<sup>th</sup> order field approximation is made. That is, the field within each corrugation is assumed to be constant in the  $z$ -direction. Attenuation for the wave guide is calculated under this assumption and is plotted as a function of  $s$ , the periodicity of the structure, for a given value of  $p$ , the normalized  $x$ -decay constant, defined  $p = \alpha_x/k$ ,  $\alpha_x$  being the  $x$ -decay constant.

### 6.3 Method of Solution

To facilitate the solution, that portion of the guide for  $x \geq 0$  may be considered along, placing a perfect electrically conducting plane at  $x = 0$ , to be removed later. Generally applicable expressions for the field are found; one set useful above the corrugations and another for below. The field matching technique is employed to assure continuity of tangential (and it may so happen normal also) field components at the boundary  $x = a$ . The field now having been completely specified, the conducting plane may be removed and a

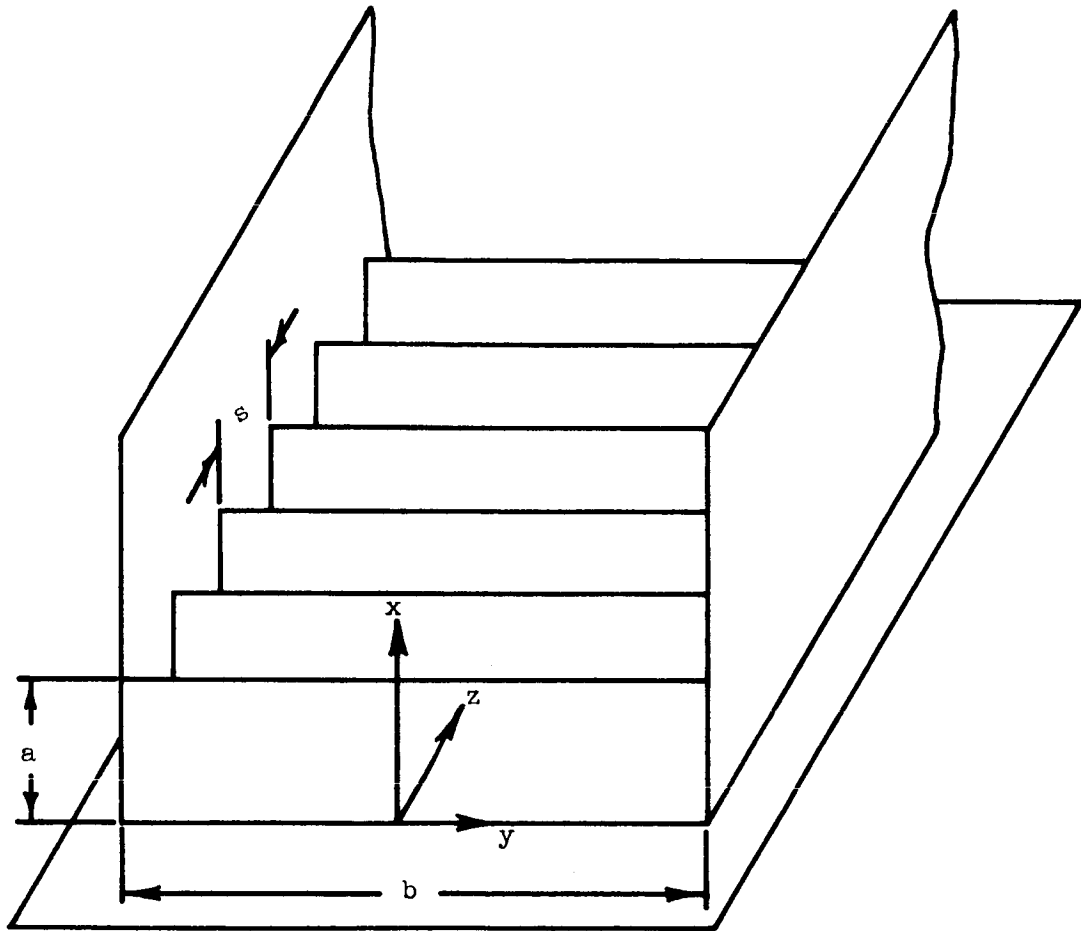


Figure 6.1 Corrugated H-guide over perfectly conducting plane

symmetrical portion of guide revealed in the region where  $x < 0$ , as predicted by the method of images. Excitation must be forced to meet the symmetry requirements imposed by this technique.

It should be noted that the above considers only one-half of the total solution to the problem; that is, there also exists a set of field components which would arise from placing a perfect magnetically conducting plane at the center of the wave guide. In this case, the tangential magnetic field would be zero at the center rather than the electric, the electric being a maximum in this case. These two types of solutions are sometimes denoted the even and odd modes, depending on whether the transverse tangential magnetic field is odd or even with respect to the center of the wave guide.

#### 6.4 Development of a Wave Equation

The total field in a region which is linear, isotropic, homogeneous and source-free with sinusoidal time variation must satisfy the Maxwell equations in the complex form:

$$\nabla \times \underline{E} = -j \omega \mu \underline{H} , \quad (6.1)$$

$$\nabla \times \underline{H} = j \omega \epsilon \underline{E} , \quad (6.2)$$

$$\nabla \cdot \underline{E} = 0 , \quad (6.3)$$

and

$$\nabla \cdot \underline{H} = 0 . \quad (6.4)$$

If the curl operator is applied to both sides of (6.1), with the aid of (6.2) and (6.3), a wave equation for  $\underline{E}$  is obtained; namely

$$\nabla^2 \underline{E} + k^2 \underline{E} = 0 , \quad (6.5)$$

where

$$k^2 = \omega^2 \mu \epsilon . \quad (6.6)$$

Similarly, applying the curl to (6.2) and using (6.1) and (6.4), yields a wave equation for  $\underline{H}$ , that is

$$\nabla^2 \underline{H} + k^2 \underline{H} = 0 . \quad (6.7)$$

In the case of a rectangular coordinate system, any one of the six field components, denoted  $f(x,y,z)$ , can be seen, by (6.5) and (6.7), to satisfy

$$\frac{\partial^2 f(x,y,z)}{\partial x^2} + \frac{\partial^2 f(x,y,z)}{\partial y^2} + \frac{\partial^2 f(x,y,z)}{\partial z^2} + k^2 f(x,y,z) = 0 . \quad (6.8)$$

Therefore, by knowing any two electric (or magnetic) components, then the remaining component is given by (6.3) [or (6.4)] specifying completely the electric (or magnetic) portion of the field. The remaining portion, magnetic (or electric) can be found from (6.1) [or (6.2)]. In general, one electric and one magnetic component could be known and the remaining components found, but this would be somewhat more involved, and since the choice will be free, two components of the same type will be chosen.

The problem is now to find solutions of (6.8) for two field components.

#### 6.5 Solution of the Wave Equation Under Special Periodic Conditions

From physical considerations of the problem, it would be expected that the field would have the same complex amplitude at any two points separated by the distance  $s$  in the  $z$ -direction, since the structure is periodic with period  $s$ . The field would not be periodic within some region near the excitation point, but as  $z$  increases further down the structure, the field would assume a periodic behavior, and the periodicity,  $s$ , of the physical structure would be imposed upon the field. This can be stated mathematically as

$$f(x,y,z+s) = f(x,y,z) e^{-jk_z s} , \quad (6.9)$$

where the exponential term allows for a phase change in the  $z$ -direction. This is known as Floquet's theorem and can be established somewhat more rigorously (Collin, 1960). If (6.9) is to be satisfied, then it must be that

$$f(x,y,z) = \varphi(x,y,z) e^{-jk_{z0}z},$$

where

$$\varphi(x,y,z+s) = \varphi(x,y,z).$$

That is  $\varphi(x,y,z)$  is a periodic function with a period  $s$ . This being the case,  $\varphi(x,y,z)$  may be expanded in a Fourier series, that is

$$\varphi(x,y,z) = \sum_{n=-\infty}^{\infty} g_n(x,y) e^{-j\frac{2n\pi}{s}z}.$$

This means the total  $z$ -variation is of the form

$$f(x,y,z) = \sum_{n=-\infty}^{\infty} g_n(x,y) e^{-jk_{zn}z}, \quad (6.10)$$

where

$$k_{zn} = k_{z0} + \frac{2n\pi}{s}. \quad (6.11)$$

Here it should be noticed that the  $x$ - and  $y$ -variation have not been separated from the  $z$ -variation, since the Fourier coefficients are, in fact, functions of  $x$  and  $y$ . The uniform convergence of the Fourier series is guaranteed if the function to be expanded,  $f(x,y,z)$ , is continuous (Lanczos, 1966) which is assumed for physical reasons. This being the case

$$\frac{\partial^2 f(x,y,z)}{\partial z^2} = - \sum_{n=-\infty}^{\infty} k_{zn}^2 g_n(x,y) e^{-jk_{zn}z}, \quad (6.12)$$

however for the  $x$ - and  $y$ -variation, uniform convergence must be assumed in order to write formally

$$\frac{\partial^2 f(x,y,z)}{\partial x^2} = \sum_{n=-\infty}^{\infty} \frac{\partial^2 g_n(x,y)}{\partial x^2} e^{-jk_{zn}z}, \quad (6.13)$$

and

$$\frac{\partial^2 f(x,y,z)}{\partial y^2} = \sum_{n=-\infty}^{\infty} \frac{\partial^2 g_n(x,y)}{\partial y^2} e^{-jk_{zn}z}. \quad (6.14)$$

Substitution of (6.12) through (6.14) into (6.8) now yields

$$\begin{aligned} & \sum_{n=-\infty}^{\infty} \frac{\partial^2 g_n(x,y)}{\partial x^2} e^{-jk_{zn}z} + \sum_{n=-\infty}^{\infty} \frac{\partial^2 g_n(x,y)}{\partial y^2} e^{-jk_{zn}z} \\ & - \sum_{n=-\infty}^{\infty} k_{zn}^2 g_n(x,y) e^{-jk_{zn}z} + k^2 \sum_{n=-\infty}^{\infty} g_n(x,y) e^{-jk_{zn}z} = 0. \end{aligned} \quad (6.15)$$

If each series is assumed convergent, then (6.15) becomes

$$\sum_{n=-\infty}^{\infty} \left[ \frac{\partial^2 g_n(x,y)}{\partial x^2} + \frac{\partial^2 g_n(x,y)}{\partial y^2} + (k^2 - k_{zn}^2) g_n(x,y) \right] e^{-jk_{zn}z} = 0. \quad (6.16)$$

This must be true for arbitrary values of  $x$  and  $y$ ; therefore, it must be that each "coefficient" is zero. That is

$$\frac{\partial^2 g_n(x,y)}{\partial x^2} + \frac{\partial^2 g_n(x,y)}{\partial y^2} + (k^2 - k_{zn}^2) g_n(x,y) = 0. \quad (6.17)$$

The method of separation of variables may now be employed. That is, let

$$g_n(x,y) = X_n(x) Y_n(y). \quad (6.18)$$

Simply substituting (6.18) into (6.17) yields

$$\frac{1}{X_n(x)} \frac{\partial^2 X_n(x)}{\partial x^2} + \frac{1}{Y_n(y)} \frac{\partial^2 Y_n(y)}{\partial y^2} + (k^2 - k_{zn}^2) = 0,$$

which must be true for arbitrary values  $x$  and  $y$ ; therefore, each of the two variable terms must be a constant, defining these constants

$$\alpha_{xn}^2 = \frac{1}{X_n(x)} \frac{\partial^2 X_n(x)}{\partial x^2}, \quad (6.19)$$

and

$$-k_{yn}^2 = \frac{1}{Y_n(y)} \frac{\partial^2 Y_n(y)}{\partial y^2}, \quad (6.20)$$

then

$$\alpha_{xn}^2 - k_{yn}^2 + k^2 - k_{zn}^2 = 0. \quad (6.21)$$

The signs in (6.19) through (6.21) were chosen such that the decay exponentially in the x-direction, which, by definition, leads to surface waves propagating in the z-direction. The choice of the negative sign for the y-variation is in anticipation of standing waves in this direction, due to reflections between the two walls. Solutions of (6.19) and (6.20) can be written in the form

$$X_n(x) = a_n e^{-\alpha_{xn} x} + b_n e^{+\alpha_{xn} x} \quad (6.22)$$

and

$$Y_n(y) = c_n \cos(k_{yn} y) + d_n \sin(k_{yn} y), \quad (6.23)$$

but  $b_n$  must be zero, since the energy is unlikely to become unbounded for large  $x$ .

The total variation for any field component is therefore given by

$$f(x, y, z) = \sum_{n=-\infty}^{\infty} [a_n \cos(k_{yn} y) + b_n \sin(k_{yn} y)] e^{-\alpha_{xn} x} e^{-jk_{zn} z} \quad (6.24)$$

after redefining the constants. Equation (6.24) now represents the general variation of any field component. Of course, as yet, boundary conditions have not been applied.

### 6.6 The Field Above the Corrugations

Any two field components may be selected at random, e.g.,  $E_z$  and  $E_x$ , and from these the remaining field components can be calculated. The two field components must be described, in general terms, by (6.24); therefore let

$$E_z = \sum_{n=-\infty}^{\infty} [a_n \cos(k_{yn}y) + b_n \sin(k_{yn}y)] e^{-\alpha_{xn}x} e^{-jk_{zn}z} \quad (6.25)$$

and

$$E_x = \sum_{n=-\infty}^{\infty} [c_n \cos(k_{yn}y) + d_n \sin(k_{yn}y)] e^{-\alpha_{xn}x} e^{-jk_{zn}z} . \quad (6.26)$$

Boundary conditions require

$$E_x = E_z = 0 \quad (6.27)$$

for

$$y = \pm b/2 .$$

This does not mean that, in general, each individual term (harmonic) of the series must satisfy the boundary conditions, but only the entire field quantity. However, later a finite approximation in connection with the matching of the field components will be made where the matched terms of the series satisfy individually the boundary conditions.

If the wave guide is excited by a rectangular wave guide or horn carrying the  $TE_{10}$  field, the energy traveling in the guide will primarily have only a single half-sinusoidal variation in the transverse direction. This assumption will simplify analysis greatly; it must be realized that higher order modes may exist, but will hopefully contribute little to the power transport.

Upon application of the boundary conditions, (6.27), to each term of the series, the field components become



$$E_z = \cos(k_{y0}y) \sum_{n=-\infty}^{\infty} a_n e^{-\alpha_{xn}x} e^{-jk_{zn}z}, \quad (6.28)$$

$$E_x = \cos(k_{y0}y) \sum_{n=-\infty}^{\infty} b_n e^{-\alpha_{xn}x} e^{-jk_{zn}z}, \quad (6.29)$$

and

$$\alpha_{xn}^2 - k_{y0}^2 + k^2 - k_{zn}^2 = 0, \quad (6.21a)$$

where

$$k_{y0} = \frac{\pi}{b} \quad (6.30)$$

after substituting  $b_n$  for  $c_n$ .

$E_y$  may be found from (6.3); that is

$$E_y = - \int \left( \frac{\partial E_x}{\partial x} + \frac{\partial E_z}{\partial z} \right) dy + c.$$

This becomes, upon substitution for  $E_x$  and  $E_z$

$$E_y = \frac{1}{k_{y0}} \sin(k_{y0}y) \left[ \sum_{n=-\infty}^{\infty} b_n \alpha_{xn} e^{-\alpha_{xn}x} e^{-jk_{zn}z} + \sum_{n=-\infty}^{\infty} j a_n k_{zn} e^{-\alpha_{xn}x} e^{-jk_{zn}z} \right] + c.$$

This may be written

$$E_y = \frac{\sin(k_{y0}y)}{k_{y0}} \sum_{n=-\infty}^{\infty} (b_n \alpha_{xn} + j a_n k_{zn}) e^{-\alpha_{xn}x} e^{-jk_{zn}z}, \quad (6.31)$$

$c$  being chosen zero, since this would correspond to a static field.

The total electric part of the field being now known allows the magnetic part to be found by utilization of (6.1). Carrying out the differentiation yields

$$H_x = \frac{j}{\omega\mu} [-k_{y0} \sin(k_{y0}y) \sum_{n=-\infty}^{\infty} a_n e^{-\alpha_{xn}x} e^{-jk_{zn}z} - \frac{\sin(k_{y0}y)}{k_{y0}} \sum_{n=-\infty}^{\infty} (-jk_{zn})(b_n \alpha_{xn} + ja_n k_{zn}) e^{-\alpha_{xn}x} e^{-jk_{zn}z}],$$

$$H_y = \frac{j}{\omega\mu} [\cos(k_{y0}y) \sum_{n=-\infty}^{\infty} b_n (-jk_{zn}) e^{-\alpha_{xn}x} e^{-jk_{zn}z} - \cos(k_{y0}y) \sum_{n=-\infty}^{\infty} a_n (-\alpha_{xn}) e^{-\alpha_{xn}x} e^{-jk_{zn}z}],$$

and

$$H_z = \frac{j}{\omega\mu} \left[ \frac{\sin(k_{y0}y)}{k_{y0}} \sum_{n=-\infty}^{\infty} (-\alpha_{xn})(b_n \alpha_{xn} + ja_n k_{zn}) e^{-\alpha_{xn}x} e^{-jk_{zn}z} + k_{y0} \sin(k_{y0}y) \sum_{n=-\infty}^{\infty} b_n e^{-\alpha_{xn}x} e^{-jk_{zn}z} \right],$$

which becomes upon simplification

$$H_x = \frac{j}{\omega\mu} \sin(k_{y0}y) \sum_{n=-\infty}^{\infty} \left[ \frac{jk_{zn}}{k_{y0}} (b_n \alpha_{xn} + ja_n k_{zn}) - k_{y0} a_n \right] e^{-\alpha_{xn}x} e^{-jk_{zn}z}, \quad (6.32)$$

$$H_y = \frac{j}{\omega\mu} \cos(k_{y0}y) \sum_{n=-\infty}^{\infty} [a_n \alpha_{xn} - jb_n k_{zn}] e^{-\alpha_{xn}x} e^{-jk_{zn}z}, \quad (6.33)$$

and

$$H_z = \frac{j}{\omega\mu} \sin(k_{y0}y) \sum_{n=-\infty}^{\infty} \left[ b_n k_{y0} - \frac{\alpha_{xn}}{k_{y0}} (b_n \alpha_{xn} + ja_n k_{zn}) \right] e^{-\alpha_{xn}x} e^{-jk_{zn}z}. \quad (6.34)$$

The total field above the corrugations is now known in terms of four constants:  $a_n$ ,  $b_n$ ,  $\alpha_{xn}$ , and  $k_{z0}$ , which will be interrelated by field matching at  $x = a$ .

### 6.7 The Field Within the Corrugations

The same procedure will be used as before, that is, all of the field components must satisfy the wave equation, (6.8). Choosing again  $E_x$  and  $E_z$  as potential functions, solutions can be separated as

$$f(x,y,z) = X(x)Y(y)Z(z) . \quad (6.35)$$

Upon substitution of (6.35) into (6.8) yields

$$\frac{1}{X(x)} \frac{\partial^2 X(x)}{\partial x^2} + \frac{1}{Y(y)} \frac{\partial^2 Y(y)}{\partial y^2} + \frac{1}{Z(z)} \frac{\partial^2 Z(z)}{\partial z^2} + k^2 = 0 , \quad (6.36)$$

which means each term is constant; therefore, constants may be defined

$$k_x^2 = - \frac{1}{X(x)} \frac{\partial^2 X(x)}{\partial x^2} , \quad (6.37)$$

$$k_y^2 = - \frac{1}{Y(y)} \frac{\partial^2 Y(y)}{\partial y^2} , \quad (6.38)$$

and

$$\beta_z^2 = - \frac{1}{Z(z)} \frac{\partial^2 Z(z)}{\partial z^2} ; \quad (6.39)$$

therefore,

$$k_x^2 + k_y^2 + \beta_z^2 = k^2 . \quad (6.40)$$

Solutions of (6.37) through (6.39) are of the form

$$X(x) = a \cos(k_x x) + b \sin(k_x x) , \quad (6.41)$$

$$Y(y) = c \cos(k_y y) + d \sin(k_y y) , \quad (6.42)$$

and

$$Z(z) = e \cos(\beta_z z) + f \sin(\beta_z z) . \quad (6.43)$$

Therefore

$$\begin{aligned} E_{xc} = & [a \cos(k_x x) + b \sin(k_x x)] [c \cos(k_y y) + d \sin(k_y y)] \\ & \cdot [e \cos(\beta_z z) + f \sin(\beta_z z)] \end{aligned} \quad (6.44)$$

and

$$\begin{aligned} E_{zc} = & [g \cos(k_x x) + h \sin(k_x x)] [i \cos(k_y y) + p \sin(k_y y)] \\ & \cdot [u \cos(\beta_z z) + v \sin(\beta_z z)] . \end{aligned} \quad (6.45)$$

Boundary conditions require

$$E_{xc} = E_{zc} = 0 \quad (6.46)$$

for

$$y = \pm b/2 ,$$

and

$$E_{xc} = E_{yc} = 0 \quad (6.47)$$

for

$$z = 0 , s .$$

Further

$$E_{zc} = E_{yc} = 0 \quad (6.48)$$

for

$$x = 0 .$$

Applying these boundary conditions to (6.44) and (6.45) yields

$$E_{xc} = c [\cos(k_x x) + b \sin(k_x x)] \cos(k_y y) \sin(\beta_z z) \quad (6.49)$$

and

$$E_{zc} = \sin(k_x x) \cos(k_y y) [d \cos(\beta_z z) + e \sin(\beta_z z)] , \quad (6.50)$$

after redefining the constants. The boundary conditions also stipulate

$$k_{yp} = \frac{p\pi}{b} ; p = 0, \pm 1, \pm 2, \dots \quad (6.51)$$

and

$$\beta_{zm} = \frac{m\pi}{s} ; m = 0, \pm 1, \pm 2, \dots ; \quad (6.52)$$

the subscripts, p and m, denoting the number of half-sinusoidal variations in the y- and z-directions respectively. The individual field modes must satisfy (6.37) through (6.40). This yields

$$k_{xpm}^2 = - \frac{1}{X_{pm}(x)} \frac{\partial^2 X_{pm}(x)}{\partial x^2} , \quad (6.37a)$$

$$k_{yp}^2 = - \frac{1}{Y_p(y)} \frac{\partial^2 Y_p(y)}{\partial y^2} , \quad (6.38b)$$

$$\beta_{zm}^2 = - \frac{1}{Z_m(z)} \frac{\partial^2 Z_m(z)}{\partial z^2} , \quad (6.39c)$$

and

$$k_{xpm}^2 + k_{yp}^2 + \beta_{zm}^2 = k^2 , \quad (6.40a)$$

and therefore

$$E_{xcpm} = [\cos(k_{xpm} x) + b_{pm} \sin(k_{xpm} x)] \cos(k_{yp} y) \cdot c_{pm} \sin(\beta_{zm} z) \quad (6.49a)$$

and

$$E_{zcpm} = \sin(k_{xpm} x) \cos(k_{yp} y) [d_{pm} \cos(\beta_{zm} z) + e_{pm} \sin(\beta_{zm} z)] . \quad (6.50a)$$

Now restricting the solution, by means of proper excitation to a single half sinusoidal variation in the y-direction, that is, let  $p = 1$ . Equation (6.50a) must become

$$k_{xm}^2 + k_{y0}^2 + \beta_{zm}^2 = k^2, \quad (6.50b)$$

where

$$k_{y0} = \frac{\pi}{b},$$

$k_{y0}$  denoting the fundamental variation in the y-direction. With these changes, (6.49a) and (6.50a) become

$$E_{xcm} = \cos(k_{y0}y) c_m [\cos(k_{xm}x) + b_m \sin(k_{xm}x)] \cdot \sin(\beta_{zm}z) \quad (6.49b)$$

and

$$E_{zcm} = \cos(k_{y0}y) \sin(k_{xm}x) [d_m \cos(\beta_{zm}z) + e_m \sin(\beta_{zm}z)]. \quad (6.50b)$$

The total field must be a linear combination of these individual wave modes, therefore, the total variation of  $E_{xc}$  and  $E_{zc}$  is

$$E_{xc} = \cos(k_{y0}y) \sum_{m=-\infty}^{\infty} c_m [\cos(k_{xm}x) + b_m \sin(k_{xm}x)] \sin(\beta_{zm}z) \quad (6.49c)$$

and

$$E_{zc} = \cos(k_{y0}y) \sum_{m=-\infty}^{\infty} \sin(k_{xm}x) [d_m \cos(\beta_{zm}z) + e_m \sin(\beta_{zm}z)]. \quad (6.50c)$$

$E_y$  can now be found from (6.3), that is

$$E_{yc} = - \int \left( \frac{\partial E_{xc}}{\partial x} + \frac{\partial E_{zc}}{\partial z} \right) dy + D.$$

Upon substitution for  $E_{xc}$  and  $E_{zc}$

$$E_{yc} = - \sin(k_{y0}y) \left\{ \sum_{m=-\infty}^{\infty} k_{xm} [-\sin(k_{xm}x) + b_m \cos(k_{xm}x)] \right. \\ \left. \cdot c_m \sin(\beta_{zm}z) + \sum_{m=-\infty}^{\infty} \sin(k_{xm}x) \beta_{zm} [-d_m \sin(\beta_{zm}z) + e_m \cos(\beta_{zm}z)] \right\} + D ;$$

simplification yields

$$E_{yc} = \frac{\sin(k_{y0}y)}{k_{y0}} \sum_{m=-\infty}^{\infty} \left\{ k_{xm} [\sin(k_{xm}x) - b_m \cos(k_{xm}x)] c_m \right. \\ \left. \cdot \sin(\beta_{zm}z) + j \sin(k_{xm}x) \beta_{zm} [d_m \sin(\beta_{zm}z) - e_m \cos(\beta_{zm}z)] \right\} .$$

Here, as for the field above the corrugations, D is zero. Equation (6.47)

specifies

$$e_m = 0 , \quad (6.53)$$

and (6.48) specifies

$$b_m = 0 . \quad (6.54)$$

It will be assumed later that the field can be approximated by a finite number of terms, each of which must necessarily meet all the boundary conditions.

The total electric portion of the field becomes, after enforcing boundary conditions

$$E_{xc} = \cos(k_{y0}y) \sum_{m=-\infty}^{\infty} c_m \cos(k_{xm}x) \sin(\beta_{zm}z) , \quad (6.55)$$

$$E_{zc} = \cos(k_{y0}y) \sum_{m=-\infty}^{\infty} d_m \sin(k_{xm}x) \cos(\beta_{zm}z) , \quad (6.56)$$

and

$$E_{yc} = \frac{\sin(k_{y0}y)}{k_{y0}} \sum_{m=-\infty}^{\infty} \sin(k_{xm}x) [k_{cm} c_m + \beta_{zm} d_m] \sin(\beta_{zm}z) . \quad (6.57)$$

The total magnetic portion may now be found from (6.1); performing the differentiation yields

$$H_{xc} = \frac{j}{\omega\mu} \left\{ -k_{y0} \sin(k_{y0}y) \sum_{m=-\infty}^{\infty} d_m \sin(k_{xm}x) \cos(\beta_{zm}z) \right. \\ \left. - \frac{\sin(k_{y0}y)}{k_{y0}} \sum_{m=-\infty}^{\infty} \sin(k_{xm}x) \beta_{zm} [k_{xm} c_m + \beta_{zm} d_m] \cdot \cos(\beta_{zm}z) \right\} ,$$

$$H_{yc} = \frac{j}{\omega\mu} \left\{ \cos(k_{y0}y) \sum_{m=-\infty}^{\infty} \cos(k_{xm}x) \beta_{zm} c_m \cos(\beta_{zm}z) \right. \\ \left. - \cos(k_{y0}y) \sum_{m=-\infty}^{\infty} d_m k_{xm} \cos(k_{xm}x) \cos(\beta_{zm}z) \right\} ,$$

and

$$H_{zc} = \frac{j}{\omega\mu} \frac{\sin(k_{y0}y)}{k_{y0}} \sum_{m=-\infty}^{\infty} k_{xm} \cos(k_{xm}x) [k_{xm} c_m + \beta_{zm} d_m] \\ \cdot \sin(\beta_{zm}z) + k_{y0} \sin(k_{y0}y) \sum_{m=-\infty}^{\infty} c_m \cos(k_{xm}x) \sin(\beta_{zm}z) ,$$

and simplifying yields

$$H_{xc} = \frac{j}{\omega\mu} \sin(k_{y0}y) \sum_{m=-\infty}^{\infty} \sin(k_{xm}x) \left[ -k_{y0} d_m - \frac{\beta_{zm}}{k_{y0}} (k_{xm} c_m + \beta_{zm} d_m) \right] \\ \cdot \cos(\beta_{zm}z) , \quad (6.58)$$

$$H_{yc} = \frac{j}{\omega\mu} \cos(k_{y0}y) \sum_{m=-\infty}^{\infty} \cos(k_{xm}x) [\beta_{zm} c_m - k_{xm} d_m] \cos(\beta_{zm}z) , \quad (6.59)$$

and

$$H_{zc} = \frac{j}{\omega\mu} \sin(k_{y0}y) \sum_{m=-\infty}^{\infty} \cos(k_{xm}x) \left[ \frac{k_{xm}}{k_{y0}} (k_{xm} c_m + \beta_{zm} d_m) \right. \\ \left. + k_{y0} c_m \right] \sin(\beta_{zm}z) . \quad (6.60)$$



The total field within the corrugated region has been found in terms of three constants:  $c_m$ ,  $d_m$ , and  $k_{xm}$ .

### 6.8 Field Matching

The method of field matching is based on the assumption of continuity of certain properly chosen field components at the boundary between any two regions, in this case, at  $x = a$ . Continuity of all field components is not necessarily guaranteed. Matching at the boundary will lead to a set of equations which may be solved for the unknown constants of the field.

Tangential field components will be matched first. That is

$$E_z = E_{zc} , \quad (6.61)$$

$$E_y = E_{yc} , \quad (6.62)$$

$$H_z = H_{zc} , \quad (6.63)$$

and

$$H_y = H_{yc} \quad (6.64)$$

for

$$x = a .$$

Equations (6.28), (6.56), and (6.61) yield for  $E_z$

$$\sum_{n=-\infty}^{\infty} a_n e^{-\alpha_{xn}a} e^{-jk_{zn}z} = \sum_{m=-\infty}^{\infty} d_m \sin(k_{xm}a) \cos(\beta_{zm}z) ; \quad (6.65)$$

(6.31), (6.56), and (6.62) yield for  $E_y$

$$\sum_{n=-\infty}^{\infty} (b_n \alpha_{xn} + ja_n k_{zn}) e^{-\alpha_{xn}a} e^{-jk_{zn}z} = \sum_{m=-\infty}^{\infty} \sin(k_{xm}a) [k_{xm} c_m + \beta_{zm} d_m] \sin(\beta_{zm}z) ; \quad (6.66)$$

(6.34), (6.60), and (6.63) yield for  $H_z$

$$\sum_{n=-\infty}^{\infty} \left[ b_n k_{y0} - \frac{\alpha_{xn}}{k_{y0}} (b_n \alpha_{xn} + j a_n k_{zn}) \right] e^{-\alpha_{xn} a} e^{-jk_{zn} z} =$$

$$\sum_{m=-\infty}^{\infty} \cos(k_{xm} a) \left[ \frac{k_{xm}}{k_{y0}} (k_{xm} c_m + \beta_{zm} d_m) + k_{y0} c_m \right] \sin(\beta_{zm} z); \quad (6.67)$$

(6.33), (6.59), and (6.64) yield for  $H_y$

$$\sum_{n=-\infty}^{\infty} (a_n \alpha_{xn} - j b_n k_{zn}) e^{-\alpha_{xn} a} e^{-jk_{zn} z} =$$

$$\sum_{m=-\infty}^{\infty} \cos(k_{xm} a) [\beta_{zm} c_m - k_{xm} d_m] \cos(\beta_{zm} z). \quad (6.68)$$

The matching of the normal components requires, if there is no charge or current on the boundary

$$E_x = E_{xc} \quad (6.69)$$

and

$$H_x = H_{xc} \quad (6.70)$$

at

$$x = a.$$

Equations (6.29), (6.55), and (6.69) yield for  $E_x$

$$\sum_{n=-\infty}^{\infty} b_n e^{-\alpha_{xn} a} e^{-jk_{zn} z} = \sum_{m=-\infty}^{\infty} c_m \cos(k_{xm} a) \sin(\beta_{zm} z); \quad (6.71)$$

(6.32), (6.58), and (6.70) yield for  $H_x$

$$\sum_{n=-\infty}^{\infty} \left[ \frac{jk_{zn}}{k_{y0}} (b_n \alpha_{xn} + j a_n k_{zn}) - k_{y0} a_n \right] e^{-\alpha_{xn} a} e^{-jk_{zn} z} =$$

$$\sum_{m=-\infty}^{\infty} \sin(k_{xm} a) \left[ -k_{y0} d_m - \frac{\beta_{zm}}{k_{y0}} (k_{xm} c_m + \beta_{zm} d_m) \right] \cos(\beta_{zm} z). \quad (6.72)$$

There now exist seven unknown quantities,  $a_n$ ,  $b_n$ ,  $c_m$ ,  $d_m$ ,  $\alpha_{xn}$ ,  $k_{z0}$ , and  $k_x$ , of which one will depend on the excitation amplitude, and seven equations, (6.21), (6.65) through (6.68), (6.71), and (6.72) for their determination. There will have to be made an approximation for the solution; therefore, the assumption can be made that the major contribution to the total field will result from the fundamental modes within the corrugations; that is, let  $m = 0$ . The field components within the corrugations reduce to

$$E_{zc} = \cos(k_{y0}y) d_0 \sin(k_{x0}x) ,$$

$$H_{xc} = \frac{j}{\omega\mu} \sin(k_{y0}y) \sin(k_{x0}x) (-k_{y0}d_0) ,$$

and

$$H_{yc} = \frac{j}{\omega\mu} \cos(k_{y0}y) \cos(k_{x0}x) (-k_{x0}d_0) .$$

These components are a standing  $TE_{10}$  mode in the x-direction; that is, the corrugated region may be considered a shorted section of rectangular wave guide. This wave guide is considered to be operating at a frequency such that only the  $TE_{10}$  mode is present; all other modes cut-off. This assumption further reduces the unknowns since  $k_{x0}$  can now be approximated by  $k = \sqrt{\mu\epsilon}$ .

The  $TE_{10}$  field can now be written

$$E_{zc} = d_0 \sin(kx) \cos(k_{y0}y) , \quad (6.73)$$

$$H_{xc} = \frac{-jd_0 k_{y0}}{\omega\mu} \sin(kx) \sin(k_{y0}y) , \quad (6.74)$$

and

$$H_{yc} = \frac{-jd_0 k}{\omega\mu} \cos(kx) \cos(k_{y0}y) . \quad (6.75)$$

Field matching may now be performed on the above components: for  $E_z$ ,

$$\sum_{n=-\infty}^{\infty} a_n e^{-\alpha_{xn} a} e^{-jk_{zn} z} = d_0 \sin(ka) ; \quad (6.76)$$

for  $H_x$ ,

$$\sum_{n=-\infty}^{\infty} \left[ \frac{jk_{zn}}{k_{y0}} (b_n \alpha_{xn} + j a_n k_{zn}) - k_{y0} a_n \right] e^{-\alpha_{xn} a} e^{-jk_{zn} z} = \sin(ka) (-k_{y0} d_0) ; \quad (6.77)$$

and for  $H_y$ ,

$$\sum_{n=-\infty}^{\infty} [a_n \alpha_{xn} - j b_n k_{zn}] e^{-\alpha_{xn} a} e^{-jk_{zn} z} = \cos(ka) (-k_{y0} d_0) . \quad (6.78)$$

The orthogonality of the z-variation may be employed to eliminate the summation over n; that is multiply by  $e^{+jk_{zv} z}$  and integrate from 0 to s.

Equations (6.76) through (6.78) become respectively

$$a_v e^{-\alpha_{xv} a} s = d_0 \sin(ka) I , \quad (6.79)$$

$$\left[ \frac{jk_{zv}}{k_{y0}} (b_v \alpha_{xv} + j a_v k_{zv}) - k_{y0} a_v \right] e^{-\alpha_{xv} a} s = -\sin(ka) k_{y0} d_0 I , \quad (6.80)$$

and

$$[a_v \alpha_{xv} - j b_v k_{zv}] e^{-\alpha_{xv} a} s = \cos(ka) (-k_{y0} d_0) I , \quad (6.81)$$

where

$$I = \int_0^s e^{-jk_{zv} z} dz .$$

The unknowns are now  $a_v$ ,  $d_0$ ,  $\alpha_{xv}$ ,  $k_{x0}$ ,  $k_{zv}$ , and  $b_v$ ; simplification will result if a new constant  $b'_v$  is defined such that

$$b_v = j b'_v .$$

Equations (6.79) through (6.81) now become

$$a_v e^{-\alpha_{xv} a} s = d_0 \sin(ka) I , \quad (6.82)$$

$$\left[ \frac{k_{zv}}{k_{y0}} (b'_v \alpha_{xv} + a_v k_{zv}) + k_{y0} a_v \right] e^{-\alpha_{xv} a} s = \sin(ka) k_{y0} d_0 I , \quad (6.83)$$

and

$$(a_v \alpha_{xv} + b'_v k_{zv}) e^{-\alpha_{xv} a} s = -\cos(ka) k d_0 I . \quad (6.84)$$

Division of (6.83) by (6.82) yields

$$\frac{k_{zv} (b'_v \alpha_{xv} + a_v k_{zv}) + k_{y0}^2 a_v}{a_v k_{y0}} = k_{y0} , \quad (6.85)$$

and simplifying yields

$$b'_v = -a_v \frac{k_{zv}}{\alpha_{xv}} . \quad (6.86)$$

Substitution of (6.86) into (6.84) now specifies

$$a_v \frac{(-\alpha_{xv}^2 + k_{zv}^2)}{\alpha_{xv}} e^{-\alpha_{xv} a} s = \cos(ka) k d_0 I ,$$

and division by (6.82) further simplifies to

$$k_{zv}^2 - \alpha_{xv}^2 = k \alpha_{xv} \cot(ka) ; \quad (6.87)$$

however the left side is reduced by (6.21) to

$$k^2 - k_{y0}^2 = k \alpha_{xv} \cot(ka) . \quad (6.88)$$

It must be concluded from (6.88) that there exists only a single value for  $\alpha_{xv}$  which may be denoted  $\alpha_{x0}$ ; that is, there is only a single term present in

the Fourier expansion representing the field components above the corrugations, the fundamental mode. Equation (6.88) may be now written

$$\alpha_{x0} = \frac{(k^2 - k_y^2) \tan(ka)}{k}; \quad (6.89)$$

(6.86) becomes

$$b'_0 = -a_0 \frac{k_{z0}}{\alpha_{x0}}. \quad (6.90)$$

(6.82) can also be written

$$d_0 = \frac{a_0 e^{-\alpha_{x0} a}}{\sin(ka) \Gamma}. \quad (6.91)$$

The field components above the corrugations are now greatly simplified; that is, (6.28), (6.29), (6.31) and (6.32) through (6.34) become respectively

$$E_z = a_0 \cos(k_{y0} y) e^{-\alpha_{x0} x} e^{-jk_{z0} z}, \quad (6.92)$$

$$E_x = jb'_0 \cos(k_{y0} y) e^{-\alpha_{x0} x} e^{-jk_{z0} z}, \quad (6.93)$$

$$E_y = j \frac{(a_0 k_{z0} + b'_0 \alpha_{x0})}{k_{y0}} \sin(k_{y0} y) e^{-\alpha_{x0} x} e^{-jk_{z0} z}, \quad (6.94)$$

$$H_x = \frac{-j}{\omega \mu} \left[ \frac{k_{z0}}{k_{y0}} (b'_0 \alpha_{x0} + a_0 k_{z0}) + k_{y0} a_0 \right] \sin(k_{y0} y) \cdot e^{-\alpha_{x0} x} e^{-jk_{z0} z}, \quad (6.95)$$

$$H_y = \frac{j}{\omega \mu} (a_0 \alpha_{x0} + b'_0 k_{z0}) \cos(k_{y0} y) e^{-\alpha_{x0} x} e^{-jk_{z0} z}, \quad (6.96)$$

and

$$H_z = \frac{-1}{\omega \mu} \left[ b'_0 k_{y0} - \frac{\alpha_{x0}}{k_{y0}} (b'_0 \alpha_{x0} + a_0 k_{z0}) \right] \sin(k_{y0} y) \cdot e^{-\alpha_{x0} x} e^{-jk_{z0} z}. \quad (6.97)$$

Equation (6.90) now eliminates one variable allowing (6.90) through (6.97) to be written

$$E_z = a_0 \cos(k_{y0}y) e^{-\alpha_{x0}x} e^{-jk_{z0}z}, \quad (6.98)$$

$$E_x = -ja_0 \frac{k_{z0}}{\alpha_{x0}} \cos(k_{y0}y) e^{-\alpha_{x0}x} e^{-jk_{z0}z}, \quad (6.99)$$

$$E_y = 0, \quad (6.100)$$

$$H_x = \frac{-jk_{y0}a_0}{\omega\mu} \sin(k_{y0}y) e^{-\alpha_{x0}x} e^{-jk_{z0}z}, \quad (6.101)$$

$$H_y = \frac{ja_0}{\omega\mu} \frac{(\alpha_{x0}^2 - k_{z0}^2)}{\alpha_{x0}} \cos(k_{y0}y) e^{-\alpha_{x0}x} e^{-jk_{z0}z}, \quad (6.102)$$

and

$$H_z = \frac{a_0 k_{z0} k_{y0}}{\omega\mu \alpha_{x0}} \sin(k_{y0}y) e^{-\alpha_{x0}x} e^{-jk_{z0}z}. \quad (6.103)$$

The field components are now known in terms of a single variable  $a_0$ ; however, it will be advantageous to define a new constant  $H'_0$  such that the work may be compared with that of the chapter entitled ATTENUATION OF A DIELECTRIC SLAB; that is, let

$$H'_0 = \frac{ja_0(\alpha_{x0}^2 - k_{z0}^2)}{\omega\mu \alpha_{x0}}. \quad (6.104)$$

The field components may now be written in terms of  $H'_0$  since

$$a_0 = \frac{-j\omega\mu\alpha_{x0}}{(\alpha_{x0}^2 - k_{z0}^2)} H'_0.$$

Before doing this, (6.21a) allows  $a_0$  to be written

$$a_0 = \frac{j\omega\mu \alpha_{x0}}{k^2 - k_{y0}^2} H'_0, \quad (6.105)$$

$k_{y0}$  being given by (6.30). Now (6.98) through (6.103) become respectively

$$E_z = \frac{j\omega\mu \alpha_{x0} H'_0}{k^2 - k_{y0}^2} \cos(k_{y0}y) e^{-\alpha_{x0}x} e^{-jk_{z0}z}, \quad (6.106)$$

$$E_x = \frac{\omega\mu k_{z0} H'_0}{k^2 - k_{y0}^2} \cos(k_{y0}y) e^{-\alpha_{x0}x} e^{-jk_{z0}z}, \quad (6.107)$$

$$H_x = \frac{\alpha_{x0} k_{z0} H'_0}{k^2 - k_{y0}^2} \sin(k_{y0}y) e^{-\alpha_{x0}x} e^{-jk_{z0}z}, \quad (6.108)$$

$$H_y = H'_0 \cos(k_{y0}y) e^{-\alpha_{x0}x} e^{-jk_{z0}z}, \quad (6.109)$$

and

$$H_z = \frac{jk_{z0} k_{y0} H'_0}{k^2 - k_{y0}^2} \sin(k_{y0}y) e^{-\alpha_{x0}x} e^{-jk_{z0}z}. \quad (6.110)$$

### 6.9 Power Transport

The determination of the attenuation requires knowledge of the power transmitted and the power dissipated within the wave guide. The power transmitted will now be calculated. The Poynting identity specifies it to be

$$P = \frac{1}{2} \int \int \underline{E} \times \underline{H}^* \cdot d\underline{s}. \quad (6.111)$$

In the present case, this reduces to

$$P = \frac{1}{2} \int \int E_x H_y^* dx dy. \quad (6.112)$$

Substitution from (6.107) and (6.109) yields



$$P = \frac{\omega \mu k_{z0} H_0' H_0'^*}{2(k^2 - k_{y0}^2)} \int_{-b/2}^{b/2} \int_a^\infty \frac{(1 + \cos(2k_{y0}y))}{2} e^{-2\alpha_{x0}x} dx dy . \quad (6.113)$$

Upon integration, this becomes

$$P = \frac{\omega \mu k_{z0} H_0' H_0'^* b e^{-2\alpha_{x0}a}}{8\alpha_{x0}(k^2 - k_{y0}^2)} . \quad (6.114)$$

### 6.10 Power Loss

The total power dissipated will have two contributing factors, the power loss within the walls above the corrugations,  $P_a$ , and the power loss within the corrugations themselves,  $P_b$ ; the total power loss is therefore given by

$$P_L = P_a + P_b . \quad (6.115)$$

In either case, the power loss will be given by

$$P_L = \frac{R}{2} \iint |H_t|^2 ds , \quad (6.116)$$

$H_t$  being the total tangential magnetic component of the field evaluated at the surface under consideration.  $P_a$  now becomes, for a single corrugated section

$$P_a = (2) \frac{R}{2} \int_0^s \int_a^\infty (|H_x|^2 + |H_z|^2) dx dz ,$$

$y$  being held constant at the value  $b/2$ . Substitution from (6.108) and (6.110) yields

$$P_a = \frac{R k_{y0}^2 H_0' H_0'^*}{(k^2 - k_{y0}^2)^2} \int_0^s \int_a^\infty (\alpha_{x0}^2 + k_{z0}^2) \sin^2(k_{y0}b/2) e^{-2\alpha_{x0}x} dx dz .$$

Upon simplification this becomes

$$P_a = \frac{R k^2 H'_0 H'_0^* (\alpha_{x0}^2 + k_{z0}^2)}{(k^2 - k_{y0}^2)^2} \int_0^s \int_a^\infty e^{-2\alpha_{x0} x} dx dz ,$$

and finally integrating, the power loss is

$$P_a = \frac{R k^2 H'_0 H'_0^* (\alpha_{x0}^2 + k_{z0}^2)}{2\alpha_{x0} (k^2 - k_{y0}^2)^2} e^{-2\alpha_{x0} a} , \quad (6.117)$$

after division by  $s$  since there are  $1/s$  corrugations per meter.

The power loss within the corrugations will have two contributing factors, the power loss on the sidewalls,  $P_w$ , and the power loss on the end plates,  $P_e$ , the total given by

$$P_b = P_w + P_e . \quad (6.118)$$

As before in either case, the power loss is given by (6.166). On the sidewalls, (6.116) becomes

$$P_w = (2) \frac{R}{2} \int_0^s \int_0^a |H_x|^2 dx dz , \quad (6.119)$$

where  $y$  is evaluated at  $b/2$ . Upon substitution of (6.74) this becomes

$$P_w = \frac{R k^2 d_0^2}{2\omega^2 \mu^2} \int_0^s \int_0^a [1 - \cos(2kx)] dx dz . \quad (6.120)$$

Yielding upon integration

$$P_w = \frac{R d_0^2 k^2}{4\omega^2 \mu^2 k} [2ka - \sin(2ka)] . \quad (6.121)$$

Again, dividing by  $s$  since there are  $1/s$  corrugations per meter. For the contribution due to the corrugations, (6.116) becomes

$$P_c = (2) \frac{R}{2} \int_{-b/2}^{b/2} \int_0^a |H_y|^2 dx dy . \quad (6.122)$$

Substitution from (6.75) yields

$$P_c = \frac{R_s k^2 d_0^2}{4\omega^2 \mu^2} \int_{-b/2}^{b/2} \int_0^a [1 + \cos(2kx)] [1 + \cos(2k_{y0}y)] dx dy ,$$

which yields upon integration

$$P_c = \frac{R_s k d_0^2 b}{8\omega^2 \mu^2} [2ka + \sin(2ka)] , \quad (6.123)$$

as the power loss for the two end plates per corrugation, after again, division by  $s$ .

The total power dissipated within the corrugated region is now given by (6.118), which becomes, upon substitution from (6.121) and (6.123)

$$P_b = \frac{R_s d_0^2}{2\omega^2 \mu^2} \left\{ a(k_{y0}^2 + \frac{k^2 b}{2s}) + \frac{\sin(2ka)}{2} \left[ \frac{kb}{2s} - \frac{k_{y0}^2}{k} \right] \right\} . \quad (6.124)$$

The total power dissipated could now be found from (6.117) and (6.124); however the resulting expression would be quite unwieldy and therefore the attenuation for the wave guide will be found in parts, each part due to a given dissipation term.

### 6.11 Identities

Before the calculating the attenuation for the wave guide, it is advantageous to consider some identities and define two new quantities,  $p$ , the normalized decay constant in the  $x$ -direction and  $q$ , the normalized propagation constant in the  $y$ -direction, as

$$p = \frac{\alpha_{x0}}{k} \quad (6.125)$$

and

$$q = \frac{k_{y0}}{k} . \quad (6.126)$$

A relationship will be needed between the two amplitude constants,  $H_0$  and  $d_0$ ; this may be found by considering (6.91) and (6.105), which yield

$$\frac{d_0^2}{H_0 H_0^*} = \left[ \frac{\omega \mu_s \alpha_{x0} e^{-\alpha_{x0} a}}{\sin(ka)(k^2 - k_{y0}^2) I} \right]^2, \quad (6.127)$$

where

$$I = \int_0^s e^{-jk_{z0} z} dz. \quad (6.128)$$

Evaluating the integral yields

$$I = \frac{j}{k_{z0}} (e^{-jk_{z0} s} - 1),$$

and expanding further

$$I = \frac{j}{k_{z0}} [\cos(k_{z0} s) - 1 - j \sin(k_{z0} s)].$$

Now forming the square of the magnitude,

$$I^2 = \frac{2}{k_{z0}^2} [1 - \cos(k_{z0} s)],$$

(6.127) becomes

$$\frac{d_0^2}{H_0 H_0^*} = \frac{(\omega \mu_s \alpha_{x0} k_{z0})^2 e^{-2\alpha_{x0} a}}{2 \sin^2(ka)(k^2 - k_{y0}^2)^2 [1 - \cos(k_{z0} s)]}. \quad (6.129)$$

Consider, also, the following identities

$$\sin(ka) = \frac{1}{\sqrt{1 + \cot^2(ka)}} \quad (6.130)$$

and

$$\cos(ka) = \frac{1}{\sqrt{1 + \tan^2(ka)}} . \quad (6.131)$$

Rewriting (6.89) in terms of  $p$  and  $q$  yields

$$\tan(ka) = \frac{p}{1-q^2} , \quad (6.132)$$

and substitution of this into (6.129) and (6.130) yield

$$\sin(ka) = \frac{p}{\sqrt{p^2 + (1-q^2)^2}} \quad (6.133)$$

and

$$\cos(ka) = \frac{1-q^2}{\sqrt{p^2 + (1-q^2)^2}} . \quad (6.134)$$

Since

$$\sin(2ka) = 2 \sin(ka) \cos(ka) ,$$

(6.133) and (6.134) specify

$$\sin(2ka) = \frac{2p(1-q^2)}{p^2 + (1-q^2)^2} . \quad (6.135)$$

It is further advantageous to write (6.21a) in terms of  $p$  and  $q$ ; that is

$$k_{z0} = k \sqrt{p^2 + 1 - q^2} . \quad (6.136)$$

## 6.12 Attenuation

The normalized power dissipated per meter of length in the direction of propagation is the attenuation, denoted  $\alpha$ , this is given by

$$\alpha = \frac{P_L}{2P} . \quad (6.137)$$

The attenuation can be separated into three terms; that due to the walls above the corrugations  $\alpha_{wa}$ , that due to the walls within the corrugated region  $\alpha_{wb}$ , and that due to the corrugations themselves  $\alpha_c$ ; that is

$$\alpha = \alpha_{wa} + \alpha_{wb} + \alpha_c . \quad (6.138)$$

The first term may be obtained from (6.114) and (6.117), using (6.137) then

$$\alpha_{wa} = \frac{P_a}{2P} ;$$

that is

$$\alpha_{wa} = \frac{R_s H'_0 H'_0^* k_{y0}^2 (\alpha_{x0}^2 + k_{z0}^2) e^{-2\alpha_{x0} a}}{4\alpha_{x0} (k^2 - k_{y0}^2)^2 \frac{\omega \mu k_{z0} H'_0 H'_0^* b e^{-2\alpha_{x0} a}}{8\alpha_{x0} (k^2 - k_{y0}^2)}} .$$

Simplifying yields

$$\alpha_{wa} = \frac{2R_s k_{y0}^2 (\alpha_{x0}^2 + k_{z0}^2)}{\omega \mu b k_{z0} (k^2 - k_{y0}^2)} ,$$

and in terms of p and q it becomes

$$\alpha_{wa} = \frac{2R_s k^2 q^2 [p^2 + (\frac{k_{z0}}{k})^2]}{\omega \mu k_{z0} b (1 - q^2)} .$$

Substituting (6.136) for  $k_{z0}$  then yields

$$\alpha_{wa} = \frac{2R_s \omega \epsilon_0 \epsilon_r q^2 [2p^2 + 1 - q^2]}{kb(1 - q^2) \sqrt{p^2 + 1 - q^2}} . \quad (6.139)$$

The attenuation due to the walls within the corrugations may be calculated from (6.114) and (6.121), therefore

$$\alpha_{wb} = \frac{P_w}{2P} ;$$

that is

$$\alpha_{wb} = \frac{R_s d_0^2 k^2 [2ka - \sin(2ka)]}{8\omega^2 \mu^2 k \frac{\omega \mu k_{z0} H_0' H_0'^* b e}{8\alpha_{x0} (k^2 - k_{y0}^2)} e^{-2\alpha_{x0} a}}$$

Simplification yields this as

$$\alpha_{wb} = \frac{R_s k_{y0}^2 \alpha_{x0} (k^2 - k_{y0}^2) [2ka - \sin(2ka)]}{\omega^3 \mu^3 k_{z0} b e^{-2\alpha_{x0} a}} \left( \frac{d_0^2}{H_0' H_0'^*} \right)$$

Substituting (6.129) for the ratio of the square of the amplitude coefficients yields

$$\alpha_{wb} = \frac{R_s k_{y0}^2 \alpha_{x0} (k^2 - k_{y0}^2) [2ka - \sin(2ka)] \omega^2 \mu^2 s^2 \alpha_{x0}^2 k_{z0}^2 e^{-2\alpha_{x0} a}}{\omega^3 \mu^3 k_{z0} b e^{-2\alpha_{x0} a} 2 \sin^2(ka) (k^2 - k_{y0}^2)^2 [1 - \cos(k_{z0} s)]},$$

and simplifying,

$$\alpha_{wb} = \frac{R_s k_{y0}^2 k_{z0} \alpha_{x0}^3 s^2 [2ka - \sin(2ka)]}{2\omega \mu k_{z0} b \sin^2(ka) (k^2 - k_{y0}^2) [1 - \cos(k_{z0} s)]}$$

Substitution of (6.133), (6.135), and the definition of p and q yields

$$\alpha_{wb} = \frac{R_s q^2 k^2 k_{z0} s^2 p \{ 2ka[p^2 + (1-q^2)^2] - 2p(1-q^2) \}}{2\omega \mu b (1-q^2) [1 - \cos(k_{z0} s)]}$$

Simplification and substitution for  $k_{z0}$ , (6.136), it becomes

$$\alpha_{wb} = \frac{R_s k \omega \epsilon_0 \epsilon_r q^2 s^2 p \{ 2ka[p^2 + (1-q^2)^2] - 2p(1-q^2) \} \sqrt{p^2 + 1 - q^2}}{2b(1-q^2) [1 - \cos(ks \sqrt{p^2 + 1 - q^2})]}$$

(6.140)

Finally, the attenuation due to the corrugations can be calculated from (6.114) and (6.123), then

$$\alpha_c = \frac{P_c}{2P};$$

that is

$$\alpha_c = \frac{R_s k d_0^2 b [2ka + \sin(2ka)] e^{-2\alpha_{x0} a}}{16s\omega^2 \mu^2 \frac{\omega \mu k_{z0} H'_0 H'^*_{0'} b e^{-2\alpha_{x0} a}}{8\alpha_{x0} (k^2 - k_{y0}^2)}}$$

Simplifying yields

$$\alpha_c = \frac{R_s k [2ka + \sin(2ka)] \alpha_{x0} (k^2 - k_{y0}^2)}{2s\omega^3 \mu^3 k_{z0} e^{-2\alpha_{x0} a}} \left( \frac{d_0^2}{H'_0 H'^*_{0'}} \right),$$

and substitution of (6.129) into  $\alpha_c$ , becomes

$$\alpha_c = \frac{R_s k [2ka + \sin(2ka)] \alpha_{x0} (k^2 - k_{y0}^2) \omega^2 \mu^2 s^2 \alpha_{x0}^2 e^{-2\alpha_{x0} a} k_{z0}^2}{2s\omega^3 \mu^3 k_{z0} e^{-2\alpha_{x0} a} \sin^2(ka) (k^2 - k_{y0}^2)^2 2[1 - \cos(k_{z0} s)]}$$

Further simplification yields

$$\alpha_c = \frac{R_s k \alpha_{x0}^3 k_{z0} [2ka + \sin(2ka)]}{4\omega \mu \sin^2(ka) (k^2 - k_{y0}^2) [1 - \cos(k_{z0} s)]}$$

Substitution of (6.133), (6.135), and (6.136), in terms of p and q into  $\alpha_c$ , it becomes

$$\alpha_c = \frac{R_s k \omega \epsilon_0 \epsilon_r s p \{ 2ka[p^2 + (1-q^2)^2] + 2p(1-q^2) \} \sqrt{p^2 + 1 - q^2}}{4(1-q^2)[1 - \cos(ks \sqrt{p^2 + 1 - q^2})]}$$



Equation (6.132) can now be substituted for  $k_a$ , eliminating the  $a$ -dependency; that is

$$\alpha_c = \frac{R_s k w \epsilon_0 \epsilon_r p s \sqrt{p^2 + 1 - q^2}}{4(1-q^2)} \cdot \frac{\{ 2[p^2 + (1-q^2)^2] \tan^{-1}\left(\frac{p}{1-q^2}\right) + 2p(1-q^2) \}}{1 - \cos(ks \sqrt{p^2 + 1 - q^2})} . \quad (6.141)$$

The total attenuation is now the sum of (6.139), (6.140) and (6.141). Equation (6.141) may be compared with the attenuation for an infinite corrugated wave guide, Section 4, as  $b$  becomes infinite the two attenuations become identical; further, (6.139) and (6.140) become zero as expected.

### 6.13 Group Velocity

The group velocity of a wave traveling in the  $z$ -direction is given by

$$v_g = \frac{\partial \omega}{\partial k_z} , \quad (6.142)$$

which may be written

$$\frac{1}{v_g} = \frac{\partial k_z}{\partial \omega} . \quad (6.143)$$

Equation (6.136) then specifies

$$\frac{1}{v_g} = \frac{\partial}{\partial \omega} [ k \sqrt{p^2 + 1 - q^2} ] . \quad (6.144)$$

Differentiating this yields

$$\frac{1}{v_g} = \frac{k}{2} \frac{1}{\sqrt{p^2 + 1 - q^2}} \frac{\partial}{\partial \omega} (p^2 + 1 - q^2) , \quad (6.145)$$

and simplifying

$$\frac{1}{v_g} = \frac{k_p}{\sqrt{p^2 + 1 - q^2}} \frac{\partial p}{\partial \omega}, \quad (6.146)$$

(6.89) can be written in terms of  $p$  and  $q$  as

$$p = (1 - q^2) \tan(ka). \quad (6.147)$$

Differentiating (6.147) yields

$$\frac{\partial p}{\partial \omega} = -2q \frac{\partial q}{\partial \omega} \tan(ka) + (1 - q^2) \sec^2(ka) \frac{\partial(ka)}{\partial \omega}, \quad (6.148)$$

since

$$q = \frac{k_y}{k}.$$

Then

$$\frac{\partial q}{\partial \omega} = \frac{-k_y}{\sqrt{\mu \epsilon}} \frac{1}{\omega^2}$$

and

$$\frac{\partial(ka)}{\partial \omega} = a \sqrt{\mu \epsilon}.$$

Equation (6.148) then becomes

$$\frac{\partial p}{\partial \omega} = \frac{2q^2}{\omega} \tan(ka) + (1 - q^2) \sec^2(ka) a \sqrt{\mu \epsilon};$$

simplifying,

$$\frac{\partial p}{\partial \omega} = \frac{2q^2}{\omega} \tan(ka) + \frac{(1 - q^2)a}{c} \frac{1}{\cos^2(ka)}. \quad (6.149)$$

The group velocity, (6.146), now becomes

$$\frac{1}{v_g} = \frac{k_p}{\sqrt{p^2 + 1 - q^2}} \left[ \frac{2q^2}{\omega} \tan(ka) + \frac{(1 - q^2)a}{c} \frac{1}{\cos^2(ka)} \right]. \quad (6.150)$$

6.14 Numerical Results6.14.1 Introduction

The attenuations  $\alpha_{wa}$ ,  $\alpha_{wb}$ , and  $\alpha_c$ , as well as the total attenuation, are calculated for various values of  $p$ , the normalized x-decay constant. The periodic plate spacing,  $s$ , is varied from one-tenth to six-tenths wavelength at the four frequencies considered, 10, 35, 70, and 150 GHz.

A computer program was written to facilitate the computations. The computer used was an IBM System/360 Model 30 and the language, Fortran IV. The program is given below along with a flow chart, and the numerical results in Figures (6.2) through (6.12).

6.14.2 Computer Program

```

S.0001      DIMENSION ALPHA(55),ALFWA(55),ALFWB(55),ALFC(55),ALFWC(55),
            *XNLAM(55)
            C   CORRUGATED H-GUIDE ATTENUATION
            C
            C---DEFINE VARIABLES---
            C   F=FREQUENCY IN GIGAHERTZ
            C   RS=SURFACE RESISTIVITY (TO BE MULTIPLIED BY 1.E-07*SQRT OF F)
            C   P=NORMALIZED DECAY CONSTANT IN X-DIRECTION--ALPHA/XK
            C   XK=OMEGA*SQRT(MU*EPSILON)
            C   B=WALL SEPARATION IN CENTIMETERS
            C   Q=NORMALIZED PROPAGATION CONSTANT IN Y-DIRECTION--XKYO/XK
            C   XKYO=PROPAGATION CONSTANT IN Y-DIRECTION--PI/B
S.0002      PI=3.1415926536
            C   S=PERIOD OF WAVE GUIDE
            C   A=HALF HEIGHT OF CORRUGATIONS
            C   XLAM IS WAVELENGTH, XNLAM(I) IS NUMBER OF WAVELENGTHS TAKEN FOR S
            C
            C   GET DATA
            C
S.0003      1 READ(1,100)P,F,B,RS
S.0004      100 FORMAT(4F10.5)
            C
            C   CALCULATE XKS--(XK SQUARED) AND XK
S.0005      XKS=(4./9.)*PI*PI*F*F*(1.E+02(
S.0006      XK=SQRT(XKS)
            C
            C   CALCULATE Y-PROPAGATION CONSTANT KYKO
S.0007      XKYO=PI/(B*(1.E-02))

```

```

C
C   CALCULATE Q
S.0008   Q=XKYO/XK
C
C
C   CALCULATE ONE HALF THE HEIGHT OF THE CORRUGATIONS A
S.0009   A=ATAN(P/(1.-Q*Q))/XK
C
C   ADJUST RS TO ACTUAL VALUE
S.0010   RS=RS*(1.E-07)*SQRT(F*(1.E+09))
C
C   CALCULATE Z-PROPAGATION CONSTANT---XKZO---
S.0011   XKZO=XK*SQRT(P*P+1.-Q*Q)
C
C   CALCULATE X-DECAY CONSTANT---ALFXO---
S.0012   ALFXO=XK*P
C
C   DEFINE EPSILON---EPSIL
S.0013   EPSIL=(1./(36.*PI))*(1.E-09)
C
C   DEFINE MU (XMU)
S.0014   XMU=4.*PI*(1.E-07)
C
C   CALCULATE FREE SPACE WAVELENGTH
S.0015   XLAMF=(3.E+08)/(F*(1.E+09))
C
C   CALCULATE GUIDE WAVELENGTH AND PHASE VELOCITY
S.0016   XLAMG=2.*PI/XKZO
S.0017   VPHAS=F*(1.E+09)*XLAMG
C
C   CALCULATE GROUP VELOCITY   VGRP=1./(X*(Y+Z))
S.0018   X=XK*P/SQRT(P*P+1.-Q*Q)
S.0019   Y=2.*Q*Q*(SIN(XK*A)/COS(XK*A))/(2.*PI*F*(1.E+09))
S.0020   Z=(1.-Q*Q)*A/(COS(XK*A)*COS(XK*A)*(3.E+08))
S.0021   VGRP=1./(X*(Y+Z))
C
C
C   CALCULATE ALFWA(1)---UPPER WALL ATTENUATION---ALFWA(1)=X*Y/Z
S.0022   X=RS*Q*Q
S.0023   Y=2.*P*P+1.-Q*Q
S.0024   Z=B*SQRT(XMU/EPSIL)*SQRT(P*P+1.-Q*Q)*(1.-Q*Q)*(1.E-02)
S.0025   ALFWA(1)=X*Y/Z

```

```

C
C PRINT OUT PARAMETERS WHICH ARE NOT DEPENDENT UPON S(1)
C
S.0026 WRITE(3,101)P,F,B,A
S.0027 101 FORMAT('1','P=',F4.3,2X,'F=',F9.4,1X,'GHZ',4X,'SIDEWALL SPACING=',
      *F6.4,1X,'CM',16X,'ONE HALF CORRUGATION HEIGHT=',E15.8,1X,'METERS')
S.0028 WRITE(3,208)VPHAS,VGRP
S.0029 208 FORMAT(1X,'PHASE VELOCITY=',1X,E15.8,3X,'METERS PER SECOND',15X,
      *'GROUP VELOCITY=',1X,E15.8,1X,'METERS PER SECOND')
S.0030 WRITE(3,207)XLAMF,XLAMG
S.0031 207 FORMAT(1X,'FREE SPACE WAVELENGTH=',1X,E15.8,3X,'METERS',19X,
      *'GUIDE WAVELENGTH=',1X,E15.8,3X,'METERS')
S.0032 WRITE(3,201)RS,ALFXO
S.0033 201 FORMAT(' ','SURFACE RESISTANCE=',E15.8,2X,'OHMS PER SQUARE',15X,
      *'X-DECAY CONSTANT=',E15.8,2X,'RADIANS PER METER')
S.0034 WRITE(3,202)XKYO,XKZO
S.0035 202 FORMAT(' ','Y-PROPAGATION CONSTANT=',E15.8,2X,'RADIANS PER METER',
      *9X,'Z-PROPAGATION CONSTANT=',E15.8,2X,'RADIANS PER METER')
S.0036 WRITE(3,210)ALFWA(1)
S.0037 210 FORMAT(1X,35X,'UPPER WALL ATTENUATION=',1X,E15.8,3X,
      *'NEPERS PER METER')

C
C ADJUST F TO ACTUAL VALUE
C
S.0038 F=F*(1.E+09)

C
C ADJUST B TO ACTUAL VALUE
C
S.0039 B=B*(1.E-02)

C
C ESTABLISH DO LOOP FOR VARYING S FROM .1 LAMBDA TO .5 LAMBDA IN 50 STEPS
C
C
S.0040 DO 10 I=1,50
S.0041 VAR=I
S.0042 VAR=VAR*.01
S.0043 XLAM=(.3E+09)/F
S.0044 XNLAM(I)=(.09+VAR)
S.0045 S(I)=XNLAM(I)*XLAM

C
C CALCULATE ALFWB(I)---LOWER WALL ATTENUATION---ALFWB(I)=X*Y/Z
C
S.0046 X=RS*2.*PI*F*EPSIL*XK*Q*Q*S(I)*S(I)*P
S.0047 Y=SQRT(P*P+1.-Q*Q)
S.0048 Y=Y*(2.*XK*A*(P*P+(1.-Q*Q)*(1.-Q*Q))-2.*P*(1.-Q*Q))
S.0049 Z=B*(1.-Q*Q)*(1.-COS(XK*SQRT(P*P+1.-Q*Q)*S(I)))*2.
S.0050 ALFWB(I)=X*Y/Z

C
C CALCULATE ALFC(I)---ATTENUATION DUE TO CORRUGATIONS ALFC=U*V*(W+X)/Z
C

```

```

S.0051      U=RS*XK*2.*PI*F*EPSIL*P*S(I)/4.
S.0052      V=SQRT(P*P+1.-Q*Q)/(1-Q*Q)
S.0053      W=2.*XK*A*(P*P+(1.-Q*Q)*(1.-Q*Q))
S.0054      X=2.*P*(1.-Q*Q)
S.0055      Z=1.-COS(XK*SQRT(P*P+1.-Q*Q)*S(I))
S.0056      ALFC(I)=U*V*(W+X)/Z
           C
           C      CALCULATE TOTAL WALL ATTENUATION---ALFC(I)---
           C
S.0057      ALFC(I)=ALFWA(I)+ALFWB(I)
           C
           C      CALCULATE TOTAL ATTENUATION ALPHA(I)=ALFWA(I)+ALFWB(I)+ALFC(I)
           C
S.0058      10 ALPHA(I)=ALFWA(I)+ALFWB(I)+ALFC(I)
           C
           C      PRINT OUT TABLE HEADING
           C
S.0059      WRITE(3,103)
S.0060      103 FORMAT('0',13X,'PERIODIC PLATE SPACING',12X,
           *'LOWER WALL ATTN',7X,'TOTAL WALL ATTN',7X,
           *'CORRUGATION ATTN',9X,'TOTAL ATTN')
           C
S.0061      WRITE(3,104)
S.0062      104 FORMAT(1X,8X,'LAMBDA',16X,'METERS',11X,
           *'NEPERS PER METER',6X,'NEPERS PER METER',6X,
           *'NEPERS PER METER',6X,'NEPERS PER METER')
           C
           C
           C      PRINT OUT DATA
           C
S.0063      DO 20 I=1,50
S.0064      20 WRITE(3,105)XNLAM(I),S(I),ALFWB(I),ALFC(I),ALPHA(I)
S.0065      105 FORMAT(' ',3X,E15.8,5(7X,E15.8))
S.0066      GO TO 1
S.0067      STOP
S.0068      END

```

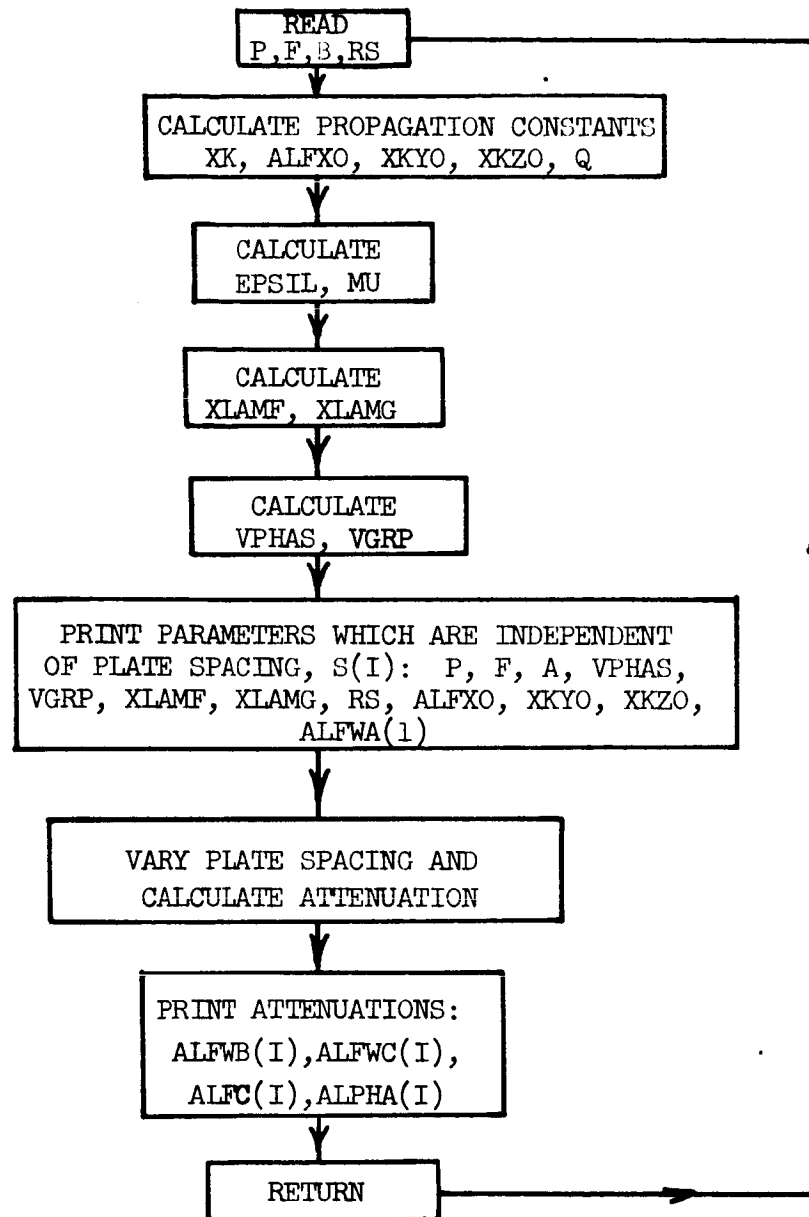


Figure 6.2 Flow chart

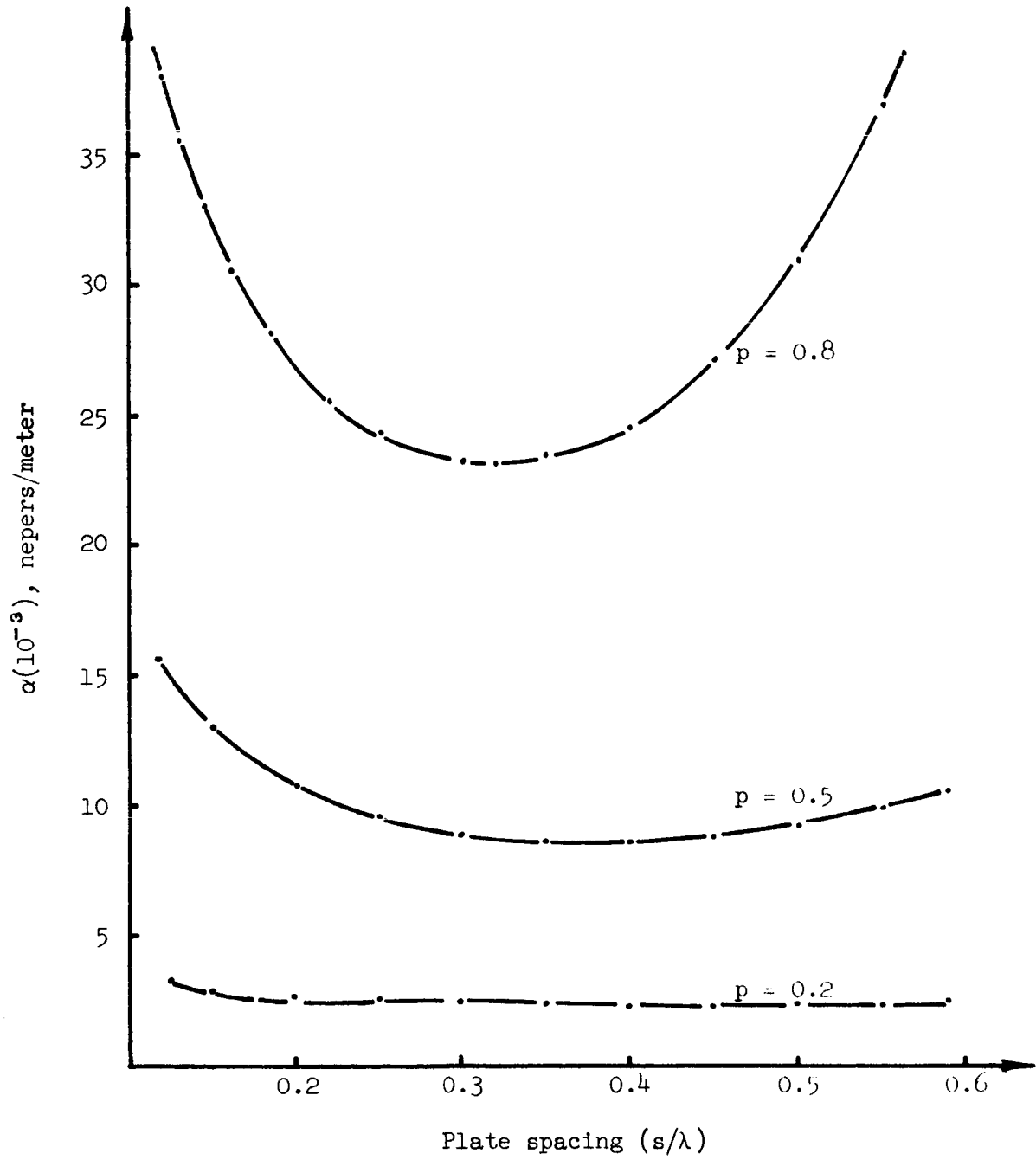


Figure 6.3 Attenuation of corrugated H-guide at 10 GHz with 2.286 cm sidewall spacing



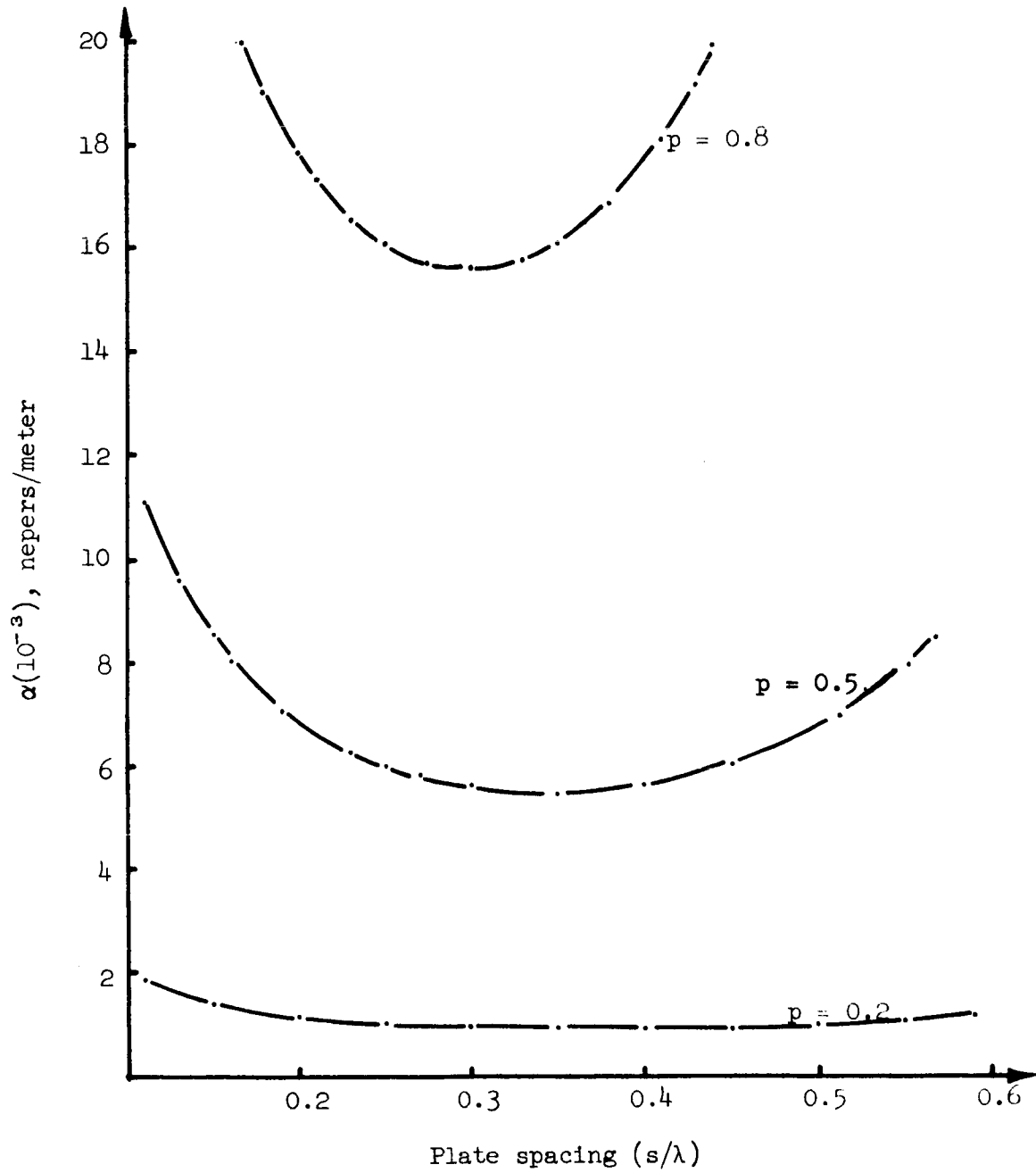


Figure 6.4 Attenuation of corrugated H-guide at 10 GHz with 4.572 cm sidewall spacing

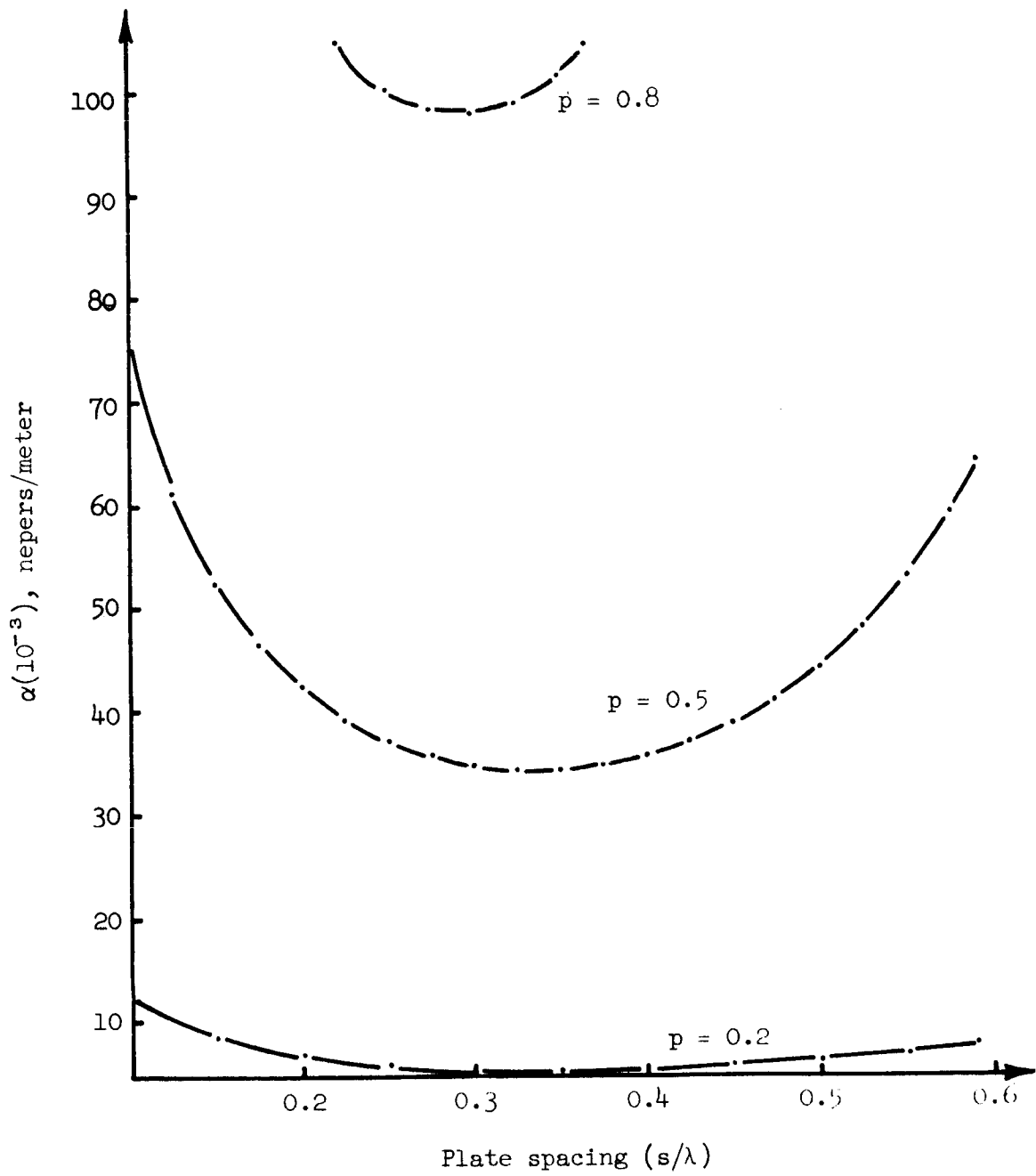


Figure 6.5 Attenuation of corrugated H-guide at 35 GHz with 2.286 cm sidewall spacing

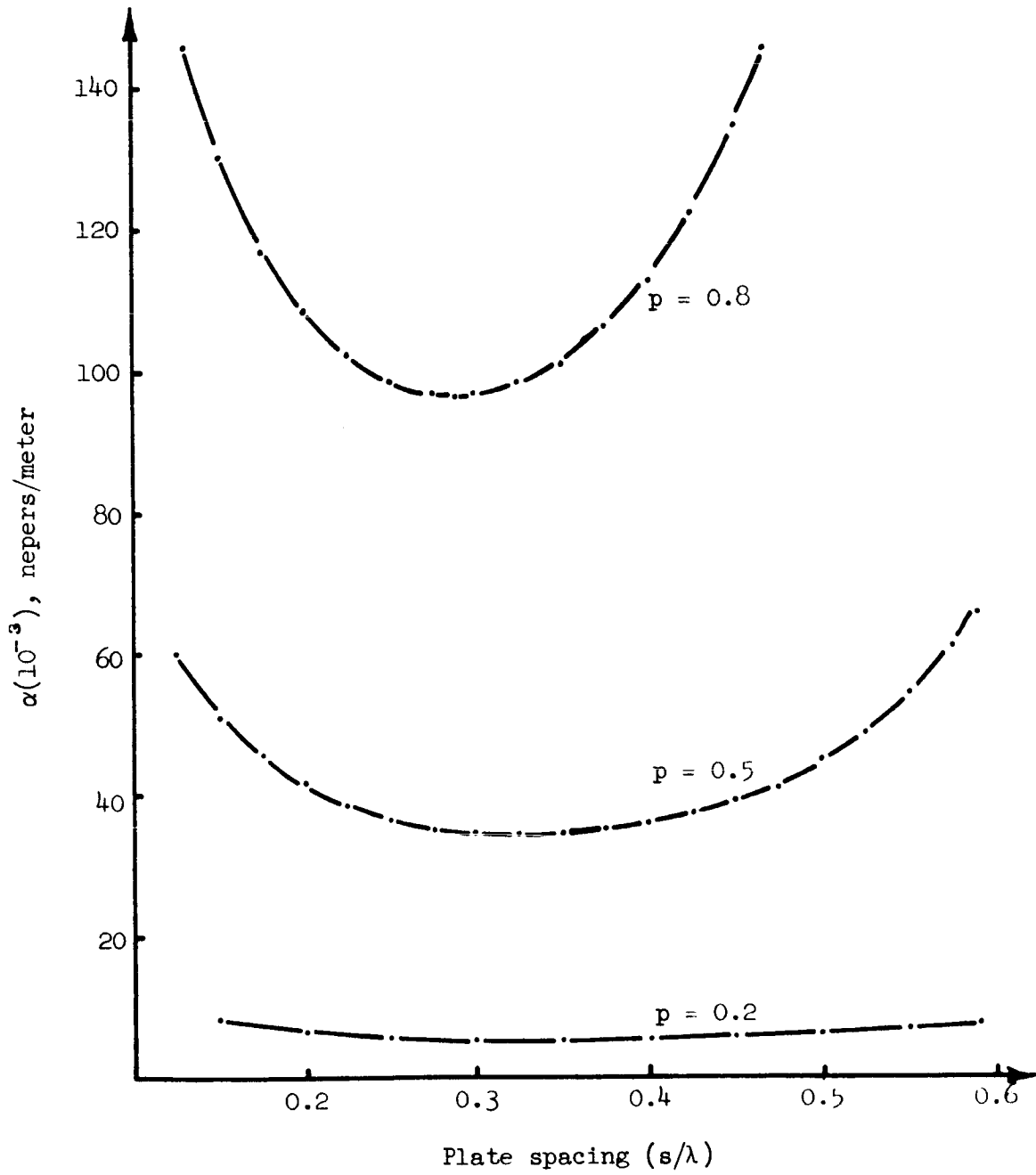


Figure 6.6 Attenuation of corrugated H-guide at 35 GHz with 4.572 cm sidewall spacing

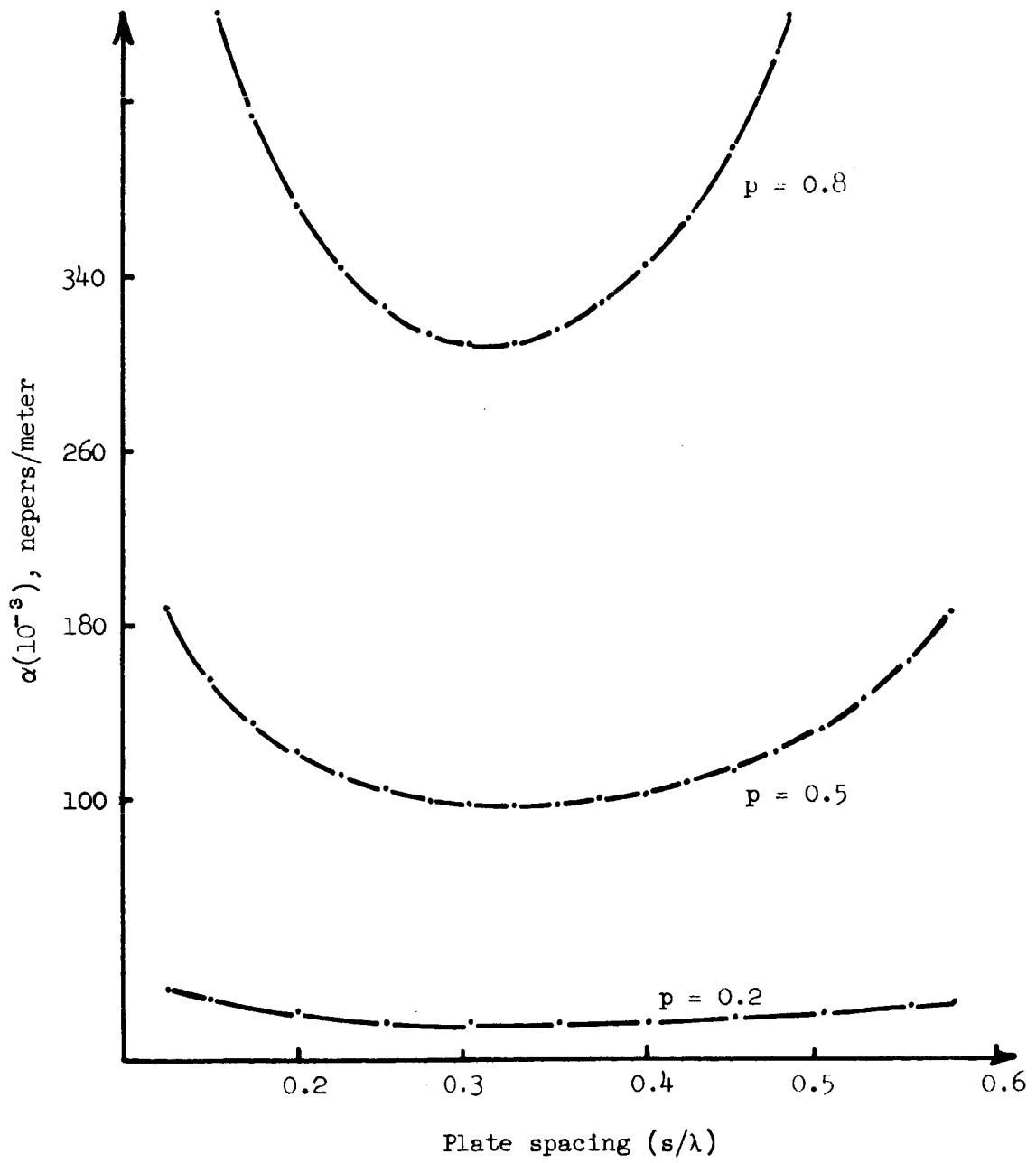


Figure 6.7 Attenuation of corrugated H-guide at 70 GHz with 2.286 cm sidewall spacing

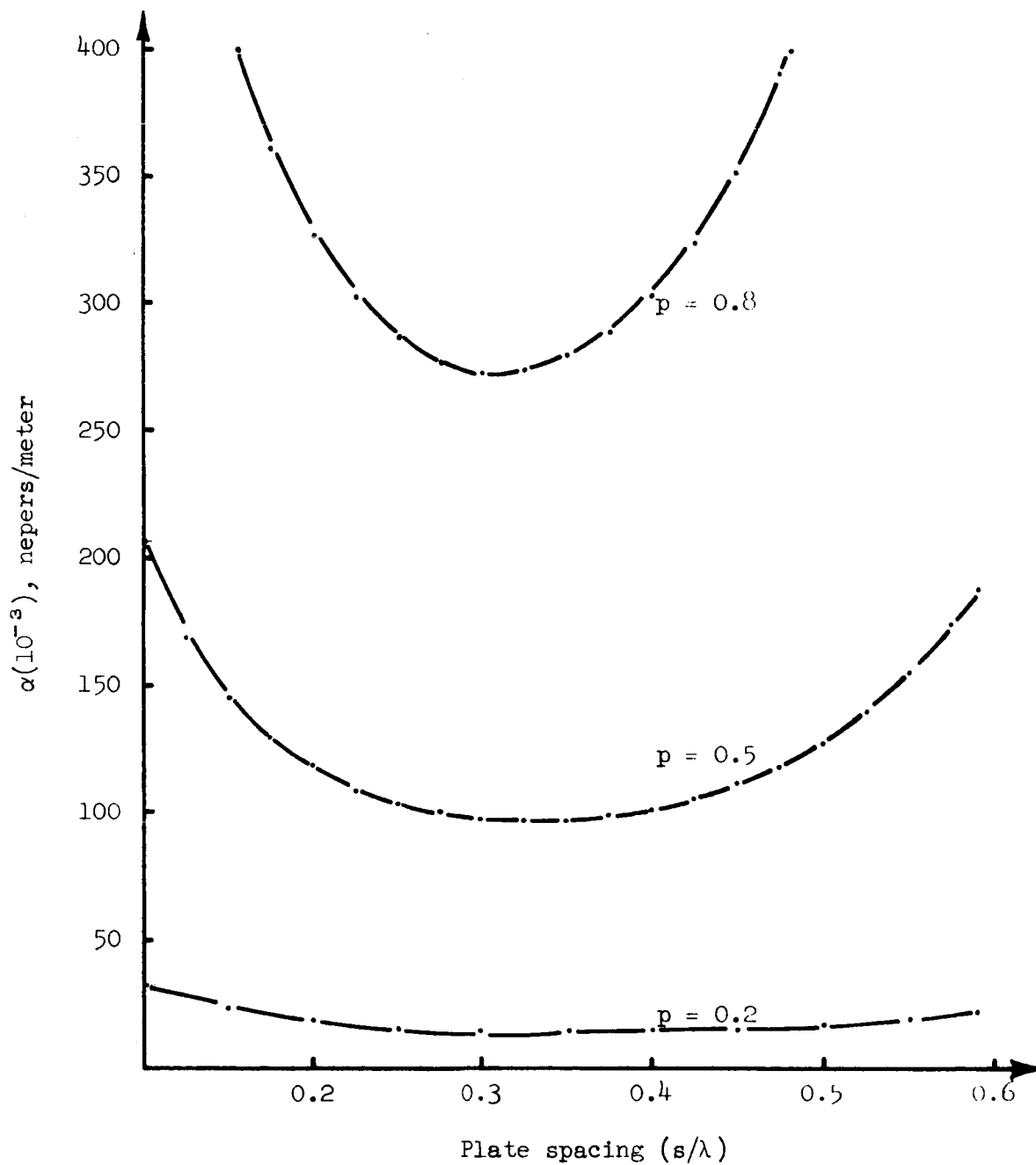


Figure 6.8 Attenuation of corrugated H-guide at 70 GHz with 4.572 cm sidewall spacing

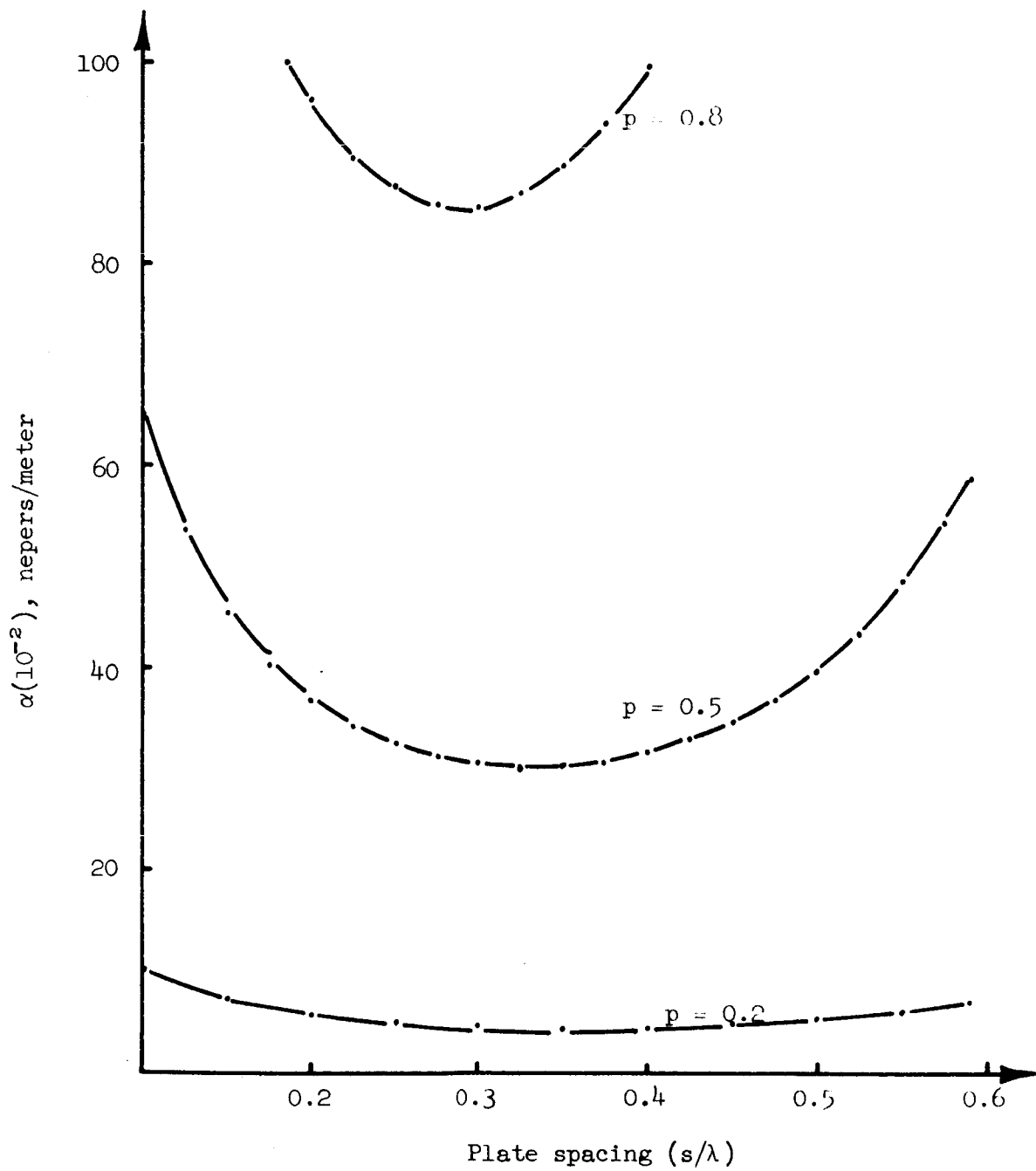


Figure 6.9 Attenuation of corrugated H-guide at 150 GHz with 2.286 cm or 2.572 cm sidewall spacing

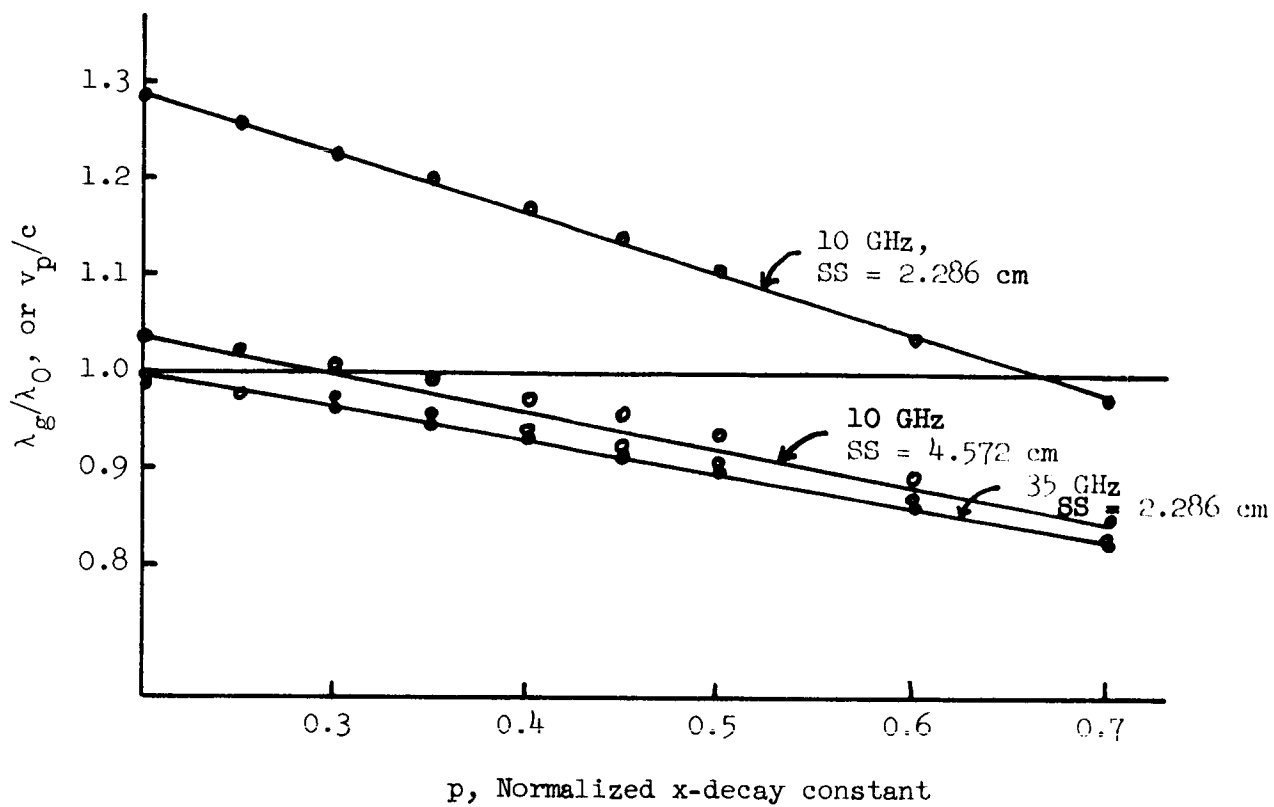


Figure 6.10 Normalized phase velocity or guide wavelength for the corrugated H-guide

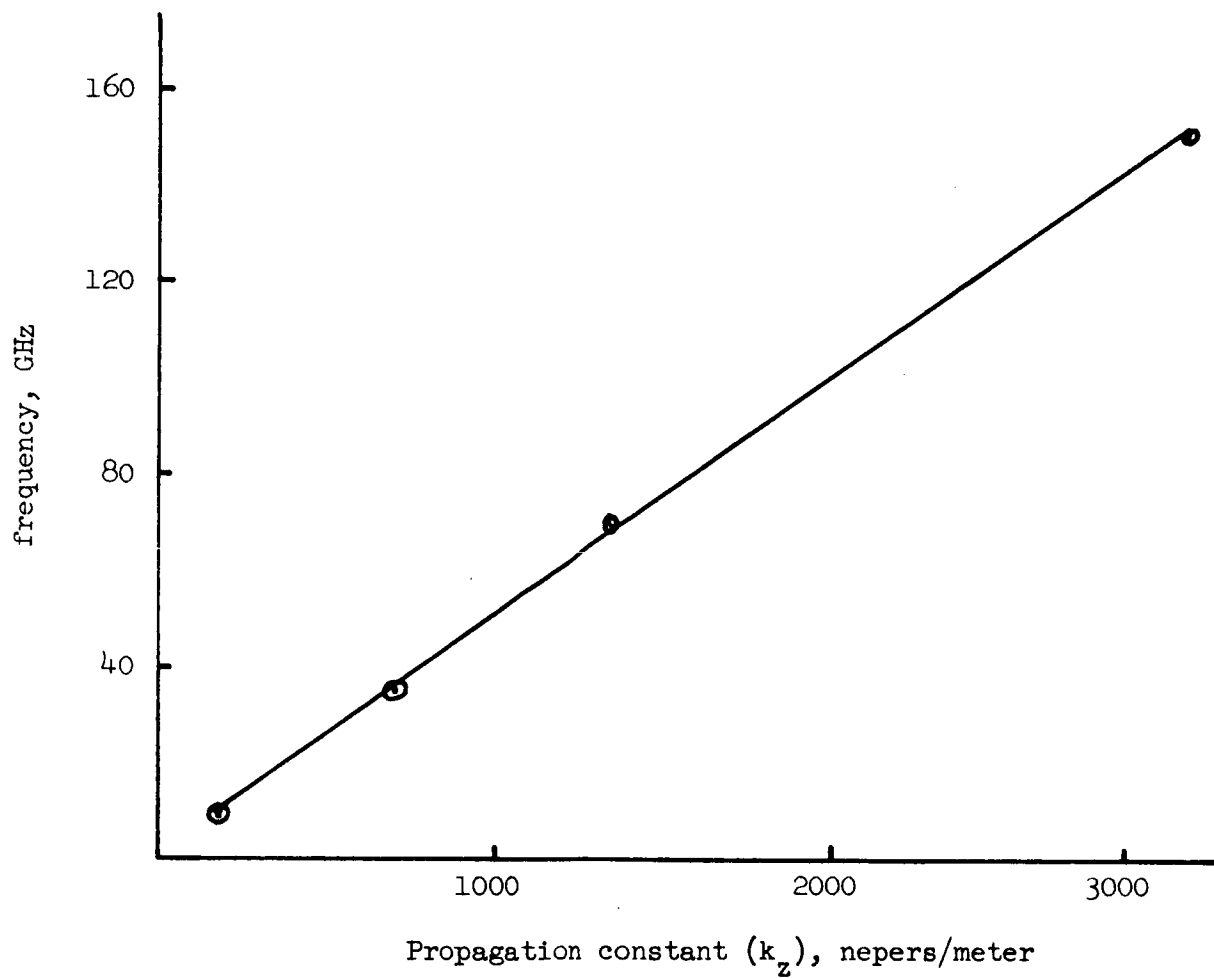


Figure 6.11 Omega-beta diagram for corrugated H-guide with  $p$ , a normalized x-decay constant of two-tenths and a sidewall spacing of 2.286 cm



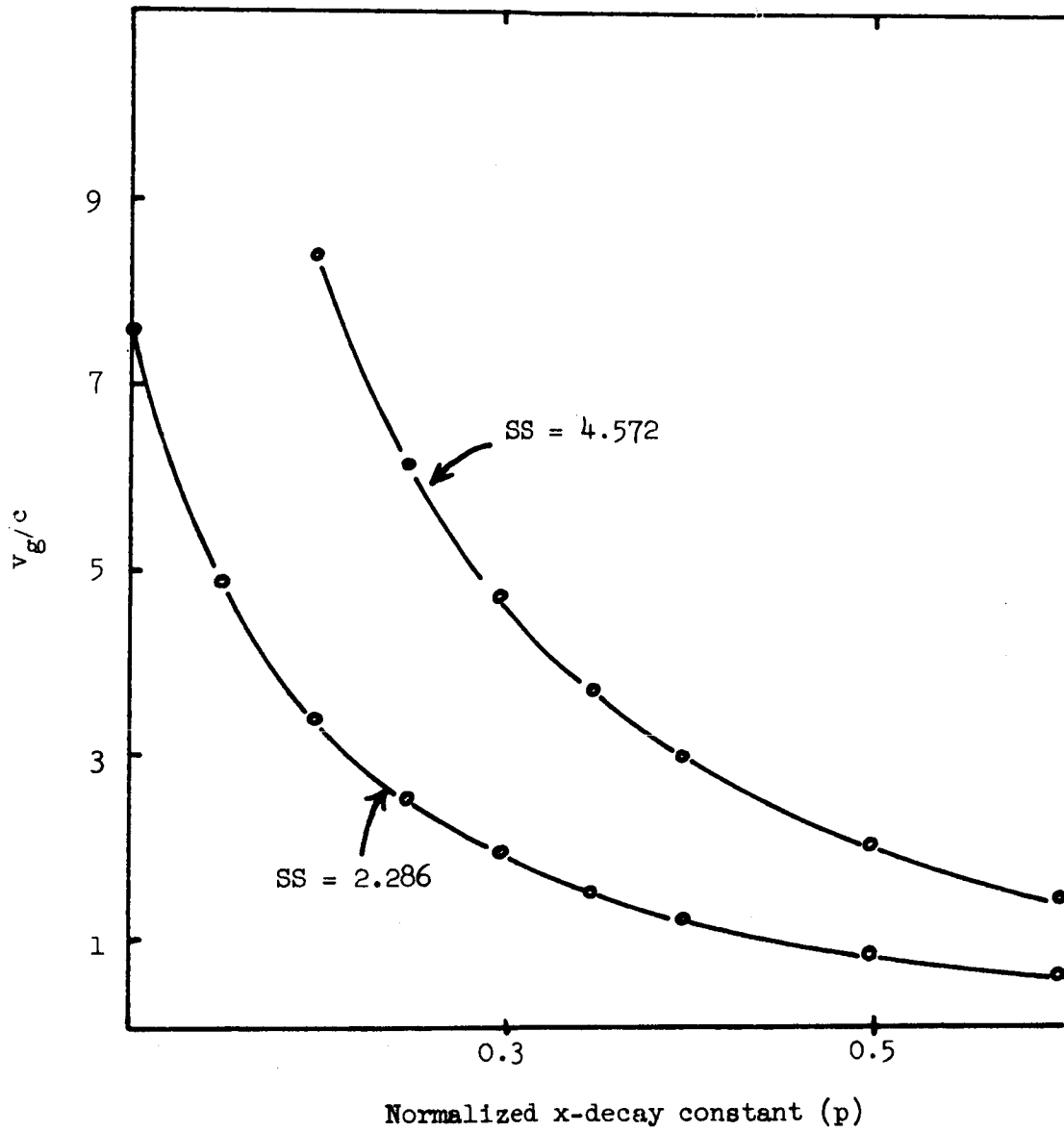


Figure 6.12 Normalized group velocity for corrugated H-guide at 10 GHz for two sidewall spacing (SS) values

## 7. COMPARISON OF ATTENUATIONS

7.1 Laminated Dielectric H-Guide

The attenuation for a dielectric H-guide ( $\alpha_{dH}$ ) will be considered in detail and some conclusions drawn on the minimization of the attenuation.

The attenuation is due to two sources, the dielectric, and the walls; it may be separated into two terms as

$$\alpha_{dH} = \alpha_d + \alpha_w ,$$

the subscripts referring to dielectric and wall respectively. The dielectric attenuation may be written in the form [see (5.85)]

$$\alpha_d = \tan(\delta) \frac{\epsilon_r[A - \epsilon_r]}{B[C + \epsilon_r(\epsilon_r - 1)]} , \quad (7.1)$$

where A, B, and C are independent of  $\epsilon_r$  and  $\tan(\delta)$ . This can be written in a further simplified form as

$$\alpha_d = \tan(\delta) \varphi(\epsilon_r) , \quad (7.2)$$

where

$$\varphi(\epsilon_r) = \frac{\epsilon_r[A - \epsilon_r]}{B[C + \epsilon_r(\epsilon_r - 1)]} . \quad (7.3)$$

It is now apparent that  $\alpha_d$  varies directly with  $\tan(\delta)$ ; further Figure 5.2 shows there is a minimum for  $\varphi(\epsilon_r)$  near  $\epsilon_r = 4$ . To minimize  $\alpha_d$ ,  $\epsilon_r$  should be chosen to be approximately four, and  $\tan(\delta)$ , should be minimized.

If the dielectric is laminated rather than solid, and yet has an equivalent relative permittivity of about four, the attenuation may be reduced. The laminations will need to have a relative permittivity greater than four to achieve this, which means generally that the loss tangent,  $\tan(\delta_{slab})$ , of each lamination will be greater than that of some solid

dielectric with  $\epsilon_r = 4$  and a loss tangent of  $\tan(\delta_4)$ . However, the equivalent loss tangent of the laminated structure,  $\tan(\delta_{eq.})$ , will be less than  $\tan(\delta_{slab})$ , and it may be possible to make  $\tan(\delta_{eq.})$  less than  $\tan(\delta_4)$ . If this is possible, then the laminated structure will have all of the necessary properties of the optimum solid dielectric and will have a smaller value for the loss tangent.

The case for a laminated dielectric in a static electric field considering only normal components has been examined by C. W. Bostian.<sup>3</sup> The optimum material for this application seems to be Eccoceram Hi K [ $\epsilon_r = 90$ ,  $\tan(\delta) = 0.001$ ].<sup>4</sup> The relative permittivity and loss tangent for various common materials appear in Table 7.1.

For the desired equivalent permittivity of four, an equivalent loss tangent of 0.000035 can be obtained. This represents a reduction in the loss tangent of about twenty [assuming  $\tan(\delta) = 0.0007$  originally].

If this analysis were exact, then the dielectric attenuation would be reduced by a factor of twenty. However, the analysis considers only the normal electric component, and in the case of an H-guide there exist tangential components also. The assumption will be made that the attenuation due to these components is not reduced significantly. It, therefore, seems reasonable in this approximation to let the reduction in the loss tangent be a factor of seven, since only one-third of the total electric field experiences a reduction. It was found that  $\alpha_d$  and  $\alpha_w$  are different by a

---

<sup>3</sup>F. J. Tischer, Principal Investigator (C. W. Bostian, Instructor; Roy Propst, Graduate Assistant), May 15, 1967. NASA Progress Report on Study of Rectangular-Guide-Like Structures for Millimeter Wave Transmission. NGR-34-002-047. Department of Electrical Engineering, North Carolina State University, Raleigh, North Carolina.

<sup>4</sup>Emerson and Cumming, Inc., Canton, Massachusetts.

Table 7.1 Relative permittivity and loss tangent of several materials at 10 GHz

Material	Relative Permittivity	Loss Tangent (to be multiplied by $10^{-4}$ )
Styrofoam	1.03	1.5
Teflon <sup>a</sup>	2.08	3.7
Polystyrene	2.54	4.3
Rexolite <sup>b</sup>	2.54	6.6
Formica <sup>c</sup>	3.90	45.0
Pyrex glass <sup>d</sup>	4.80	98.0
Water (25° C)	55.00	5400.0
Eccoceram <sup>b</sup> Hi K	90.00	10.0

<sup>a</sup>E. I. Du Pont de Nemours and Co., Inc., Wilmington, Delaware.

<sup>b</sup>Emerson and Cumming, Inc., Canton, Massachusetts.

<sup>c</sup>The Formica Company, Cincinnati, Ohio.

<sup>d</sup>Corning Glass Works, Corning, New York.

factor of ten at 10 GHz for a sidewall spacing of 2.286 cm. Let this value of attenuation be  $D$ ; that is

$$\alpha_d = 10 \alpha_w = D, \quad (7.4)$$

which means the total attenuation is given by

$$\alpha_{dH} = 10 D + D. \quad (7.5)$$

Let  $\alpha_{dHl}$  denote the attenuation for the laminated H-guide. It was seen above that the dielectric attenuation was reduced by a factor of seven; therefore

$$\alpha_{dHl} = \frac{10}{7} D + D. \quad (7.6)$$

It follows that

$$\alpha_{dHl} = \frac{17}{77} \alpha_{dH}, \quad (7.7)$$

thus, yielding a reduction in total attenuation of about four and one-half.

### 7.2 A Comparison of Three H-Guides with the Rectangular Wave Guide

The attenuation for three H-guides (dielectric, corrugated, and laminated dielectric) has been obtained. A comparison of the attenuations can be made for a fixed value of: sidewall spacing (2.286 cm.), normalized x-decay constant ( $p = 0.2$ ), and frequency (10 GHz). This particular value of  $p$  corresponds to a field which decays by ninety percent, in a distance of five centimeters from the dielectric at the above frequency. The value of attenuation chosen will be that which is minimum in each case for the given value of  $p$ .

The values of attenuation for the dielectric and corrugated H-guides can be found directly from the curves provided in the respective sections; that of the laminated dielectric H-guide can be found from (7.7). The results are shown in Table 7.2.

Table 7.2 Attenuation for various wave guides at 10 GHz

Wave guide type	Attenuation (nepers per meter)
Rectangular (standard X-band)	$12 \times 10^{-3}$
H-guide (dielectric)	$5 \times 10^{-3}$
H-guide (laminated dielectric)	$1 \times 10^{-3}$
H-guide (corrugated)	$2 \times 10^{-3}$

## 8. EXPERIMENTAL PROCEDURES AND RESULTS

### 8.1 Introduction

The properties of surface wave guide structures can be determined by different techniques: such as, direct measurement of the structure under operational conditions or measurement of the characteristics of various types of modes when the structure is enclosed in a cavity. The cavity method offers some advantages in that probes and the change in the field due to the insertion of a probe for measurements are eliminated; further, the structure is isolated from external fields. As a first step, a test cavity, which can later be converted into a shorted section of the H-guide, must be thoroughly analyzed and pertinent parameters determined. The parameters are the resonant frequencies of the various possible modes (which may interfere with the desired mode), the frequency shifting due to various types of loading, and the Q-values of the modes.

### 8.2 Description of the Test Cavity

The rectangular cavity considered is of the transmission type coupled by circular irises between two sections of rectangular wave guide (Figure 8.1).

The inside width of the cavity was made equal to the inside width of standard X-Band wave guide (RG 52/U) to insure that only modes of one-half period sinusoidal variation in that direction would be present. The inside height was four inches and the longitudinal length six.

Coupling to the wave guide was accomplished by circular irises centered in the wave guide cross-section; hence, centered in the cavity end plates. During all of the measurements, irises of one-quarter inch diameter were

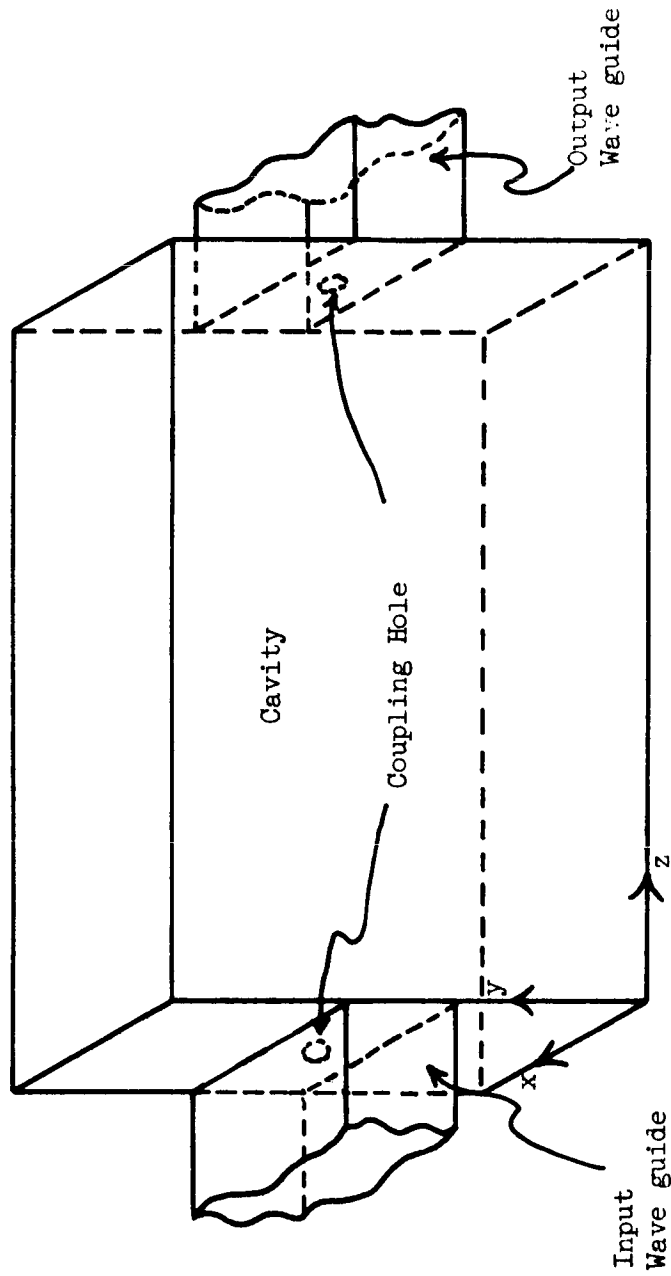


Figure 8.1 Test cavity

used since smaller diameters increase the insertion loss to an extent that the signal amplitude has approximately the amplitude of the noise level.

The cavity was constructed of one-half inch thick brass sides and one-quarter inch thick brass end plates having 0.050 inch thick inserts for changing the size of the coupling iris; the entire assembly was electroplated with several ten-thousandths thickness of silver. A detailed view of one end can be seen in Figure 8.2, the other end being identical.

### 8.3 Determination of the Resonant Frequencies for the Empty Cavity

The solution of the Maxwell equations within a closed uniform region, upon separation of variables, yields a relationship between the propagation constants as

$$k^2 = k_x^2 + k_y^2 + k_z^2, \quad (8.1)$$

where

$$k^2 = (2\pi f)^2 \mu_0 \epsilon_0 \epsilon_r, \quad (8.2)$$

and the remaining terms the squares of the propagation constants in the subscripted directions. Boundary conditions for a rectangular cavity admit only sinusoidal solutions which means that (8.1) becomes

$$f_{imn} = \frac{1}{2\pi\sqrt{\mu_0\epsilon_0}\sqrt{\epsilon_r}} \left[ \left(\frac{i\pi}{a}\right)^2 + \left(\frac{m\pi}{b}\right)^2 + \left(\frac{n\pi}{d}\right)^2 \right]^{\frac{1}{2}}, \quad (8.3)$$

where  $n, m, i = 0, 1, 2, \dots$ , and  $a, b$ , and  $d$  are the dimensions of the cavity. It can be seen that  $n, m$ , and  $i$  describe the number of half sinusoidal variations in their respective directions. For the cavity under consideration, and for the unloaded case

$$f_{imn} = \frac{3 \times 10^{10}}{2\pi} \left[ 1.893 + \left(\frac{m\pi}{4 \times 2.54}\right)^2 + \left(\frac{n\pi}{6 \times 2.54}\right)^2 \right]^{\frac{1}{2}}, \quad (8.4)$$



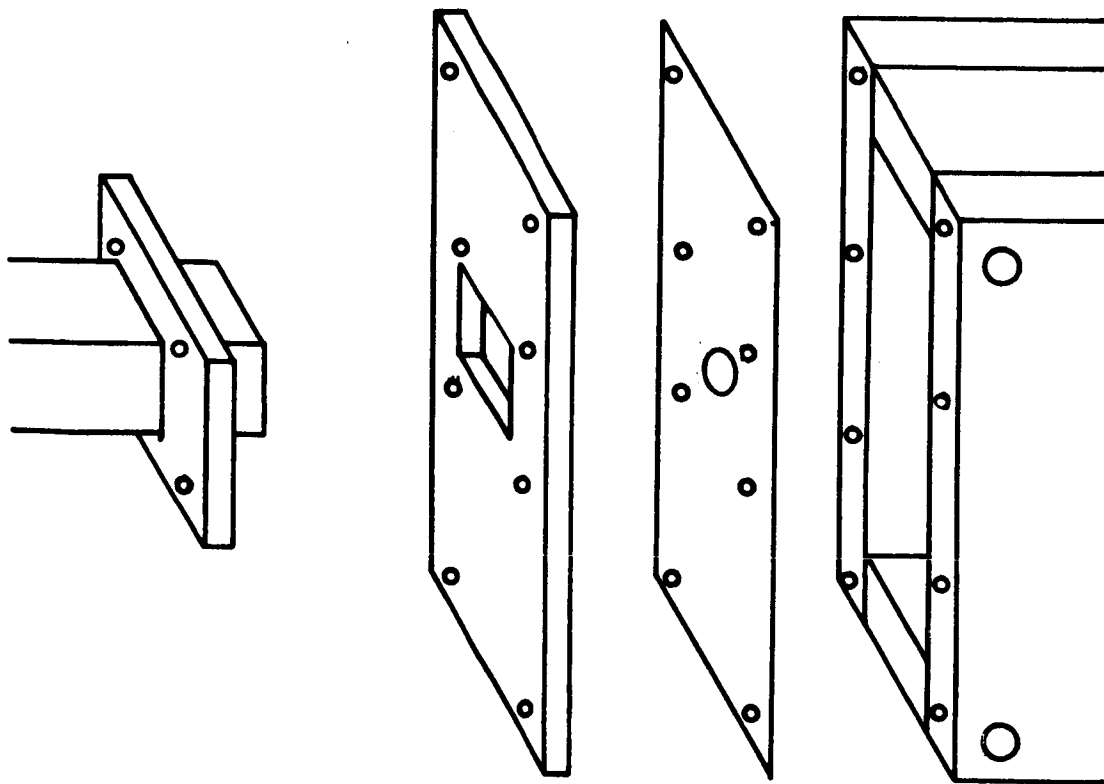


Figure 8.2 Assembly view of test cavity end section

since

$$\frac{1}{\sqrt{\mu_0 \epsilon_0}} \approx 3 \times 10^{10} \frac{\text{cm}}{\text{sec}} .$$

It is now possible to calculate all of the possible modes for the cavity. The frequency range shall be limited to 9.0 to 11.0 GHz. The results are tabulated in Table 8.1 along with the measured values. Only the modes with even numbers in the vertical direction appear in the table since the odd modes were not assumed to be excited, due to the excitation discriminating against odd modes.

It should be noted that the measured values are lower than the calculated values. This may be due to several causes: first, the velocity of light was approximated to facilitate calculations; second, losses within the cavity walls and the coupling irises will tend to lower the resonant frequencies; and third, a very slight error was made in the measurement of the cavity width (0.005 inches), implying the value 1.893 should be a small amount less. The average deviation is approximately 30 MHz.

Table 8.1 Frequencies of cavity modes

Mode TE	Calculated frequency (GHz)	Measured frequency (GHz)
107	9.515	9.502
108	10.250	10.220
109	11.030	11.000
126	9.327	9.295
127	9.955	9.944
128	10.650	10.635
142	9.020	9.032
143	9.320	9.295
144	9.690	9.651
145	10.100	10.080
146	10.615	10.580

#### 8.4 Determination of the Resonant Frequencies of the Dielectric-Loaded Cavity

In the case of a fully loaded cavity, (8.3) shows that the mode frequencies will be decreased by  $\sqrt{\epsilon_r}$ ; that is, all frequencies will be decreased by the same amount.

If the cavity is partially loaded, then the exact frequency shift determination becomes quite difficult; however, the problem may be approximated in the following manner. A typical cross-section of the loading to be considered is shown in Figure 8.3. To a first approximation, it appears that the dielectric affects primarily the x-variation of the field; in fact, the dielectric may be considered to increase the x-dimension by an amount  $(\sqrt{\epsilon_r} - 1)D$ , where  $D$  is the thickness of the dielectric. Equation (8.3) may be utilized, simply replacing  $b$  by  $b + (\sqrt{\epsilon_r} - 1)D$ . The results of the calculations for the even modes appear in Table 8.2.

Table 8.2 Frequencies of cavity modes with central slab loading

Cavity Loading	TE Mode	Calculated Frequency (GHz)
1/8" Rexolite 1422 slab in center of cavity $\epsilon_r = 2.53$ $\tan(\delta) = 0.00066$	126	9.290
	127	9.947
	128	10.620
	143	9.120
	144	9.515
	145	9.968
	146	10.490
1/4" Rexolite 1422 slab in center of cavity $\epsilon_r = 2.53$ $\tan(\delta) = 0.00066$	126	9.249
	127	9.890
	128	10.600
	143	9.005
	144	9.380
	145	9.810
	146	10.450

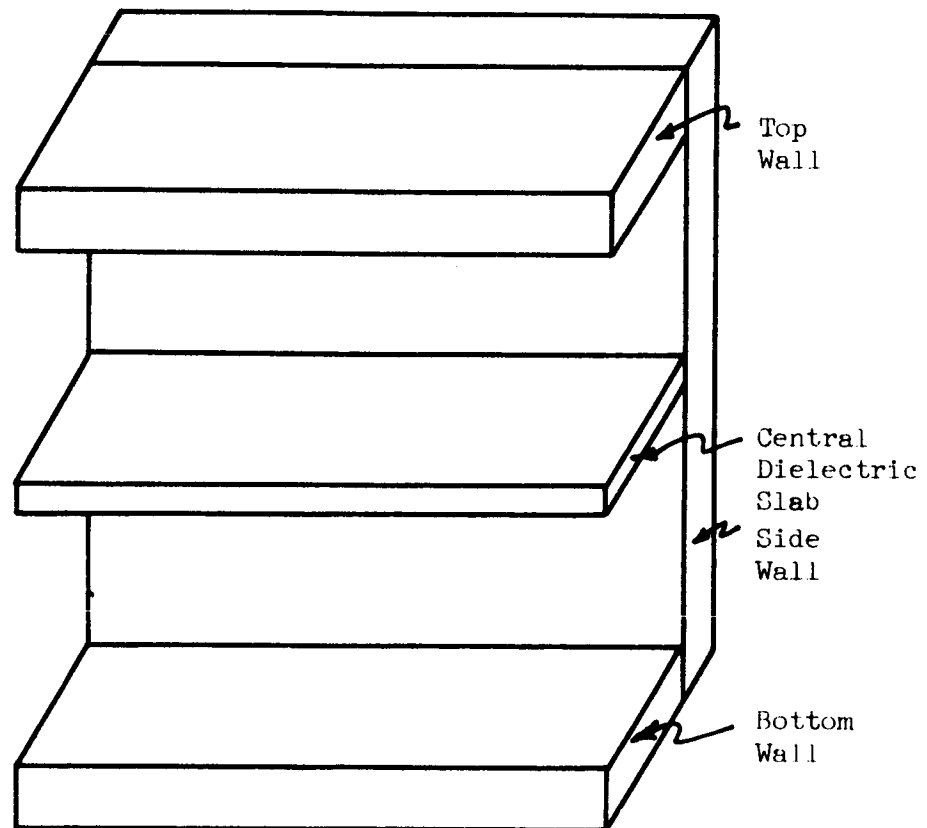


Figure 8.3 Cutaway view of test cavity with central dielectric loading

### 8.5 Excitation of Cavity Modes

The field configuration within the rectangular wave guide, which delivers energy to the cavity, is due only to the  $TE_{10}$  mode, all others being damped out since operation is not above the cutoff frequencies of the higher order modes. The field due to the  $TE_{10}$  mode is given by

$$E_y = E_0 \sin\left(\frac{\pi x}{a}\right),$$

$$H_x = \frac{E_0}{z_{TE}} \sin\left(\frac{\pi x}{a}\right),$$

and

$$H_z = \frac{jE_0 \lambda}{2a \eta} \cos\left(\frac{\pi x}{a}\right),$$

where

$$z_{TE} = \sqrt{1 - \left(\frac{\lambda}{2a}\right)^2} \eta$$

and

$$\eta = \sqrt{\frac{\mu}{\epsilon}}.$$

These are the only possible field components available for excitation of the cavity. Figure 8.4 shows the cross-sectional view of the cavity and wave guide located centrally about the iris. Boundary conditions require  $E_y$  and  $H_z$  to be zero on the wave guide end plate, leaving only the  $H_x$  component present there. If the assumption is made that the iris diameter is small enough not to appreciably disturb the field within the wave guide, within the iris itself only the  $H_x$  component will be present, since the field must be continuous. It now appears that only the  $H_x$  component of the wave guide field is present within the cavity region. Furthermore, there will be no  $E_z$  component excited within the cavity region under ideal conditions. The absence of the  $E_z$

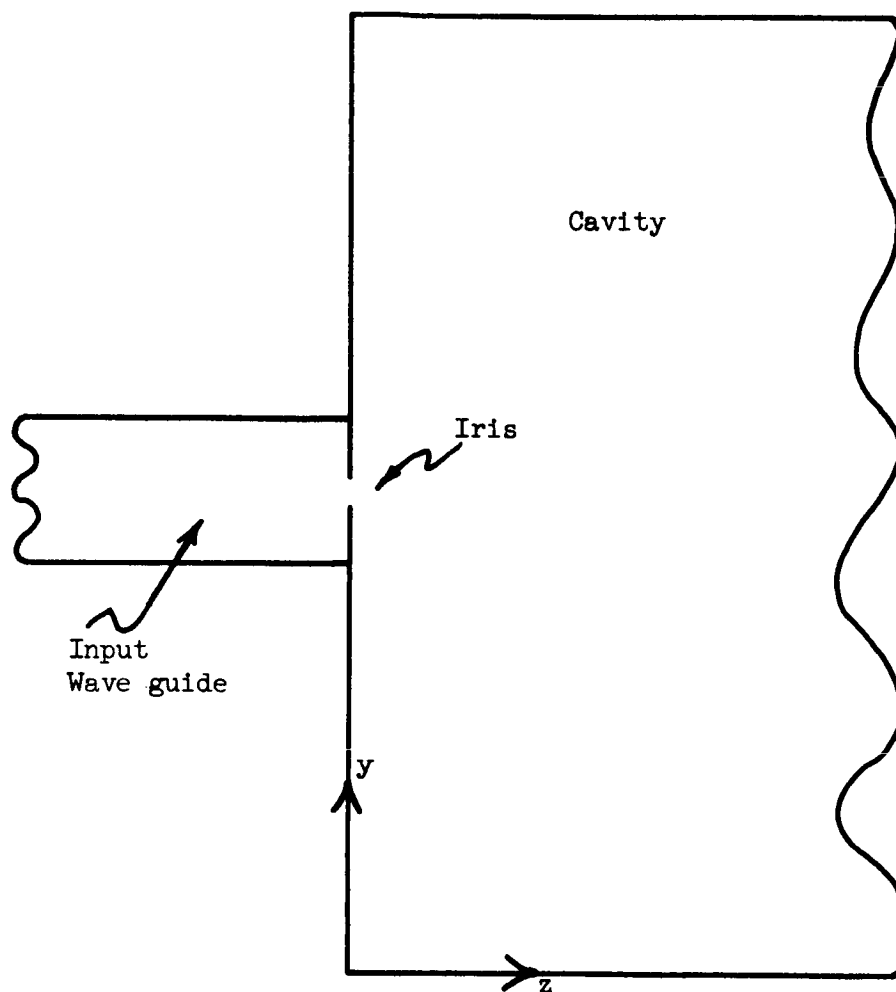


Figure 8.4 Cross-sectional view at test cavity end

component within the cavity restricts the results to  $TE_{lmn}$  modes within the cavity. Dielectric loading will possibly cause excitation of other modes.

It is possible for the  $TM_{lmn}$  modes with  $m$  even to be excited, since at the coupling hole these wave modes have transverse magnetic field components which are coupled to the fields within the wave guide. The resonant frequencies for these modes are identical with the corresponding  $TE_{lmn}$  modes for the homogeneous cavity, and it is therefore impossible to separate the two modes by examination of the cavity output.

### 8.6 Wideband Measurement Technique

A swept frequency method was used in order to facilitate the measurements, since continuous recording of data is possible. The output signal of the cavity, which is connected at the input to a swept-frequency generator, is measured at the exit port. This output may be considered as the transfer function of the cavity since the input signal is essentially independent of frequency, due to the signal leveling system of the sweep oscillator. This transfer function can be examined with an oscilloscope or, for a permanent record, a X-Y recorder which is swept by the same sawtooth voltage as the oscillator; the test circuit diagram is shown in Figure 8.5. The swept-frequency generator is an Alfred Model 650 (manufactured by Alfred Electronics, Palo Alto, California) with the 7.0-12.4 GHz plug-in unit (Model 654AK-S1) (manufactured by Alfred Electronics, Palo Alto, California). External leveling of the signal is accomplished by feeding back a portion of the input signal to the leveling input of the generator. Two frequency meters were used in the circuit since the precision (.015 percent absolute maximum frequency error) PRD Model 559-A (manufactured by PRD Electronics Inc., Westbury, New York) has a range which only extends up to 10 GHz; the Hewlett

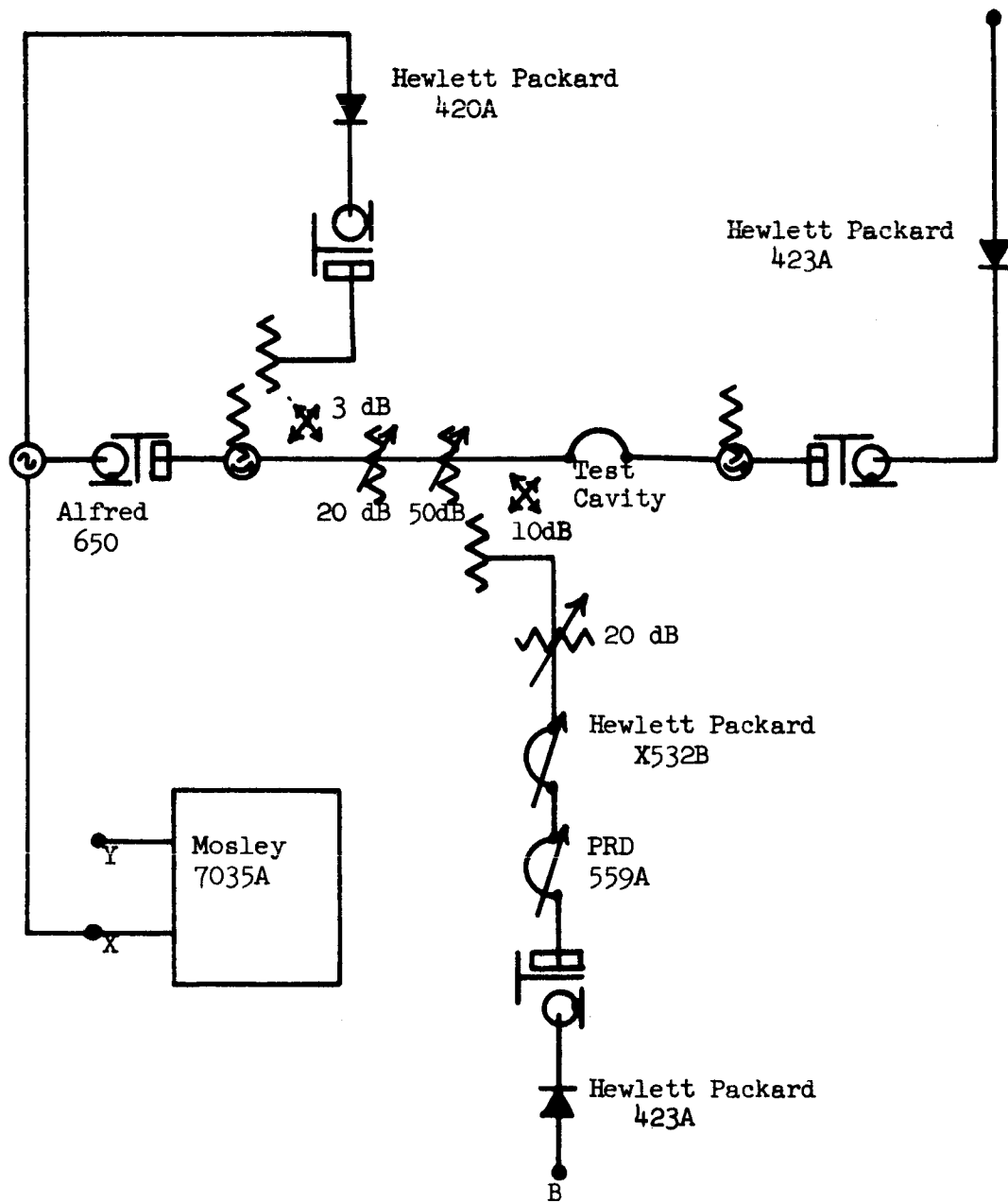


Figure 8.5 Circuit used for wideband and Q-value measurements



Packard Model X532B (manufactured by Hewlett Packard, Palo Alto, California) (.08 percent maximum error) is used for the higher frequency part of the swept spectrum. The precision type frequency meter is especially useful for narrow band measurements, as Q-measurements, since divisions of 1 MHz are directly readable on the meter.

### 8.7 Q-Value Measurement Technique

The procedure for the Q-value measurements is essentially the same as the wideband measurements except normally the sweeping range is limited to  $\Delta f = 10$  MHz rather than 2 GHz. The circuit is identical to that shown in Figure 8.5.

Initially the desired sweeping range is set, and the first two variable attenuators are adjusted for a convenient amplitude level. Two attenuators are available since it is desirable to set the second attenuator (precision type) to an even dB setting, then vary the first one for the desired amplitude at terminal A. First terminal A is connected to the y-axis input of the plotter and a Q-curve is described on the plotter, then an additional 3 dB is inserted by the second attenuator and another Q-curve is drawn--a straight line across the peak of the second curve marks the 3 dB points on the first curve. Frequency calibration is carried out in the same manner as in the case of the wideband measurement, and described below.

The x-axis of the recorder is driven by the sweep circuit of the generator; the y-axis may be excited by either terminal A or B, A being used to plot the mode spectrum of the cavity, whereas B is used for frequency calibration--the unused terminal is terminated with a 50 ohm load. The high Q-value of the absorption type frequency meter is utilized for calibration purposes. The Hewlett Packard 423A diode (manufactured by Hewlett Packard,

Palo Alto, California) has a negative response characteristic; therefore, the frequency to which the absorption meter is tuned appears as a positive peak. In this manner then, the frequency meter is adjusted to a given frequency and, after the peak is drawn, quickly advanced some predetermined interval and repeated throughout the spectrum yielding a sequence of peaks whose frequency is precisely known. During the calibration process, the sweeping speed is adjusted to 100 seconds per sweep to allow ample time for frequency changing.

The procedure, therefore, is to first connect the y-axis of the recorder to terminal A and place a 50 ohm termination on B; plot the mode spectrum of the cavity, then interchange the termination and the y-axis input and finally plot the frequency calibration peaks. It is advantageous to perform the measurements sequentially as quickly as possible, since there is some frequency drift associated with the sweeper which usually performs low amplitude drift oscillations about a center frequency for a small time interval, then shifts somewhat to a new center frequency.

### 8.8 Wideband Measurement Results

The mode spectrum of the empty cavity for a 2 GHz sweeping range can be seen in Figure 8.6. There is some degeneracy present.

The cavity was next loaded fully with very inexpensive styrofoam material purchased in a department store, normally used for Christmas decorations (Figure 8.7), which incidentally turned out to be less lossy than material purchased specifically for low-loss properties (Eccofoam, Type PS available from Emerson & Cumming, Inc., Canton, Massachusetts). The entire spectrum can be seen to be shifted approximately 75 MHz, corresponding to a relative permittivity of 1.03 for the styrofoam. There exists some mode splitting

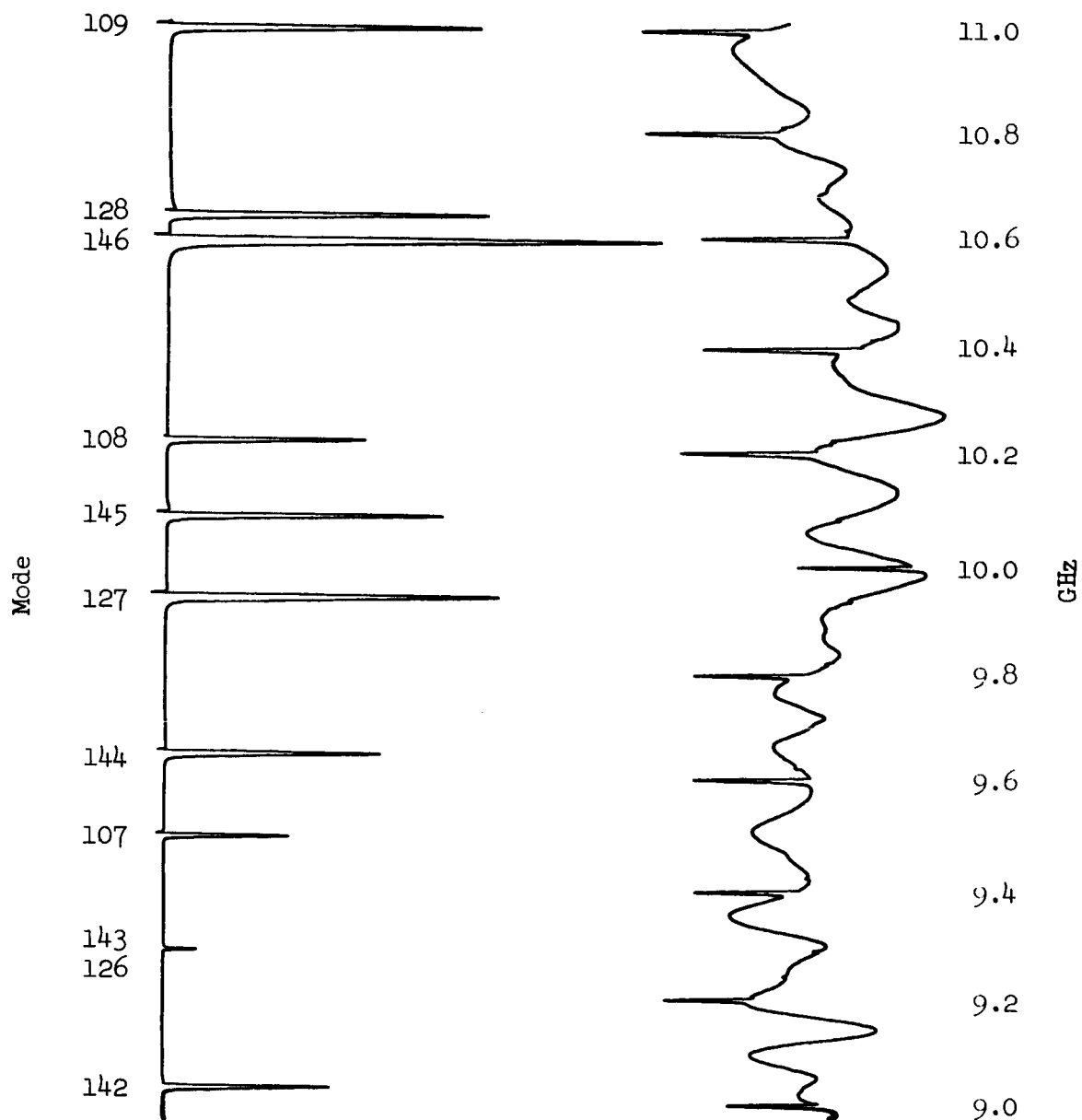


Figure 8.6 Mode spectrum of empty test cavity

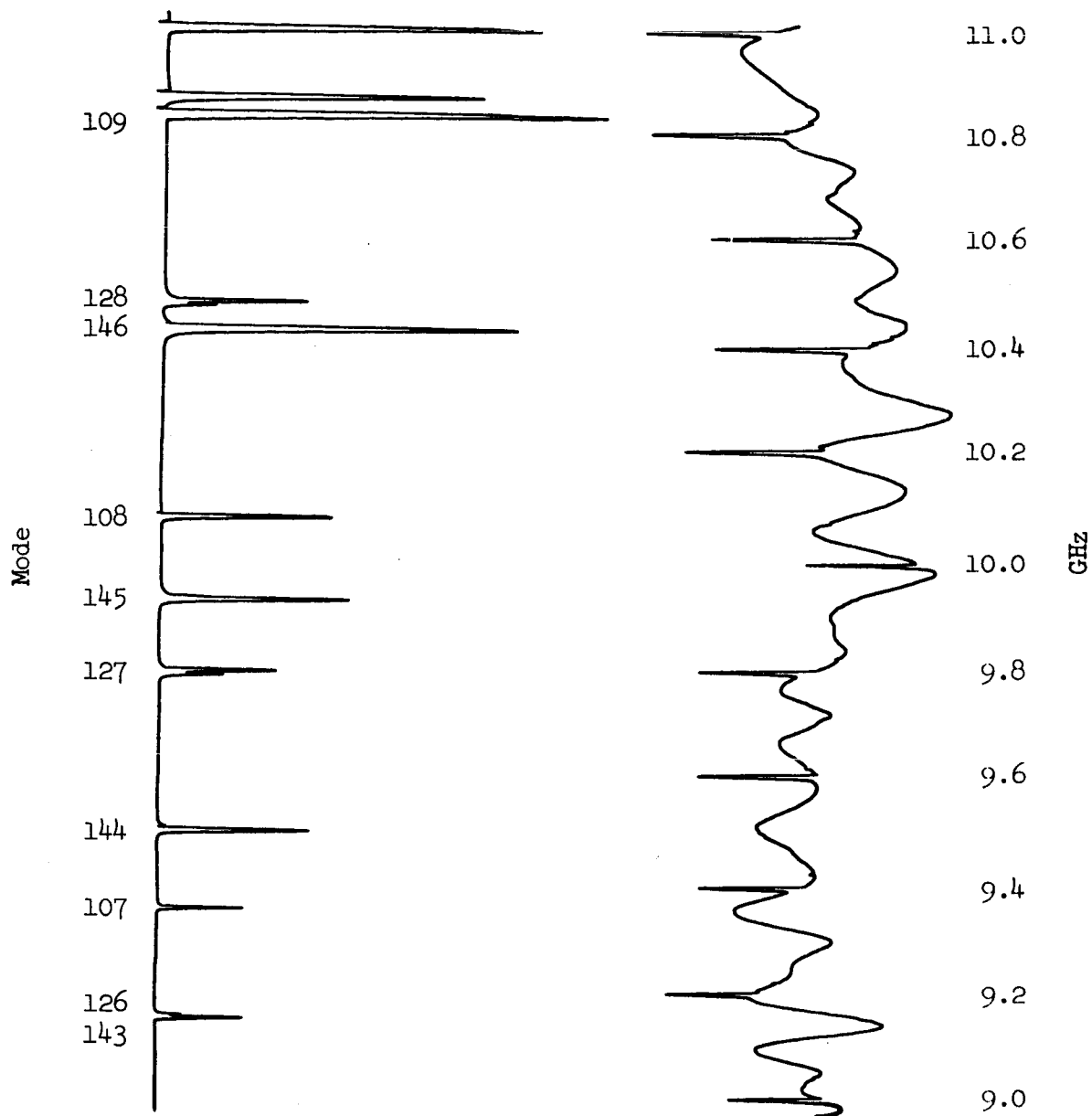


Figure 8.7 Mode spectrum of test cavity fully loaded with inexpensive dielectric described in test

(127 and 151) which is probably due to inhomogenities in the material. The variation in the relative amplitudes of the various modes is probably due to the change in the impedance which the cavity and irises present to the wave guide system which changes with frequency. Figure 8.8 shows the effects of a single one-inch thick slab of styrofoam located symmetrically in the center of the cavity (all of the slabs used for loading extend the full width of the cavity). There was only a slight shifting of the modes, perhaps 30 MHz. Again, the position occupied (in the empty cavity) by the 127, 135, and 143 modes split into two separate modes.

More could be determined about the effects of the slab by using a high permittivity dielectric [Rexolite 1422 (manufactured by Emerson & Cumming, Inc., Canton, Massachusetts)  $\epsilon_r = 2.53$ ] and comparing the spectrums for different thicknesses. The spectrum of the cavity loaded with an one-eighth-inch slab of Rexolite can be seen in Figure 8.9 and correspondingly, an one-fourth-inch slab in Figure 8.10. It should be expected that modes without any x-variation, that is 107, 108, and 109, become predominant since the dielectric behaves as a surface wave guide with the fields decaying exponentially at right angles to the surface.

There exists a transition from excitation of all cavity modes to a gradual decrease in amplitude resulting from reduced coupling, except for the 107, 108, and 109 modes. With a sufficiently thick dielectric slab in the center to cause the fields to decay to essentially zero at the top and bottom surfaces, the cavity becomes a shorted section of H-guide.

The low amplitude modes can be damped out quite effectively by placing absorbing material on the top and bottom surfaces of the cavity (Figure 8.11). The H-guide modes are not disturbed since they have essentially zero field intensity on the top and bottom surfaces.

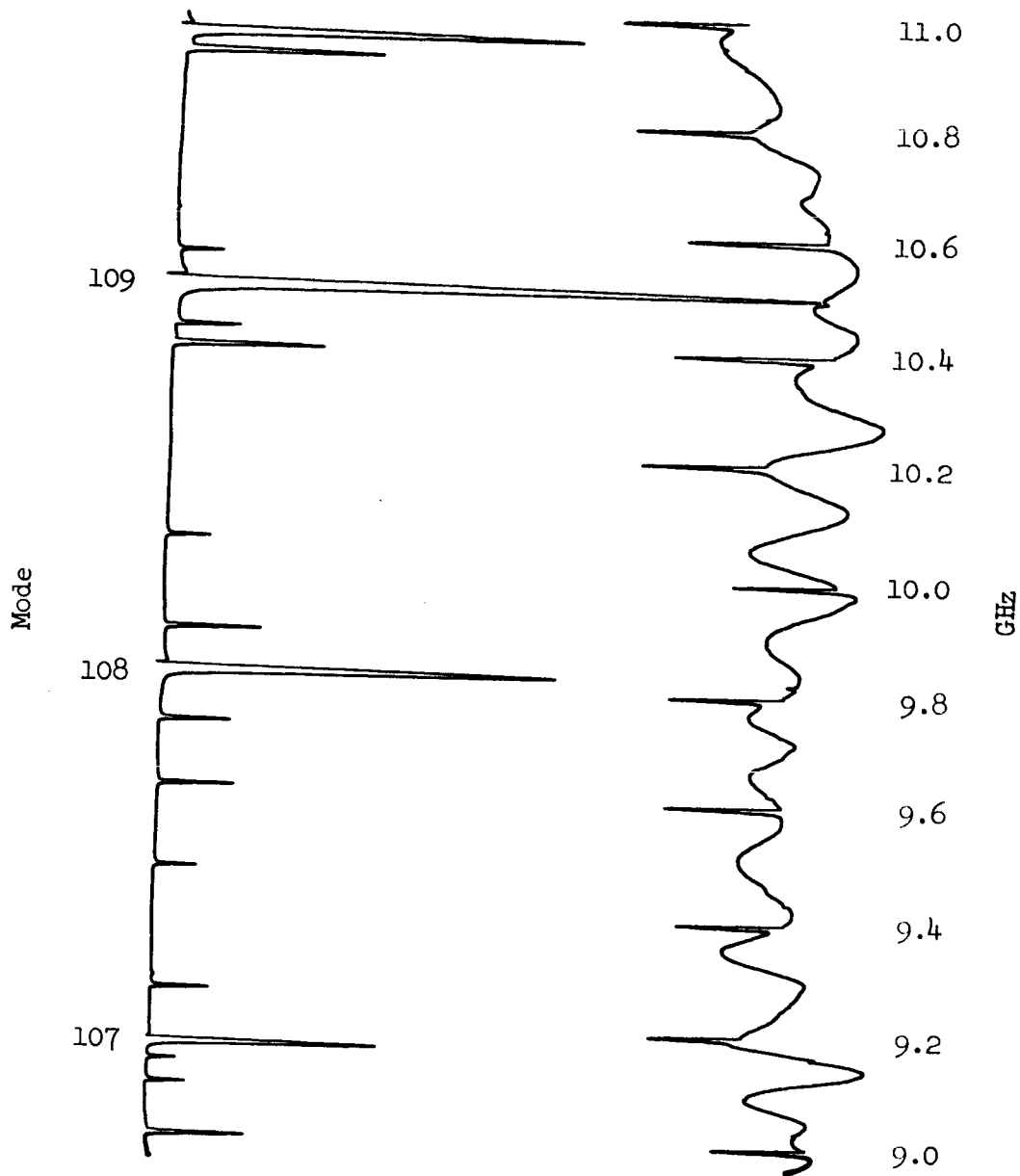


Figure 8.8 Mode spectrum of test cavity centrally loaded with a one-inch strip of inexpensive dielectric described in text

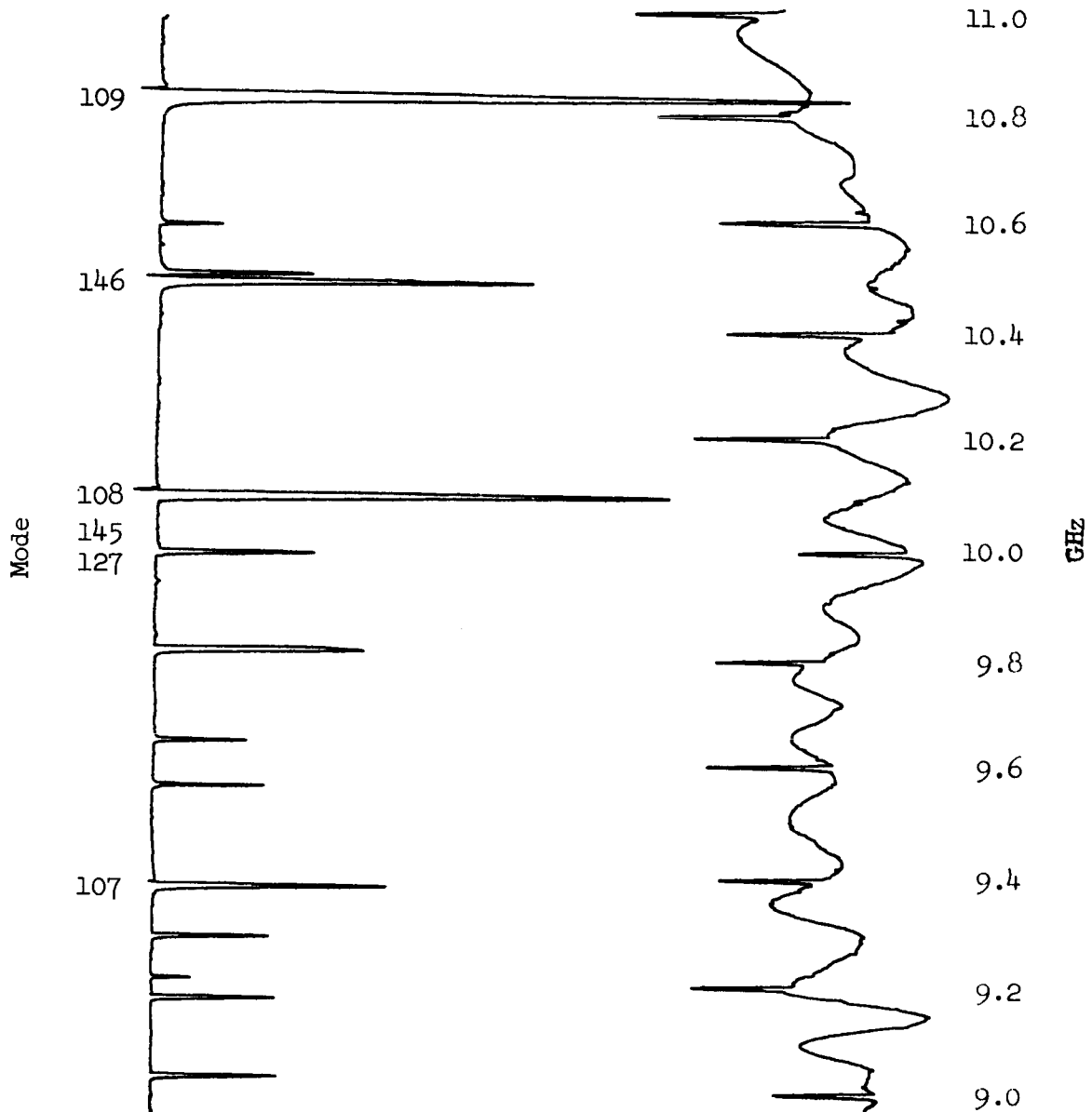


Figure 8.9 Mode spectrum of test cavity centrally loaded with a one-eighth-inch strip of Rexolite

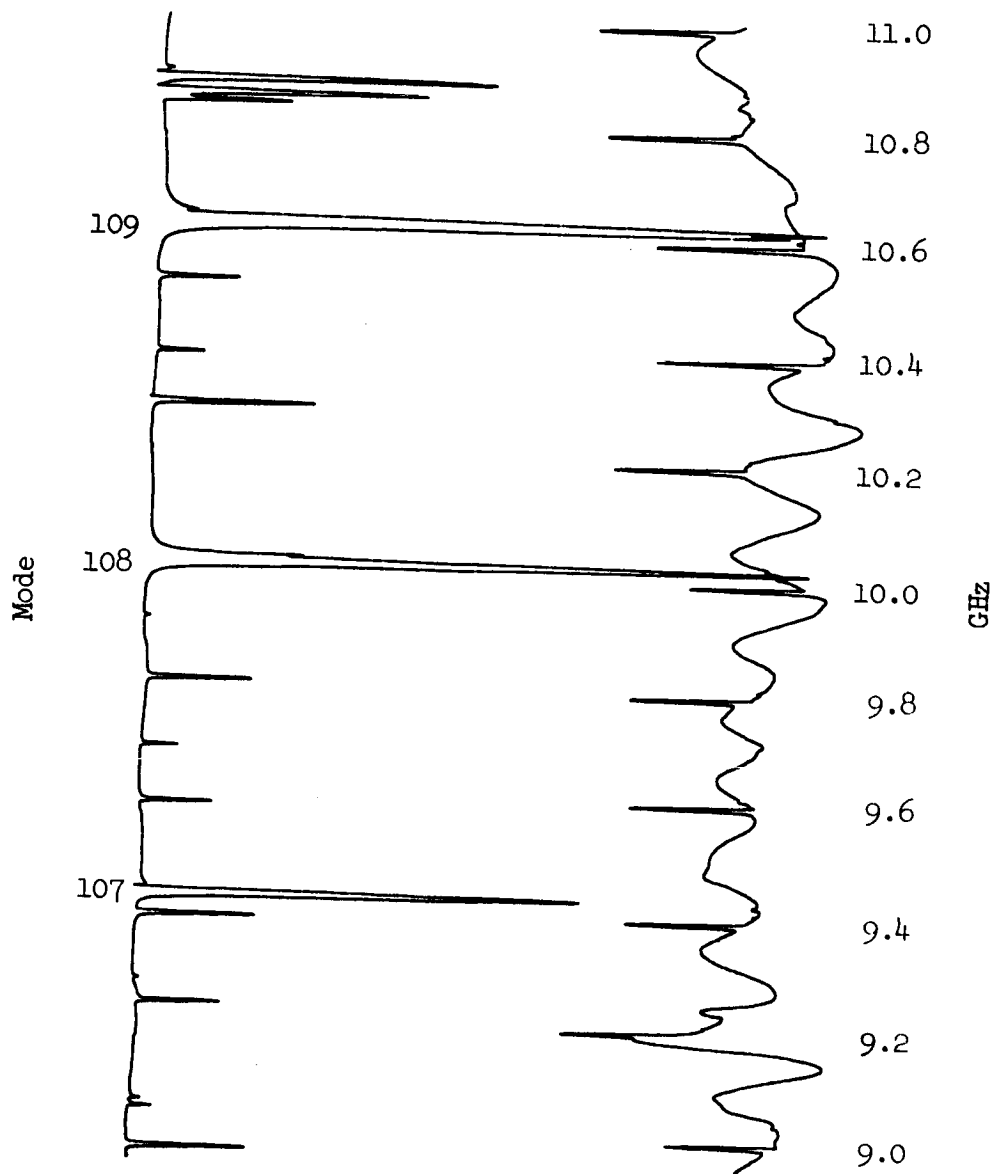


Figure 8.10 Mode spectrum of test cavity centrally loaded with a one-quarter-inch strip of Rexolite



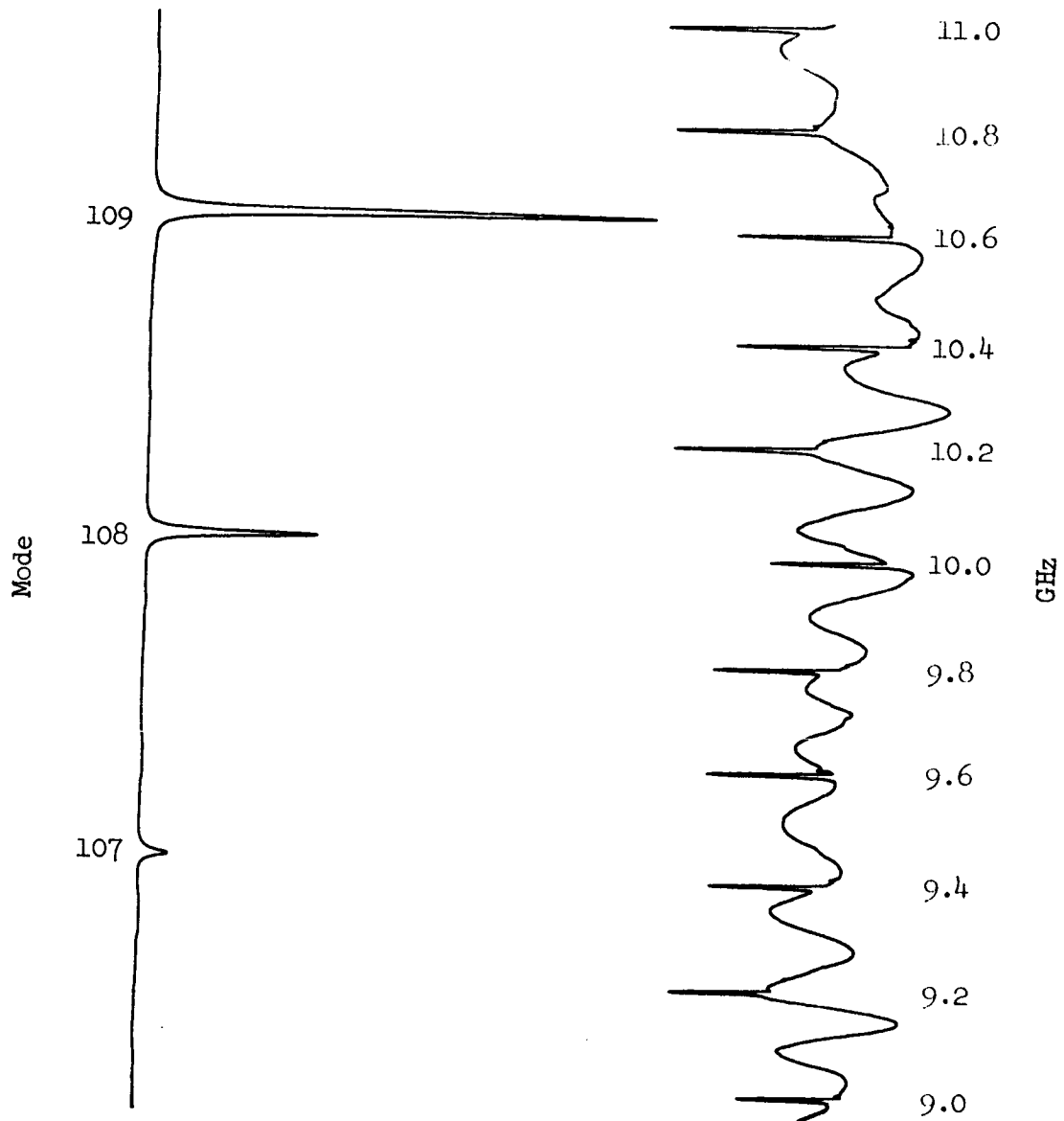


Figure 8.11 Mode spectrum of test cavity centrally loaded with a one-quarter-inch strip of Rexolite and one-quarter-inch plywood on top and bottom surfaces

The effect of the dielectric slab in the center of the cavity carrying surface waves (H-guide) can be seen more distinctly by comparing Figures 8.12 and 8.13. Figure 8.12 shows the cavity with the absorbing material on the top and bottom surfaces without the dielectric in the center. No field is excited in the cavity. A dielectric slab inserted in the center of the cavity causes the H-guide modes to be excited. They are modified 107, 108, and 109 modes, which can be seen in Figure 8.13.

The actual identification of the H-guide modes was made on the basis of Figure 8.9. The frequencies of 127, 145, and 146 modes were calculated (Table 8.2) and identified in Figure 8.9; comparison with Figure 8.6 shows that the remaining large magnitude modes must be the modified 107, 108, and 109.

### 8.9 Q-Value Measurement Results

Results of the measurements described in Section 8.7 are shown in Figure 8.14 for the empty cavity and for the 107 mode. The extraneous "spikes" in the calibration curve were caused by the technique used. At first, the frequency meter is adjusted to 9.498 GHz, then the sweeping circuit energized, and a part of the curve for this frequency setting is plotted. After the pen of the plot has passed the peak of the 9.498 GHz setting, frequency meter is quickly moved to 9.500 GHz causing a "spike." The recorder then plots a section of the frequency curve for the new setting until the frequency meter is moved to the next frequency setting. In this way, series of resonance curves are obtained as references for the frequency scale.

The Q-measurements were made with one-quarter-inch irises. The Q would be higher for smaller diameters since the coupling losses would be reduced. This size was decided upon since the insertion loss becomes

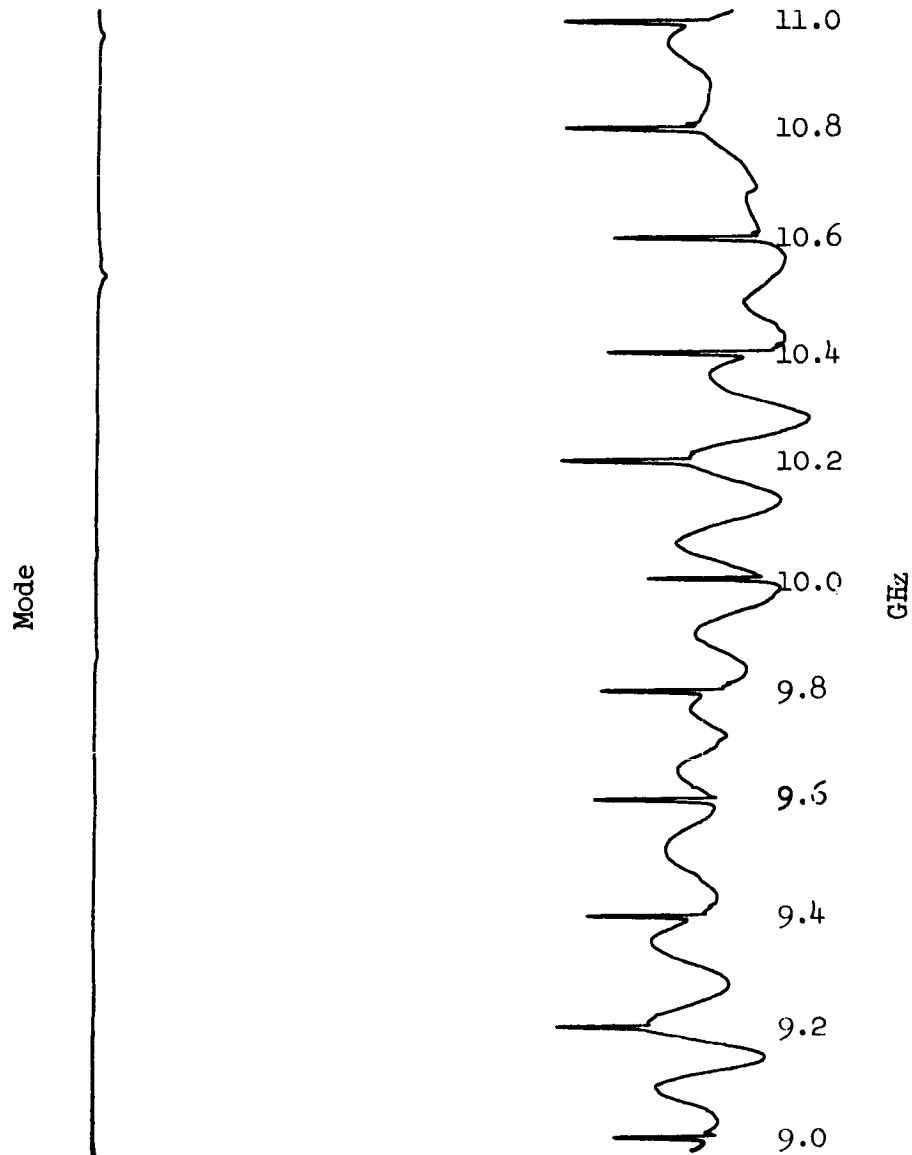


Figure 8.12 Mode spectrum of test cavity loaded with one-half-inch strips of Eccofoam absorbing material on top and bottom surfaces

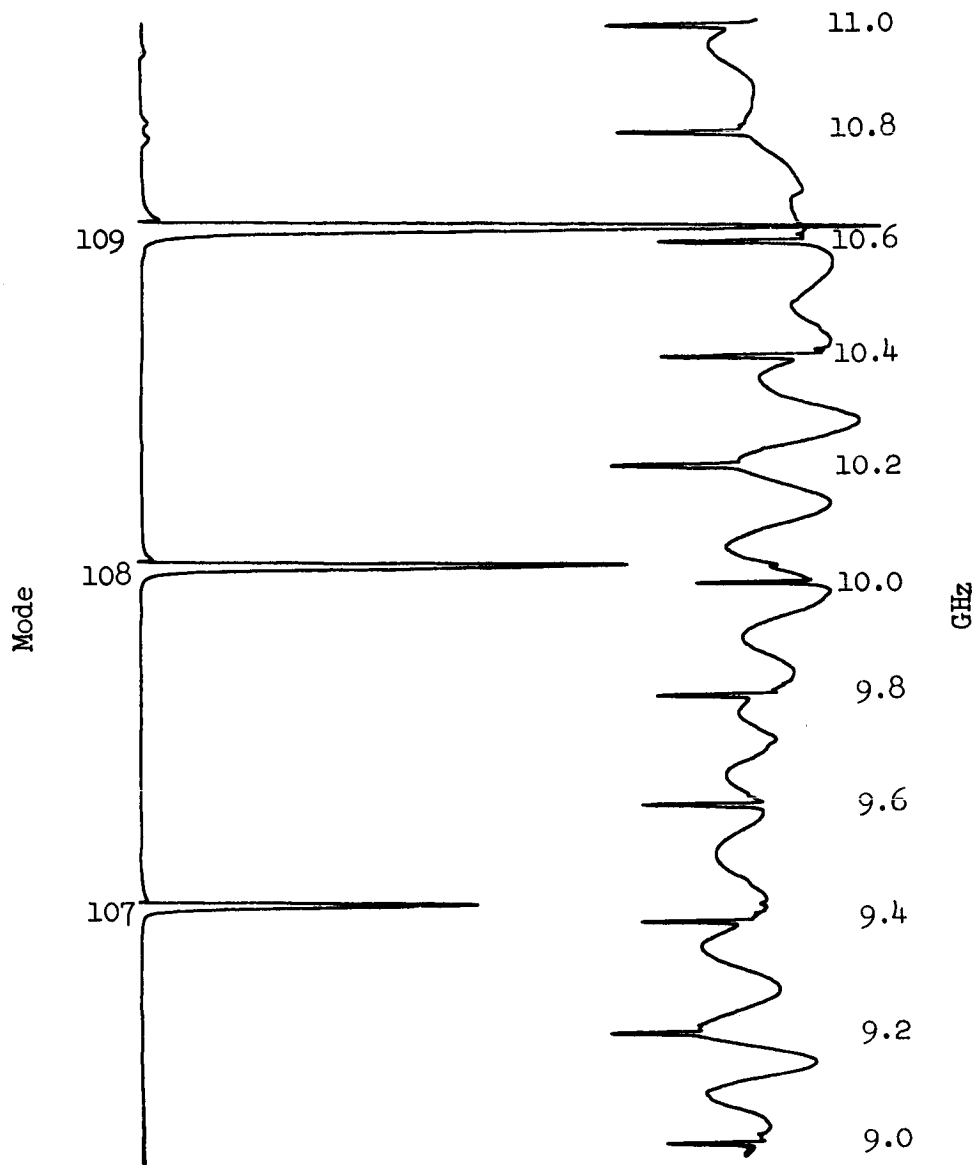


Figure 8.13 Mode spectrum of test cavity centrally loaded with one-quarter-inch strip of Rexolite and one-half-inch strips of Eccofoam absorbing material on top and bottom surfaces

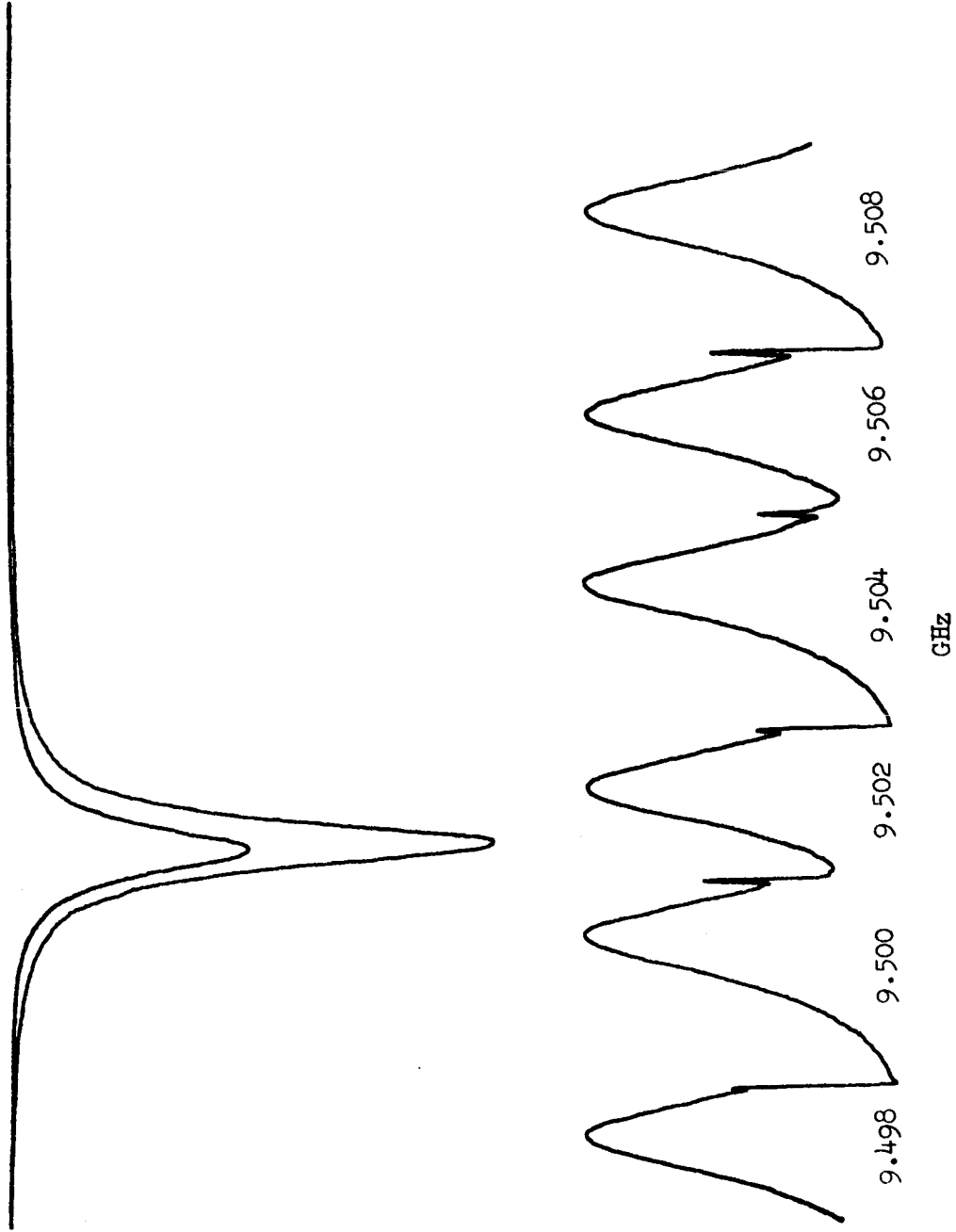


Figure 8.14 Q-value measurement spectrum of test cavity for the  $TE_{1,07}$  mode in empty cavity

objectionable for small diameters with the present power capability (10 mw.) and available detection system (crystals). The results of the measurements can be seen in Table 8.3. The 107, 108, and 109 modes were examined since they ultimately become the only modes present under all types of loading considered. As was expected, the loaded Q-value decreases with increasing dielectric loading. No specific conclusions can be made about the Q-value of the different modes for a fixed type of loading since the impedance of the irises changes with frequency and the unloaded Q would have to be isolated from the various loading factors; that is,

$$\frac{1}{Q_L} = \frac{1}{Q_u} + \frac{1}{Q_c},$$

where the subscripts specify loaded, unloaded, and coupling (irises) respectively. To determine the unloaded Q, the frequency dependent coupling Q must be separated from the loaded Q.

Table 8.3 Loaded Q-values of the test cavity

Cavity Loading	TE Mode	Loaded Q-value
Empty	107	16000
	108	16080
	109	-
Dielectric (Styrofoam $\epsilon_r = 1.03$ ) Completely filled	107	11000
	108	11160
	109	9065
Dielectric 1/4" Rexolite 1422 strip ( $\epsilon_r = 2.53$ ) centered in cavity parallel to top and bottom surfaces	107	3410
	108	3435
	109	3200
Dielectric as above except additional 1/2" thick absorbing material on top and bottom surfaces (Eccosorb LS)	107	3015
	108	2620
	109	2220

### 8.10 Theoretical Technique for Unloaded Q-Value Measurement

A transmission cavity can be considered in terms of lumped circuit parameters, Montgomery (1947); an equivalent circuit for the cavity is shown in Figure 8.15. In general, the input and output coupling would be different, but here the symmetric case is considered since the input and output irises are identical. The irises will thus be represented by ideal transformers with turn ratios  $n:1$ . If the equivalent circuits of the transformers are utilized, Figure 8.15 becomes Figure 8.16.

The loaded  $Q$ ,  $Q_L$ , for the circuit in Figure 8.16 is given by

$$Q_L = \frac{\omega_0 L}{R + n^2(R_G + R_L)} , \quad (8.5)$$

where  $\omega_0$  is the particular resonant frequency under consideration. Equation (8.5) can be written in terms of the unloaded  $Q$ ,  $Q_u$ , as

$$Q_u = Q_L \left[ 1 + \frac{n^2}{R} (R_G + R_L) \right] . \quad (8.6)$$

If the system is matched in both directions from the cavity ( $R_G = R_L$ ), which can be accomplished by making the voltage standing wave ratio, VSWR, small in both directions, then (8.6) becomes

$$Q_u = Q_L (1 + 2\beta) , \quad (8.7)$$

where the coupling parameter,  $\beta$ , has been defined as

$$\beta = \frac{n^2 Z_0}{R} \quad (8.8)$$

and

$$Z_0 = R_L = R_g .$$

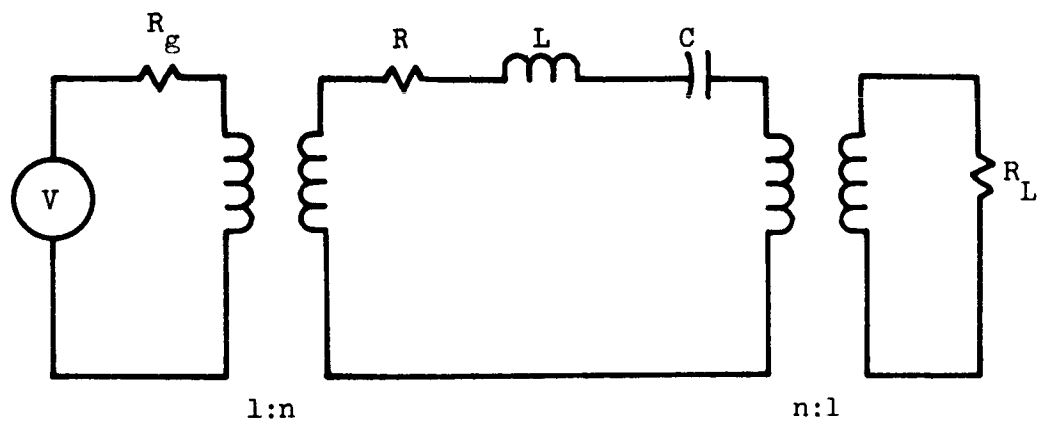


Figure 8.15 Equivalent circuit of transmission cavity with coupling irises shown as ideal transformers



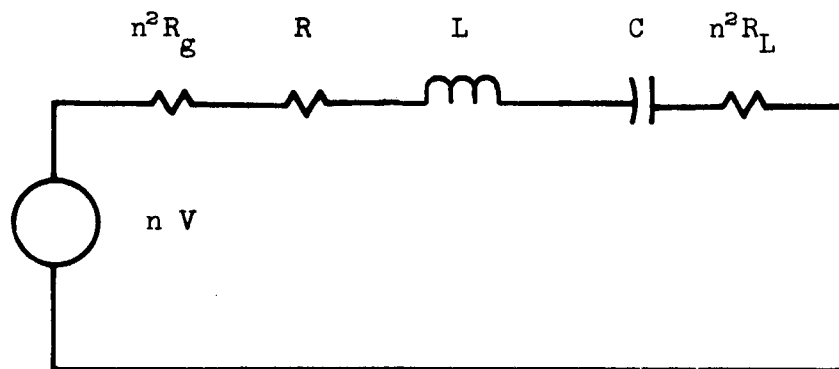


Figure 8.16 Alternative form for the circuit shown in Figure 8.15

The current for the loop in Figure 8.16 can be written in the form

$$I = \frac{nV}{R[(1+2\beta) + j Q_u (\frac{\omega}{\omega_0} - \frac{\omega_0}{\omega})]} , \quad (8.9)$$

since

$$\omega_0^2 = \frac{1}{LC} . \quad (8.10)$$

The real power delivered to the load impedance is given by

$$P_L = |I|^2 n^2 Z_0 , \quad (8.11)$$

or in terms of  $\beta$  as

$$P_L = |I|^2 \beta R . \quad (8.12)$$

Now, substituting from (8.9) into (8.12) the power becomes

$$P_L = \frac{V^2 \beta^2}{Z_0 [(1+2\beta)^2 + Q_u^2 (\frac{\omega}{\omega_0} - \frac{\omega_0}{\omega})^2]} . \quad (8.13)$$

If the generator were to see a matched load, as in Figure 8.17, the power delivered to the load would be given by

$$P = \frac{V^2}{4Z_0} . \quad (8.14)$$

A transmission function,  $T(\omega)$ , defined as  $P_L/P$ , can be found from (8.13) and (8.14), that is

$$T(\omega) = \frac{4\beta^2}{[(1+2\beta)^2 + Q_u^2 (\frac{\omega}{\omega_0} - \frac{\omega_0}{\omega})^2]} , \quad (8.15)$$

which becomes at resonance

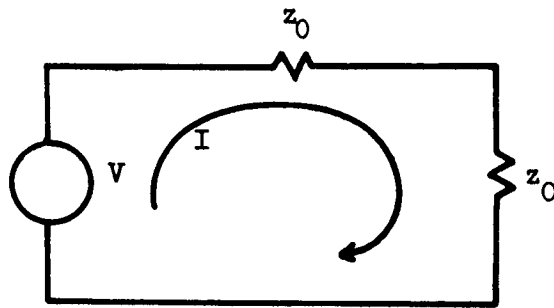


Figure 8.17 Generator,  $V$ , feeding a matched load  $z_0$

$$T(\omega_0) = \frac{4\beta^2}{(1+2\beta)^2}, \quad (8.16)$$

or for  $\beta$  in terms of  $T(\omega_0)$  as

$$\beta = \frac{\sqrt{T(\omega_0)}}{2[1 - \sqrt{T(\omega_0)}]}. \quad (8.17)$$

$T(\omega_0)$  is a measurable quantity. Upon measuring it, (8.17) yields  $\beta$ , and then (8.7) specifies  $Q_u$  after  $Q_L$  is measured.

### 8.11 Experimental Technique for Q-Value Measurements

The circuit used for loaded Q-value and insertion loss measurements is shown in Figure 8.18.

The VSWR, as seen in both directions from the cavity must have a low value if the previously described method is to be employed. This can be accomplished by inserting attenuation in the wave guide. If ten dB of attenuation is inserted by both attenuator 1 and attenuator 2, the VSWR in both directions was found to be less than 1.02:1.

The system must now be balanced. With the cavity removed from the system and attenuator 1 set to approximately ten dB, the signal is measured at B; the switch now is turned to the other arm and attenuator 2 is adjusted for the same signal amplitude at A, thus balancing the system.

A six-inch section of wave guide is inserted in the position formerly occupied by the cavity. The difference between the signals at A and B is one-quarter dB, indicating the loss for two coupling flanges and a six-inch section of wave guide, which represents the coupling loss from the wave guide to the irises.

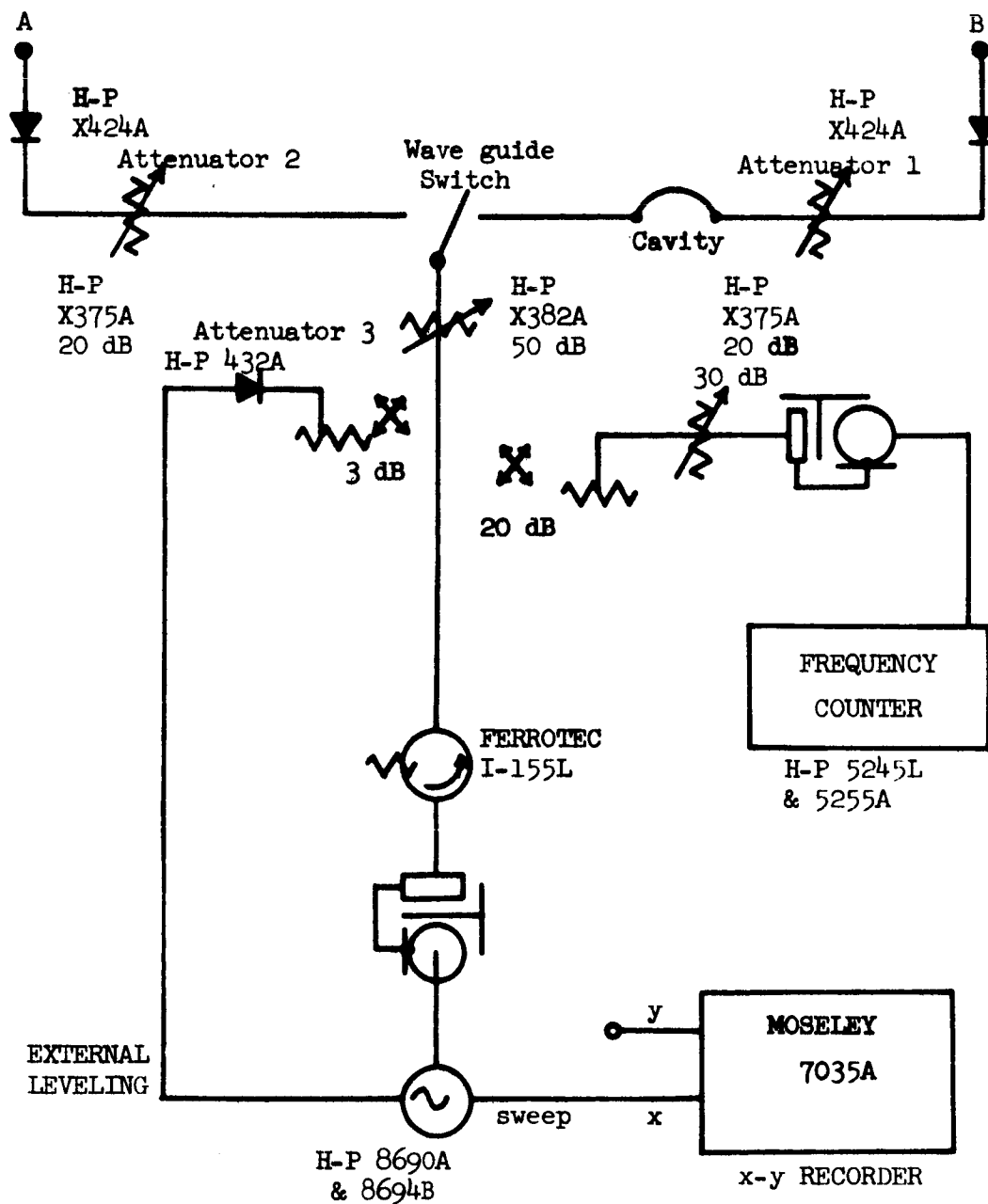


Figure 8.18 Circuit used for INSERTION LOSS and Q-value measurement

Insertion loss measurements may now be performed. An oscilloscope is connected to B, the frequency adjusted to the resonant frequency of the mode to be measured, attenuator 3 adjusted to a convenient level, and the signal level recorded. The switch is now turned to the left arm and attenuator 3 adjusted until the signal level is the same as that previously measured. The difference between the final and initial settings of attenuator 3 yields the insertion loss. The results of the measurements appear in Table 8.4.

The loaded Q-value,  $Q_L$ , is measured as follows. Terminal A is connected to the y-axis input of the X-Y recorder. Sweeping will be performed manually at the generator. The resonant frequency,  $f_0$ , of the particular mode under consideration is determined and the generator adjusted to this frequency.

A minus three-dB level is now established. A line is drawn on the paper in the plotter parallel to the x-axis and near the vertical center of the sheet. Attenuator 3 is adjusted such that the pen coincides with this line at the resonant frequency. Attenuator 3 is now adjusted to a value three dB less than before and a Q-curve is drawn on the paper by allowing the generator to sweep several MHz about the resonant frequency. The frequencies,  $f_1$  and  $f_2$ , at which the Q-curve crosses the line previously drawn are the half power frequencies. The loaded Q-value is now given by

$$Q_L = \frac{f_0}{f_2 - f_1} . \quad (8.18)$$

The loaded Q-values for the modes considered appear in Table 8.4.

The coupling parameter,  $\beta$ , can be calculated from (8.17), thus yielding  $Q_u$  from (8.7).

The Q-values for the  $TE_{107}$  mode in the empty cavity provides a validity-check on the method. Analytically, this was calculated to be 22,700 and

Table 8.4. Results of insertion loss and loaded Q-values measurements

Mode	Loading	Resonant frequency (GHz)	$1/T(\omega_0)$ (dB)	$\beta$	$Q_L$ (thousands)	$Q_U$ (thousands)	$\alpha$ nepers (per meter)	Calculated $\alpha$ nepers (per meter)
107	Empty	9.4909	12.5	0.156	16.8	22.0		
108		10.2252	9.9	0.238	16.3	24.0		
107	Corrugated H-guide $p = 0.3$	9.2560	14.0	0.121	9.3	18.2	0.0071	0.0033
108		9.9563	10.5	0.214	8.0	17.9	0.0072	
109		10.6849	7.3	0.386	7.1	20.1	0.0064	
107	Corrugated H-guide $p = 0.45$	9.6402	13.5	0.131	6.9	13.5	0.0088	0.0070
108		10.2620	9.3	0.262	5.5	13.0	0.0091	
109		10.8575	16.5	0.088	9.0	16.7	0.0071	

measured as 22,000. This result is within the experimental error of the measurement (5%), which was obtained by repeating identical measurements and noting the differences incurred.

The H-guide structure which was inserted into the cavity was supported by a rectangular piece of dielectric identical in size to the inside dimensions of the cavity. Consequently, dielectric losses are introduced and must be considered. Under earlier conditions, for a  $Q_L$  of 16,000, a value of 11,000 was measured when the cavity was filled with dielectric of the same type as used for supporting the H-guide structure. It would therefore seem reasonable to multiply the measured Q-values for the H-guide by a factor 16/11 to determine the Q-value for the H-guide structure above.

The unloaded Q-value for the H-guide,  $Q_u$ , now contains losses due to the top and bottom surfaces as well as the end plates. If the losses due to the top and bottom surfaces are neglected, since the field decays exponentially normal to the corrugations, it should have a small value of amplitude at these surfaces. The losses due to the end plates can be accounted for in terms of a Q-value,  $Q_E$ . The H-guide Q,  $Q_H$ , is now given by

$$\frac{1}{Q_H} = \frac{1}{Q_u} - \frac{1}{Q_E} . \quad (8.19)$$

$Q_E$  was calculated to be 143,000. The Q-value,  $Q_H$ , must now be related to attenuation,  $\alpha$ .

#### 8.12 A Relationship Between Attenuation and Q-Value

A cavity may be considered as a shorted section of the wave guide, whose attenuation is given by

$$\alpha = \frac{P_L}{2P} , \quad (8.20)$$



where

$$P_L = \frac{R_s}{2} \oint_C |H_t|^2 dl \quad (8.21)$$

and

$$P = \frac{1}{2} \operatorname{Re} \int_{S_c} \int (\underline{E} \times \underline{H}^*) \cdot d\underline{s} , \quad (8.22)$$

$C$  being the contour enclosing the cross-sectional area  $S_c$ . The  $Q$ -value for the cavity, excluding the losses on the end plates, is

$$Q = \frac{\omega W_{E(\max)}}{P_L'} , \quad (8.23)$$

where

$$W_{E(\max)} = \frac{\epsilon}{2} \int \int_V \underline{E} \cdot \underline{E}^* dv \quad (8.24)$$

and

$$P_L' = \frac{R_s}{2} \int_{S'} \int |H_t|^2 ds , \quad (8.25)$$

$S'$  being the internal surface area, excluding the end plates, and  $V$  the volume enclosed by the cavity.

For the case of TE waves propagating as  $e^{\pm jk_z z}$ , the tangential field components are related as (Collin, 1960)

$$|E_t| = Z_{TE} |H_t| , \quad (8.26)$$

where

$$Z_{TE} = \eta \frac{k_0}{k_z} , \quad (8.27)$$

and  $\eta$  is the intrinsic impedance of free space, defined by

$$\eta = \sqrt{\mu_0 / \epsilon_0} . \quad (8.28)$$

Applying this restriction to (8.22), (8.25) and (8.25), they become respectively

$$\underline{P} = \frac{M}{2Z_{TE}} , \quad (8.29)$$

$$W_{E(\max)} = \frac{Med}{2} , \quad (8.30)$$

and

$$P'_L = P_L d , \quad (8.31)$$

where  $d$  is the length of the cavity in the direction of propagation ( $z$ ), and for convenience  $M$  has been defined as

$$M = \int \int_{S_c} |E|^2 ds . \quad (8.32)$$

The product of  $\alpha$  and  $Q$  may now be formed, that is

$$\alpha Q = \frac{\omega W_{E(\max)} P_L}{2 P P'_L} , \quad (8.33)$$

substituting from (8.29) through (8.31) yields

$$\alpha Q = \frac{\omega Med P_L}{2 MP_L d} ,$$

$$2 \frac{2Z_{TE}}{2Z_{TE}}$$

and simplifying yields

$$\alpha Q = \frac{\omega e Z_{TE}}{2} . \quad (8.34)$$

Using the definition for  $Z_{TE}$  simplifys further, and the product becomes

$$\alpha Q = \frac{k_0^2}{2k_z} , \quad (8.35)$$

where  $Q$  is the  $Q$ -value of the cavity including the losses due to any inserted structure, but excluding the losses due to the end plates.

The attenuation for the H-guide structure may be obtained from (8.19) and (8.35). The  $z$ -propagation constant was calculated by the computer program previously written. Attenuation values appear in Table 8.4.

## 9. CONCLUSION

### 9.1 Summary

Analytical expressions for attenuations were obtained and evaluated numerically by a digital computer. Comparisons were made at a frequency of 10 GHz using the same value of  $p$ , the normalized x-decay constant, in all cases; that is, the same field confinement. A shorted section corrugated H-guide was constructed and the attenuation measured.

### 9.2 Findings

The analytical solution for the dielectric H-guide yielded the disappearance of the longitudinal wall current as expected; however, for the corrugated H-guide, the only field component disappearing was the transverse electric. This could be in fact true or could be due to the particular approximation made in the solution. It was assumed that the fundamental mode (no longitudinal variation) was dominant within the corrugations, and all other modes could be neglected. The approximation is not entirely without merit since good agreement was found with measurements.

The attenuation for the corrugated H-guide was found to be less than half that of the dielectric H-guide at a frequency of 10 GHz and the same value of x-decay constant. By using laminations rather than a solid slab for the dielectric H-guide, the attenuation could be decreased by a factor of approximately five, half that of the corrugated H-guide.

## 10. LIST OF REFERENCES

- Barlow, H. M. and J. Brown. 1962. Radio Surface Waves. Oxford University Press, London, England.
- Brillouin, L. 1948. Wave guides for slow waves. J. Appl. Phys. 19:1023-1041.
- Chodorow, M. and C. Susskind. 1964. Fundamentals of Microwave Electronics. McGraw-Hill Book Company, Inc., New York.
- Cohn, M. 1959. Propagation in a dielectric-loaded parallel plane wave guide. I.R.E. Trans. on Microwave Theory and Techniques MTT-7:202-208.
- Collin, R. E. 1960. Field Theory of Guided Waves. McGraw-Hill Book Company, Inc., New York.
- Elliott, R. S. 1954. On the theory of corrugated plane surfaces. I.R.E. Trans. on Antennas and Propagation AP-2:71-81.
- Goubau, G. 1950. Surface waves and their application to transmission lines. J. Appl. Phys. 21:1119-1128.
- Goubau, G. 1954. Designing surface wave transmission lines. Electronics 27:180-184.
- Griemsmann, J. W. E. and L. Birenbaum. 1959. A low-loss H-guide for millimeter wavelengths. Pp. 593-562. Proc. of the Symposium on Millimeter Waves. Polytechnic Institute of Brooklyn, New York.
- Harms, F. 1907. Elektromagnetische wellen an einem draht mit isolierender zylindrischer hülle. Annalen der Physik 23:44-60.
- Jones, D. E. 1893. Electric Waves. Macmillan and Company, New York. Reprinted by Dover Publications Inc., New York.
- Lanczos, C. 1966. Discourse on Fourier Series. Hafner Publishing Company, New York.
- Montgomery, C. G. 1947. Technique of Microwave Measurements. McGraw-Hill Book Company, Inc., New York.
- Ramo, S., J. R. Whinnery, and T. Van Duzer. 1965. Fields and Waves in Communications Electronics. John Wiley and Sons, Inc., New York.
- Sommerfeld, A. 1899. Über die fortpflanzung elektrodynamischer wellen längs eines drahtes. Annalen der Physik und Chemie 67:233-290.
- Stratton, J. A. 1941. Electromagnetic Theory, McGraw-Hill Book Company, Inc., New York.

## LIST OF REFERENCES (continued)

- Taylor, A. E. 1955. Advanced Calculus. Ginn and Company, Boston, Massachusetts.
- Tischer, F. J. 1953. A wave guide structure with low losses. Archiv der Elektrischen Übertragung 7:592-596.
- Tischer, F. J. 1956. The H-guide, a wave guide for microwaves. I.R.E. Convention Record (Part 5):44-47.
- Tischer, F. J. 1959. Properties of the H-guide at microwave and millimeter-wave regions. Proc. I.E.E. 106 (B-13):47-53.
- Zenneck, J. 1907. Über die fortplanzung ebener elektromagnetischer wellen längs einer ebenen leiterfläche und ihre beziehung zur drahtlosen telegraphie. Ann. Phys. 23:846-866.
- Zucker, F. J. 1954. The guiding and radiation of surface waves. In Proceedings of the Symposium on Modern Advances in Microwave Techniques. J. Fox, Editor. Pp. 403-405. Polytechnic Institute of Brooklyn, New York.